Engineering Platforms for Mimicking Cellular Processes using Cell-Free Expression Systems

by

Sagardip Majumder

A dissertation submitted in partial fulfillment
of the requirements for the degree of
Doctor of Philosophy
(Mechanical Engineering)
in the University of Michigan
2020

Doctoral Committee:

Associate Professor Allen Liu, Chair
Assistant Professor Tobias Giessen
Professor Edgar Meyhöfer
Assistant Professor Anthony Vecchiarelli

Sagardip Majumder

sagardip@umich.edu

ORCID iD: 0000-0002-4736-6945

Acknowledgments

This work wouldn't have been possible without the support of my advisor, Dr. Allen Liu. I sincerely thank Allen for providing me this wonderful opportunity to work in his lab for the last three and half years. His constant guidance during this period has helped me become a better researcher. He has been a source of tremendous inspiration for me both in terms of work ethics and as a great human being. Over the years, I have come to admire him for his discipline and dedication towards scientific research. I am also thankful to him for providing all the valuable suggestions regarding trainings and workshops and financially supporting them, to improve my knowledge and skills on this topic of research. He is a great mentor and working with him has been a phenomenal experience for me.

I would also like to extend my gratitude to all the members of Liu Lab, past and present, for maintaining a kind and supportive environment in the lab. Specifically, I thank Kenneth and Luciana for introducing me to experimental research and preaching good lab practices during my initial training. My sincere thanks to Max for all the helpful discussions regarding cell biology in general and his customized protocols which is now followed by half of the lab! I thank the newer lab members Yashar, Hossein and Alessandro for their valuable feedbacks regarding my work and all the interesting conversations we had over the last year. Finally, I would like to extend my appreciation to Jophin for being a good friend and my office neighbor since the time we joined the lab.

Outside the lab, I would like to express my sincere thanks to the staff of the Department of Mechanical Engineering who have been excellent in resolving any issues

that I had during my time here. I thank my previous roommate Aniruddhe, for feeding me with great homemade food during times when I was struggling with my research. I thank my childhood friends Supratim and Mandeep who have kept me motivated over the years to keep learning and exploring the sciences.

A huge shoutout to my sister Ena, and my fiancé Payal, for their emotional and moral support throughout my PhD. In the end, I thank my parents for making me the person that I am today. This thesis is dedicated to their well-being.

Table of Contents

List of Figures

Abstract

Bottom-up *in vitro* reconstitution has provided fundamental insights into the mechanisms of key cellular processes like cell migration, cell division, endocytosis and exocytosis. Traditional reconstitution methods rely on protein purification as the primary means of extracting functional proteins from cells. While efficient for most cytoplasmic proteins which are stable in solution, reconstitution of membrane proteins remains challenging. This is attributed to the requirement of a cellular membrane-like substrate for proper folding and functioning of membrane proteins. Reconstitution into lipid bilayer membranes is usually achieved using moderate non-ionic detergents. Such a process is non-trivial and requires excessive optimization based on the type of membrane protein that is to be reconstituted. Additionally, tagging of proteins, which facilitates purification, can hinder protein function post reconstitution.

An alternative approach is the use of cell-free expression (CFE) systems to synthesize proteins *in vitro.* Recent advances in cell-free reconstitution have enabled synthesis and insertion of membrane proteins into artificial lipid bilayer substrates. However, past studies have been primarily focused on the detergent-free reconstitution of individual membrane proteins without an attempt to recapitulate biologically relevant phenomena. In this dissertation, we demonstrate the potential of using CFE systems to directly investigate important biological processes and to mimic cell-like behavior through the creation of synthetic cells.

First, we use a HeLa CFE platform to study inner nuclear membrane proteins SUN1 and SUN2 that are involved in the formation of the linker of nucleoskeleton and cytoskeleton complex (LINC). Inner nuclear membrane proteins are difficult to study in cells and require sophisticated techniques for successful extraction and analysis. By coupling simple biochemical assays with fluorescence microscopy, we determine the membrane-inserted topology of full-length SUN1 and SUN2 and demonstrate their function *in vitro.* Further, we find evidence of previously unidentified SUN1-SUN2 heteromeric interactions and possible cation dependent enhancement in binding affinity to KASH peptides which are responsible for the formation of LINC complex in cells.

Next, we use an *E. coli* CFE system encapsulated within lipid bilayer vesicles (liposomes) to demonstrate simultaneous reconstitution of two functionally different proteins. The activity of a CFE reconstituted mechanosensitive channel (MscL) in response to hypo-osmotic shock is demonstrated using a dye leakage assay in liposomes. A calcium biosensor (G-GECO) with high ON/OFF ratio in fluorescence intensity upon calcium binding is successfully expressed using CFE. We observe spontaneous localization of MscL to lipid membranes while G-GECO is homogenously distributed within encapsulated liposomes. Co-expression inside liposomes with application of hypo-osmotic shock result in detectable calcium influx through activated MscL. Our findings present the creation of a synthetic cell which can be used as a reconstitution platform to study calcium permeable mechanosensitive channels.

Finally, we develop gene circuits to control the initiation of protein synthesis with inducer molecules in the *E. coli* CFE. Using a lac promotor to synthesize a green fluorescent protein (deGFP), we demonstrate successful induction with Isopropyl β-d-1-thiogalactopyranoside (IPTG). Next, MscL is reconstituted into liposome membranes to

mediate influx of IPTG in response to hypo-osmotic shock. A high ON/OFF ratio of deGFP synthesis post induction is observed when using a gene amplification circuit. A bacterial cytoskeletal protein MreB substituted in place of deGFP is synthesized inside liposomes in response to hypo-osmotic shock. MreB is observed to form ring-like structures on the liposome membrane. Such a system enables control over initiation of protein synthesis in synthetic cells in response to osmotic changes which is important for the study of spatio-temporal evolution of protein functions.

In summary, the results of this dissertation provide advanced tools based on CFE systems for *in vitro* reconstitution of complex biological processes with modularity in design and application.

Chapter 1: Introduction

1.1 Cell biology through bottom-up *in vitro* reconstitution.

Ever since the first cells were observed by Robert Hooke[1], scientists have been fascinated by the sheer complexity of these micron-scale living entities. With the development of advanced experimental techniques, a lot of fundamental characteristics akin to all living cells have been discovered and cell functions such as migration, division, endocytosis, exocytosis, and many others are understood as essential cellular processes. However, the assembly of component molecules and how they overcome energetic and entropic barriers to mediate such macroscale phenomena within the complex design of cells have remained elusive over the years. To address these questions, the field of bottom-up *in vitro* reconstitution has emerged over the years where individual components are assembled under controlled conditions to simulate cellular processes.

Traditional cell biology studies were primarily focused on observations of input-output relationships in cells subjected to changes in their environment. Unlike most engineered systems, such changes in cell behaviors do not seem to follow simple predictable rules but are subjected to variable constraints based on how cells adapt to these changes. This realization led to the use of a top-down experimental approach where individual parts of cells were isolated and probed to identify key molecules mediating different cell functions. More than a billion years of evolution has conferred redundancies in different functional units of cells through self-organization, crosstalk and sustained

feedback mechanisms[2] which enable cells to be robust and adaptive to external and internal stimuli.

Redundancies conferring such robustness in cells hinder the development of fundamental insights into the mechanism of a given cellular process through top-down techniques. Bottom-up reconstitution studies enable distinction between sufficient and necessary biomolecules involved in mediating different cell functions[3,4]. By isolating proteins of interest which are believed to interact in cells, one can identify a minimal system that can reliably carry out a specific function *in vitro*. Moreover, reconstitution of functional units enables control over individual protein concentrations in addition to other experimental parameters that allow for testing and refinement of mechanistic models generated from existing cell biology data. Also, quantitative predictions can be made based on the understanding gained from such *in vitro* reconstitution studies. Additionally, in some cases, reconstitution of certain proteins under a range of conditions can result in an emergent behavior, i.e. unexpected topological and functional behavior of interacting proteins can emerge *in vitro* which cannot be predicted based on their individual functions.

In recent years, bottom-up *in vitro* reconstitution has been immensely successful in understanding complex cellular processes in terms of functions of a set of proteins under specific conditions[4,5]. However, existing techniques of protein isolation and reconstitution are specific to the problem being studied and lack modularity in their use. Also, reconstitution of processes at the complexity and length scale of cells is difficult to achieve. The work presented here is an effort to advance existing tools and address these limitations with the hope of complementing traditional cell biology experiments.

1.2 Power of *in vitro* reconstitution to identify mechanisms of different cell functions.

Since proteins are the workhorses of cells, most reconstitution studies have been associated with the isolation of individual or a set of proteins from cells and probing their functions using biochemical and fluorescence-based assays. In order to maintain homeostasis, cells need a barrier to separate chemical reactions from their immediate surroundings. This barrier is present in the form of a bilayer membrane of lipids which are amphiphilic molecules that allow passive diffusion of small molecules[6]. In both prokaryotic and eukaryotic cells, a wide range of proteins are spatially distributed between the bulk phase (cytoplasm) and the membranes which support active and passive diffusion of molecules embedded in them. Despite this spatial segregation, protein functions are predominantly interdependent and require active interaction between the cytoplasmic proteins (soluble) and their membrane counterparts[7]. In the following subsections, reconstitution strategies for soluble and membrane proteins are discussed with a few selected examples, and key insights into the mechanisms of important cellular processes gained from these studies are presented.

1.2.1 Soluble proteins in bulk and encapsulated volumes

Interactions of soluble proteins in the cell cytoplasm are essential in mediating different processes within cells. Cytoplasmic proteins responsible for carrying out critical cell functions are mostly conserved across different species. The following three case studies present examples of *in vitro* reconstitution systems aimed at understanding the functions of some of these cytoplasmic proteins.

1.2.1.i Studies on actin cytoskeleton

One of the early focuses of reconstitution experiments was carried out with cytoskeleton proteins. It is widely acknowledged that the cytoskeletal proteins play diverse roles in modulating the shape and mechanics of all types of cells. These proteins are tightly regulated by the cell in response to external stimuli and show a wide range of emergent behaviors when reconstituted *in vitro*[8]. Many reconstitution studies have been carried out on the three major cytoskeletal filaments in eukaryotic cells namely actin, microtubules and intermediate filaments. Of these, the most actively remodeled cytoskeletal structure which drives the mechanics of cell migration, endocytosis, exocytosis and cell division is the actin filament network. The observation of muscle contractions *in vitro* in muscle samples supplemented with magnesium and ATP (adenosine tri-phosphate)[9] led to a series of reconstitution studies that aimed to unravel the mechanism of force generation in cells.

Actin polymerizes into long filaments which can bind to a host of proteins that control the extent of filament crosslinking and association with the plasma membrane (actin cortex). Using total internal reflection fluorescence (TIRF) microscopy, the mechanics of filament formation under a range of concentrations could be probed with high resolution and their topology could be studied[10,11]. To investigate the effect of spatial confinement on actin polymerization, several strategies were developed to force actin assembly on engineered patterns on surfaces [12,13]. Patterning of nucleation promotion factors which promote polymerization of actin enabled the study of the dynamics of actin architecture remodeling by different actin-binding proteins[13]. Advanced techniques like

AFM (atomic force microscopy) was also used to probe the effect of external forces on self-assembling actin networks *in vitro*[13]. Further reconstitution studies on the formation of actin cortex were carried out by polymerizing actin in the presence of membrane anchoring proteins on supported lipid bilayers (SLBs)[14–16].

In order to understand the effect of polymerization in confined spaces like cells, actin networks were encapsulated within liposomes[17] (lipid bilayer vesicles) or giant unilamellar vesicles (GUVs)[18]. Actin polymerization on liposomal membranes was shown to be reversibly controlled by the formation of different lipid phases[19] while the rigidity of the membrane seemed to affect the bundling of membrane-associated actin filaments[20]. Depending on filament branching, symmetry breaking was observed in liposomes which was crucial in understanding the dynamics of actin polymerization leading to cell shape changes *in vivo*[21,22]. With modern advances in nanotechnology and microscopy, single molecule resolution in structure of these filaments and networks[23] can be achieved further promoting such bottom-up approaches for deciphering the mechanics of actin and associating proteins in cells. Similar studies have been carried out for other cytoskeletal proteins which are described elsewhere[24–26]. These examples illustrate the power of reconstitution studies to dissect the mechanisms of interacting proteins in cells without the complexities associated with *in vivo* environments.

1.2.1.ii Mechanisms of protein-induced membrane curvature generation.

Another example that has benefitted immensely from *in vitro* reconstitution approaches is membrane trafficking, specifically, membrane curvature generation. Given the wide spectrum of proteins involved during membrane trafficking processes, it is difficult to delineate the function of each protein in cells. One important class of proteins which is

believed to be essential for counteracting membrane tension to induce local curvature is coat proteins[27,28]. A large portion of the current knowledge regarding the functioning of these proteins was derived from bottom-up reconstitution studies.

Coat proteins like clathrin were isolated and reconstituted on liposomes as models for cell-confined geometry with constant membrane tension. ATP was found to be dispensable to the formation of membrane invaginations and vesiculation by clathrin[29] and that it can only deform membranes below certain tension thresholds[30]. Dynamin, which is believed to mediate scission in the later stages of endocytosis[31], caused twisting of lipid tubes and also mediated scission under high longitudinal tension in the presence of guanosine tri-phosphate (GTP)[32]. Other coat proteins like COP-I and COP-II which were identified to be important for trafficking cargos between the endoplasmic reticulum (ER) and the Golgi apparatus, were found to form coats on liposomal membranes with deformations being dependent on membrane tension[33]. Further reconstitution of COP-II proteins on liposomes lead to the formation of beads-on-string-like deformation of membrane which is similar to what is observed in cells[34].

Endosomal sorting complex required for transport (ESCRT) is vital in multivesicular biogenesis and cytokinesis in cells. Given many proteins are associated with its formation, reconstitution experiments were necessary for defining a minimal functional unit[35]. A key finding in understanding the molecular mechanisms of ESCRT polymerization which drives membrane remodeling was obtained from studies of reconstituted ESCRT interaction with SLBs using AFM. This revealed the formation of spring-like regions which are hypothesized to store energy for membrane deformation to be released when triggered[36].

1.2.1.iii Understanding signaling through reconstitution.

Cells adapt in response to external and internal stimuli by cell signaling. Cell signaling is usually coupled with changes in gene expression profile and are tightly regulated. Given the large number of proteins involved in cell signaling, a controlled experimental platform is essential to probe the mechanism of activation and transmission of intracellular signals. One example where understanding such signaling events has physiological and therapeutic relevance is activation of T-cell receptor (TCR) signaling when T-cells interact with other cell membranes[37]. Because of the wide range of ligands that can lead to early activation of T-cells, semi-reconstitution studies have been very useful in probing such events.

Typically, SLBs reconstituted with adhesion proteins and specific ligands are used as model membranes with which T-cells are allowed to interact. Several studies over the years have revealed that signaling is sustained through the formation of clusters of signaling molecules with recruitment of adaptor proteins and movement towards center of cell-SLB contacts[38,39]. Further inhibition of such interactions with different sized nanostructures showed position-dependent signal activation within the cell-SLB contacts[40]. This system served as a powerful platform to probe different parameters of TCR signaling activation such as ligand density, changing contact area and composition of protein clusters[41]. Further attempts were made to reconstitute the adaptor proteins with different domains of the TCR to map out the interaction pathway and develop mathematical models for understanding the enzymatic pathways associated with T-cell activation[42,43].

The above findings illustrate the advantages of *in vitro* reconstitution with lipid bilayer membranes to delineate the complexities associated with cellular processes which require multi-protein interactions.

1.2.2 Study of proteins residing in cell membrane

Cell membrane proteins are primarily responsible for transducing extracellular signals. There are different types of membrane proteins based on their structure, function and the how they associate with their native membranes. Integral membrane proteins span the membrane with domains exposed to both sides of the membrane. Of these, integral membrane proteins of the plasma membrane are the most studied ones due to their vital importance in mediating cellular responses to environmental stimuli. It has been shown that such membrane proteins are less conserved among different species than their soluble counterparts[44]. It is speculated that surface interactions of membrane proteins with the extracellular environment provide pressure for evolving at a much faster rate than cytoplasmic proteins[44]. Therefore, studies on membrane proteins require the ability to probe both solvent-accessible domains to understand the significance of their orientation in native cell membranes. Control over these parameters is difficult to achieve in cells. The following examples illustrate the benefits of *in vitro* reconstitution in identifying minimal units to achieve a specific function and investigating functions of important membrane proteins in isolation.

1.2.2.i Reconstitution of membrane fusion machinery

Membrane fusion is a vital process of all types of cells. Transport of cargo out of a cell is predominantly mediated by such fusion events, such as in the transmission of neuronal signals across the synaptic junction in our central and peripheral nervous systems.

Signaling molecules encapsulated within small liposomes are released from the termini of one neuron and are taken up by the dendrites of another. Release of these molecules is mediated via membrane fusion between the small vesicles and the plasma membrane of cells. Fusion was initially hypothesized to be a several-part process initiating with the mixing of the outer leaflet of small vesicles and the inner leaflet of the plasma membrane[45]. *In vitro* studies on fusion between liposomes and planar lipid bilayers validated this first step of fusion[46]. Subsequent steps involve the formation of a pore in the mixed bilayer followed by mixing of encapsulated components with the cell cytoplasm or the extracellular space.

The discovery of the SNARE complex which is essential for fusion in multi-compartment eukaryotic cells was a result of careful reconstitution studies initiating with the isolation of the Golgi apparatus from Chinese hamster ovary (CHO) cells infected with vesicular stomatitis virus[47,48]. Subsequent studies led to the discovery of multiple proteins associated with the formation of this complex[49]. Ensemble fusion assays were the earliest forms of reconstitution experiments where liposome-liposome fusion was observed using fluorescently labelled lipids to understand the mechanism of fusion with these proteins[50,51]. It was found that a minimal unit comprising of three proteins syntaxin, SNAP-25 and synaptobrevin could mediate fusion between liposomes[52]. Fluorescently tagged lipids were quenched to probe lipid mixing during the docking of liposomes to a planar lipid bilayer and subsequent fusion. It was observed that the probability of lipid mixing was enhanced in the presence of divalent cations[52]. Interestingly, docking of liposomes and lipid mixing was found to be independent of the inclusion of SNAP-25, suggesting its role in the later stages of fusion post assembly of the SNARE complex[53]. Since signal propagation in neurons is sensitive to calcium influx, calcium-sensitive fusion was

reconstituted *in vitro* by the addition of synaptotagmin which is known to control fusion based on calcium concentrations[54].

Further reconstitution studies *in vitro* have succeeded in determining the effect of other proteins known to be associated with the stability and proper functioning of the SNARE complex on membrane fusion[55,56]. Recent single molecule experiments using optical tweezers revealed the energetics and kinetics of SNARE assembly under different conditions[57]. Thus, our understanding of signal transmission across neurons has been significantly enhanced though bottom-up *in vitro* reconstitution experiments.

1.2.2.ii Probing activity of ion channels

Most reconstitution studies with membrane proteins have been primarily aimed at understanding the gating mechanism of different types of ion channels that span the different membranes in cells. Many ion channels in eukaryotic and prokaryotic cells have been identified over the years and reconstituted in lipid bilayer environments. There are four major types of ion channels namely peptide-based, voltage-gated, ligand-gated and mechanosensitive ion channels. Each of these types of channels have been extensively studied in *in vitro* reconstituted setups comprising of a lipid bilayer membrane acting as a substrate for proper folding of these proteins and an electrophysiological setup to probe for ion currents in response to specific stimuli. Peptide-based ion channels are small polypeptides of about 50 amino acids in length which can self-insert into lipid bilayer membranes and form pores allowing exchange of ions. Their reconstitution into membrane substrates serve as good *in vitro* models for studying activity of other ion channels and membrane proteins[58].

Voltage-gated ion channels are mostly found in neurons and muscle cells owing to their ability to initiate action potential to relay information in the form of electrical pulses through the nervous system. Many of these channels have been extensively studied using patch clamp techniques in reconstituted lipid bilayer. Since electrophysiological data based on measurements in cells can contain interference from other ion channels and other membrane proteins, *in vitro* readings of purified ion channels more accurately reflect their voltage-current relationships. Examples include studies on voltage-gated sodium and potassium channels like Nav, KvAP and Shaker[59–61]. By probing different mutants, the movement of the voltage-sensitive domain leading to increase or decrease in channel conductance was identified which paved the way for the development of fast voltage-sensitive fluorescent biosensors to optically record action potentials in neurons with high temporal and spatial resolution[62]. Similar studies have been carried out with ligand-gated ion channels like hERG and GABAA receptors[63] to determine the effect of ligand concentrations, clustering and specificity on ion channel activity.

Mechanosensitive ion channels were first identified in bacteria[64] and identification of several mammalian counterparts have renewed interests in investigating their physiological relevance in recent years[65]. These channels are hypothesized to be solely activated in response to elevated membrane tension. This presents a major bottleneck in probing their activity in cells owing to the close interaction between the cytoskeleton and the plasma membrane in eukaryotic cells. *In vitro* reconstitution into liposomal membranes allows for direct electrophysiological measurements as a function of applied tension to monitor channel activation. Mechanosensitive channel of large inductance (MscL) is the most extensively characterized bacterial channels using this approach[64,66]. The activation properties of various mutant MscL was measured *in vitro* to better

understand MscL gating mechanism[67]. Mammalian mechanosensitive channels like TREK and TRAAK[68] (specific to potassium flux) and Piezo1 and Piezo2 (cation conducting channels)[69] were reconstituted into lipid membranes. Osmotic gradient induced changes in membrane tension could mediate Piezo1 activity when reconstituted in planar lipid bilayers[70]. Shear stress-induced activation of Piezo channels have been speculated and, in some cases (e.g., Piezo1) demonstrated in cells subjected to fluid shear stresses[71]. However, true mechanosensation by membrane tension can only be verified with reconstituted systems in the absence of other interacting proteins[72].

Despite technological advances in microscopy, electrophysiology and other tools to probe membrane protein functionality, study of membrane proteins is limited to the above-mentioned examples. This is because of the lack of significant developments in traditional reconstitution approaches to accommodate for all other types of membrane proteins. Few attempts have been made to study membrane receptors like G-protein coupled receptors (GPCRs)[73,74], TCR[75,76] and other signaling receptors. However, membrane proteins whose function depend on interactions with molecular chaperones and other proteins cannot be easily reconstituted using conventional techniques. This can be attributed to the specificity of these approaches to each type of proteins and their inability to simultaneously reconstitute multiple membrane proteins.

In the following section, the underlying principles of conventional *in vitro* reconstitution are presented and major challenges of membrane protein reconstitution are discussed.

1.3 Conventional techniques of *in vitro* reconstitution.

A reconstitution system aims to isolate the function of one or a set of proteins in a controlled environment. Since many cellular processes are regulated simultaneously, reducing the complexity of these interactions is a primary motivation for reconstitution studies. Towards this goal, the first task is to ensure the extraction of the protein of interest with sufficient purity to enable detection using available techniques. This is achieved through standard protein purification approaches which are customized based on the physical and chemical properties of individual proteins. Usually for cytoplasmic proteins with little or no membrane interaction, purification is the only step required for effective reconstitution. However, when working with proteins that need a membrane for activation or integral membrane proteins, providing a cell membrane-like substrate is an important consideration for successful reconstitution. Given the propensity of lipid molecules to spontaneously self-assemble into bilayers in aqueous solutions, artificial lipid bilayer membranes are generated using extracted or pure lipids to provide a scaffold for functional reconstitution of purified membrane proteins. This is challenging to achieve for complex membrane proteins and is the basis for the work carried out in this thesis.

1.3.1 Protein purification

The following sub-sections describe the standard techniques of isolation of recombinant proteins of interest (POI) from cells.

1.3.1.i Soluble proteins

Purification of almost all soluble proteins are carried out in bacteria because of its fast growth rate and high yield of synthesized protein. The recombinant POI is cloned into an expression vector with an appropriate affinity tag. Bacterial expression vectors mostly

have a T7 promotor for transcription of the gene of interest while some use the lac operon. Induction of protein synthesis is carried out by addition of IPTG. To prevent degradation of the POI by native proteases, protease inhibitors are added to the lysis buffer depending on the type of POI. Cell lysis is usually achieved by sonication, chemical lysis, bead-based mechanical agitation or homogenization under osmotic shock. A range of chromatography techniques are available for separating out the POI from the rest of the lysate. In some cases, acid-based purification based on pH change can also be achieved if the POI has pH dependent solubility. For most soluble proteins, the POI can be used immediately following the separation step. For affinity-based separation, the peptide tags used to create the recombinant POI can be cleaved depending on downstream applications and removed from solution by dialysis. Since bacterial codon usage for translation is different from eukaryotic cells, different strains of bacteria have been genetically engineered to synthesize proteins from other organisms. Soluble proteins purified in this manner can be studied in bulk or confined reactions.

1.3.1.ii Membrane proteins

Most membrane proteins studied to date have been purified in bacterial cells. The procedure is quite similar to soluble proteins for the most part. However, since membrane proteins have hydrophobic residues that can affect protein folding upon exposure to aqueous environment, care must be taken to solubilize the POI post cell-lysis. A standard technique is to add a detergent to the lysis buffer at concentrations below their critical micelle concentration to shield the hydrophobic region of the POI and maintain proper folding. Depending on the stability of the POI, different types of detergents are used which

are primarily non-ionic to prevent denaturation by strong electrostatic interactions. Following lysis, standard chromatographic techniques can be used to isolate the POI[77].

In case of large ion channels like Piezo1 from mammalian hosts, purification is achieved by expressing the protein in mammalian cells with high metabolic activities like HEK293 (human embryonic kidney) cells[78]. In such cases, the POI is cloned into an expression vector containing a virus-based promotor that can induce overexpression in these cells. Cells transfected to express the POI are lysed mechanically, and the POI is extracted with moderate non-ionic detergents using similar strategies as with bacterial protein purification. Other types of membrane proteins like GPCRs are purified in different hosts including yeasts, insect cells and plant cells. The inherent complexity of over-expressing membrane proteins lies in their trafficking to the host membrane upon synthesis. When such localization is not spontaneous, inclusion bodies can form at high

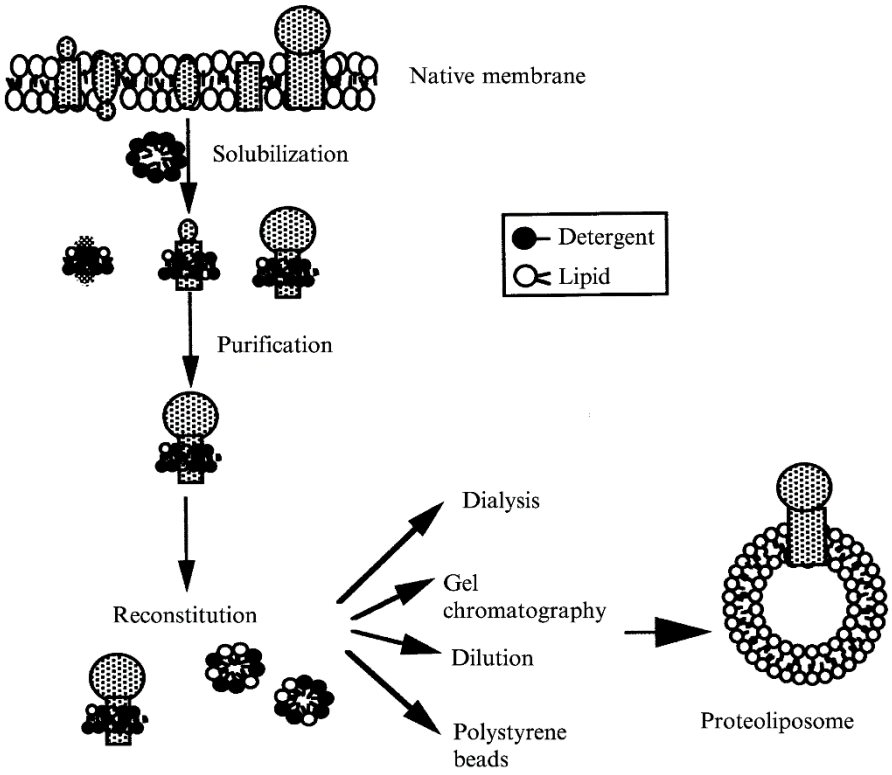

Figure 1.1: Standard procedure for the purification and reconstitution of membrane proteins[77].

concentrations of the POI[79]. Comparative studies have shown the importance of choosing the right host for expressing different types of membrane proteins[80]. To study the native structure and function of specific membrane proteins in mammalian cells, native cell membrane vesicles can be produced in the form of giant plasma membrane vesicles (GPMVs) by inducing blebbing which can then be fused with an artificial lipid bilayer[81].

1.3.2 Membrane mimics for reconstitution of membrane proteins

In order to probe the functionality of membrane proteins isolated from cells, it is important to ensure a physical and chemical environment that is similar to cell membranes. Since lipids are known to form bilayer membranes of all membrane-bound organelles in cells[82], self-assembled lipid bilayers have been the common choice of substrates for studying membrane proteins *in vitro.* Two different types of lipid environments are typically used in reconstitution experiments. The first is the use of lipids extracted from different natural sources like chicken egg or *E. coli* membranes. These lipid extracts contain a mixture of many different types of lipid headgroups with varying chain lengths and packing densities which allow for mimicking the heterogeneity of regular cell membranes around reconstituted membrane proteins. Alternatively, pure lipids with specific headgroups and chain lengths are used to form artificial lipid bilayer membranes where individual components can be altered to investigate protein-lipid interactions. In some cases, binary or tertiary mixtures of these pure lipids are also desirable to impart certain chemical properties like charge and membrane fluidity to these self-assembled bilayers.

Since membrane proteins are usually purified with detergents in aqueous solutions, their transfer to the lipid membranes of liposomes is achieved by incubating the solubilized protein solution with small preformed liposomes. Detergents can create pores

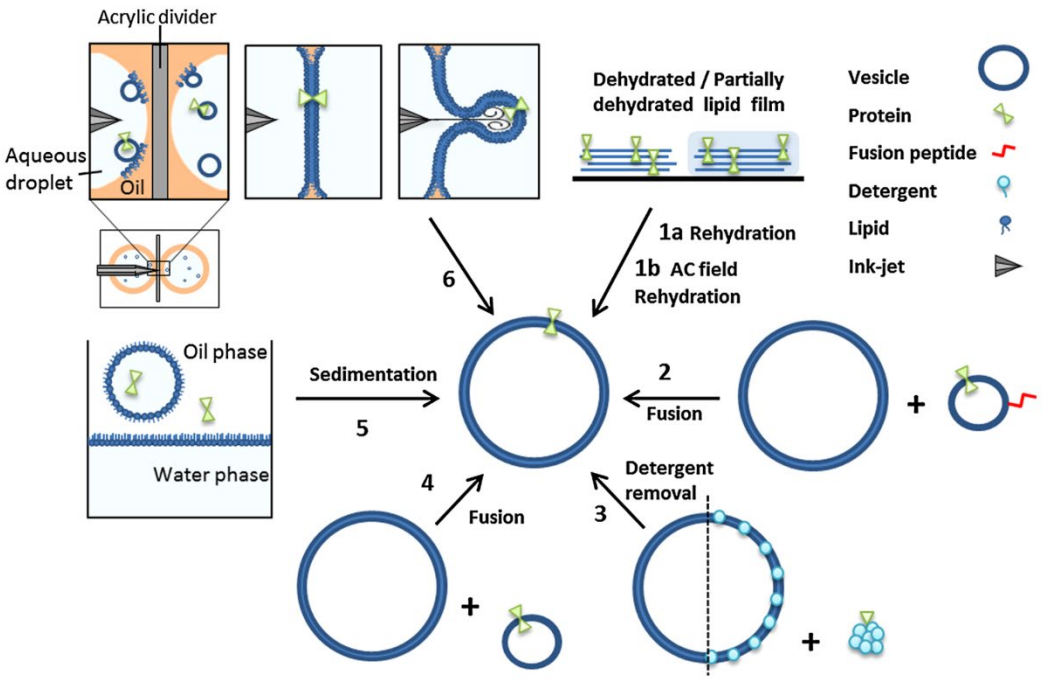

Figure 1.2: Different techniques of reconstitution of membrane proteins in liposomes[83].

in lipid bilayers at certain concentrations which is beneficial for the incorporation of the membrane proteins. To stabilize the bilayers post membrane insertion, the detergent is slowly removed from the solution by dialysis or using adsorptive substrates like bio-beads which can sequester detergents very effectively[83]. These proteoliposomes can then be fused with larger liposomes using charge-based[46] or peptide/DNA[84]-mediated vesicle fusion, for patch clamp studies or dried on glass for subsequent rehydration or electroformation to generate large lipid bilayer vesicles[85].

Another membrane model which is very popular with fluorescence microscopic techniques is the generation of supported lipid bilayers (SLBs)[86]. Small proteoliposomes are allowed to interact with a hydrophilic surface like glass/mica which causes rupture and results in the formation of a planar lipid bilayer on the surface. Other approaches for the generation of supported lipid bilayers include Langmuir Blodgett deposition, peptide-based fusion and a combined technique[87]. These SLBs are great models for studying

peripheral membrane proteins and small transmembrane proteins. Reconstitution of proteins in these bilayers along with advanced microscopic techniques allow for the measurement of diffusion rates, complex formation, clustering and oligomerization states under different experimental conditions.

Vertical planar lipid bilayers are yet another class of membrane models which have been used extensively to reconstitute and study ion channels and porins[88,89]. Earlier techniques used the Montal Mueller method where a small orifice is created in a partition between aqueous solutions with preformed lipid monolayers resulting in a vertical lipid bilayer where membrane proteins can be inserted via fusion of proteoliposomes or detergent-mediated reconstitution[88]. In recent years, a variant of the approach using droplets was developed (droplet interface bilayer, DIB)[90] and several types of ion channels studied using droplet-immersed electrodes[91,92]. Another common method for reconstitution of membrane proteins is in lipid nanodiscs[93] and DNA nano-barrels[94] which are nanoscale bilayer-like structures that can embed few membrane proteins in them allowing structural and functional studies of membrane proteins and their oligomeric states.

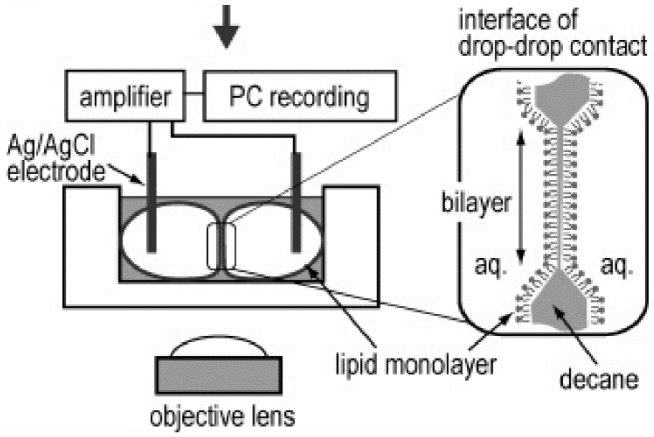

Figure 1.3: A typical droplet interface planar lipid bilayer setup with electrodes for single channel recordings of reconstituted ion channels[90].

1.3.3 Major challenges with membrane protein reconstitution

Despite the tenacious process of protein purification, isolation of soluble proteins in appropriate buffers to enhance stability serves as a good approach for dissecting complex cellular interactions by sequential addition of individual components. While a host of biochemical and mechanical assays have been developed to achieve the same for membrane proteins, several limitations remain. For instance, reconstitution of membrane proteins in liposomes is non-trivial and requires the use of detergents which can affect subsequent protein interaction if not properly removed. Past studies have shown that depending on the properties of detergents, residual amounts can be present in the final membrane which can affect the permeability and membrane integrity of the liposomes[95,96]. Methods like rehydration and electroformation of dried proteoliposome films to reconstitute membrane proteins in large vesicles do not allow for uniformity in protein orientation which is desirable for probing structural and functional roles of the intracellular and extracellular domains of proteins involved in signaling[97,98].

In the case of SLBs, reconstituting integral membrane proteins with large extracellular domains is not desirable owing to the small water gap between the lipid bilayer and the substrate which can hinder function and diffusion[86]. Spontaneous fusion of proteoliposomes or detergent-based insertion of proteins in DIBs present the same problem of orientation where directional probing of functionality of ion channels in response to ligand or voltage gradients is difficult to achieve. Apart from technical considerations, purification and isolation of toxic proteins or complex proteins with multiple transmembrane and large extracellular domains is challenging. Further purification of loss of function mutants of these proteins may not be possible due to their

inhibitory effects on cell growth in bacterial or mammalian cultures. Finally, most studies of membrane proteins have been in isolation to characterize their functions *in vitro*. But, in cells, most membrane proteins interact with other proteins and form oligomeric complexes to mediate cell-function. In order to study protein-protein interactions and formation of heteromeric complexes, simultaneous or time dependent reconstitution of several membrane proteins is desired. This would be extremely difficult if not impossible with the traditional techniques mentioned before.

In the following sections, I describe cell-free protein synthesis as a promising approach to reconstitute a wide range of proteins while alleviating some of the limitations discussed earlier.

1.4 Emergence of *in vitro* gene expression and cell-like mimics as tools for bottom-up *in vitro* reconstitution

An alternative to extracting proteins from cells after induction of protein production is *in vitro* synthesis of the protein of interest for reconstitution studies. It was discovered in the 1950's that cytoplasmic extracts from bacteria[99], human and rabbit reticulocytes[100], rat liver cells[101], ascites cells[102] and wheat germ cells[103] had the potency to carry out protein synthesis in the presence of energy molecules like ATP and GTP in a test tube. The first studies with these extracts were aimed at understanding the genetic code and how amino acids are incorporated into peptide chains to form different proteins[104]. Pioneering work was carried out in subsequent years to synthesize proteins from exogenously added mRNAs in these extracts[105]. Significant advances in improving the efficiency of these translation systems and the discovery of strong phage promotors that could sustain

simultaneous *in vitro* transcription from added DNA[106] led to the development of powerful modern cell-free expression (CFE) systems.

Given the versatility of these systems, it is now possible to synthesize a host of proteins within hours in contrast to purifying them from cells. Also, multiple supplements like molecular chaperones, membrane compartments and radioisotope labels can be added and desired post-translational modifications achieved based on the protein of interest. The range of application of CFE systems has increased over the years[107] and this dissertation extends the utility of CFE for *in vitro* reconstitution studies. The following sections discuss the relevance of CFE to bottom-up *in vitro* reconstitution and lay down the foundations behind the work presented in this thesis.

1.4.1 Coupling synthesis with reconstitution: Cell-free expression systems

CFE systems are cell extracts containing ribosomes, transcription factors and aminoacyl synthetases supplemented with charged nucleotides, an amino acid mixture and an energy regeneration mix to carry out protein synthesis outside cells. The modularity of CFE system allows expression of multiple proteins simultaneously from recombinant plasmid DNA within a few hours. Therefore, it is ideally suited for reconstitution of multiple proteins without the need for more purification steps. In case of soluble proteins, non-specific interactions with existing proteins in the CFE can result in undesirable artifacts. One can avoid such interactions by using a protein synthesis using recombinant elements (PURE) system[108] where the transcription and translation factors for protein synthesis are individually purified and used at known concentrations in the absence of other lysate proteins. This has only been possible for *E. coli* CFE so far. While higher concentrations of soluble proteins can be obtained from standard purification, temporal evolution of

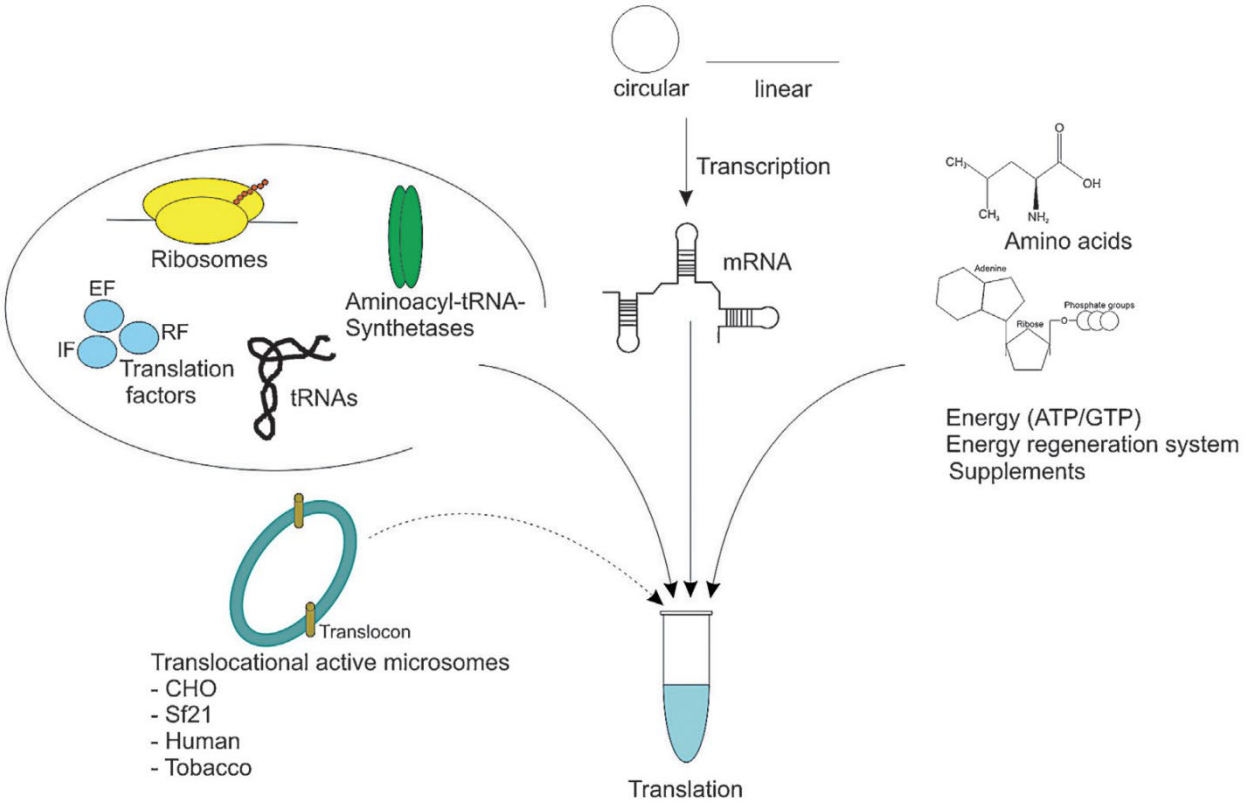

Figure 1.4: Schematic depicting the different constituents of an assembled cell-free reaction coupling transcription with translation[113].

protein-protein interactions as a function of its concentration and synthesis can only be attained using CFE setups. In the case of membrane proteins, CFE offers distinct advantages over conventional reconstitution approaches. Most of the challenges discussed in the previous section can be addressed when using CFE. Insertion of membrane proteins into lipid bilayer substrates like liposomes and planar lipid bilayers can be achieved in the absence of detergents thus alleviating the problems associated with detergent-mediated reconstitution[109,110]. Microsomes from different organelle membranes that are present in cell-free lysates can also be used as supplements for successful insertion of membrane proteins during synthesis[110–112].

Further, synthesis of toxic proteins and loss-of-function mutants can be easily carried out and complex or larger proteins can be synthesized with strong phage

polymerases in different types of lysates. A comparison of the benefits of using different sources of CFE lysates developed till date, is presented in previous review articles[107,113]. Past studies have shown expression and functional reconstitution of different kinds of membrane proteins such as ion channels[114,115], mechanosensitive channels[116,117], G protein-coupled receptors[118], enzymes for lipid synthesis[119,120], olfactory receptors[121], gap junction proteins[122], proton pumps[123] and transporter proteins[124,125]. Also, it is possible to incorporate post translational modifications in proteins using eukaryotic CFE[111].

Despite these advantages, proper design of engineered systems is essential to leverage the full potential of CFE-based reconstitution studies. These systems should have the necessary parameters to control conditions which can probe protein functionality *in vitro* to better understand its role *in vivo.* In the following final sub-section, a model for simulating protein functions in a cell-like confinement is discussed which forms the basis of the work described in later chapters.

1.4.2 Development of synthetic cells for mimicking cellular processes

While studies on microscopic effects of local stimuli on reconstituted proteins is important from a biophysics point of view, it is equally desirable to see the propagation of such an effect at a macroscopic level (i.e. at a cellular level) to better understand large-scale dynamics or possible emergent behavior. Figure 1.5 shows the span of both complexity and length scale over which bottom-up *in vitro* reconstitution has evolved in recent years[5]. In this regard, the development of synthetic cells has been influential to simulate both cellular and population level complexities *in vitro*[126]*.* In the context of the work presented here, synthetic cells are used to denote liposomes encapsulating CFE systems capable of synthesizing desired proteins of interest. By developing such a platform where multiple

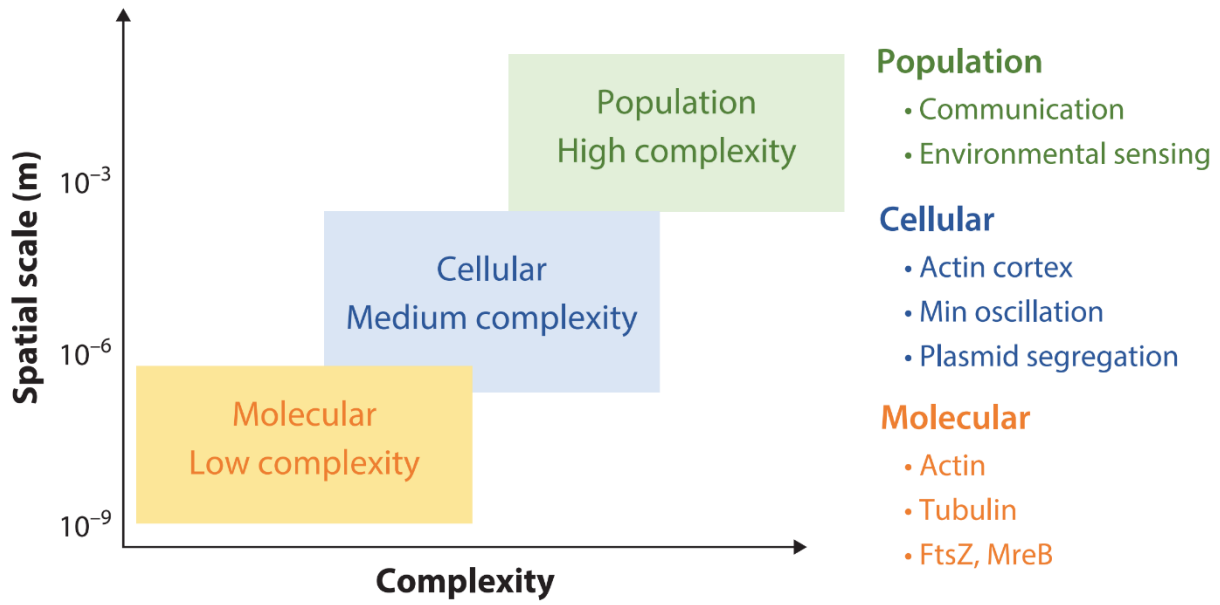

Figure 1.5: **Range of complexity and length scale involved in *in vitro* reconstitution studies[5]**.

proteins can be synthesized from encapsulated DNA, proteins with diverse functions can be simultaneously reconstituted. Thus, with appropriate choice of proteins, desirable physical and chemical properties can be imparted to synthetic cells. This will allow the coupling of function of our protein of interest to the desirable property for ease of detection and analysis. Because multiple variants of proteins can be easily expressed by tweaking their genes, a library of desirable mutants can be screened in such synthetic cell systems within a few hours as compared to days for cell-based approaches. Though generation of synthetic cells is challenging and is a topic of ongoing research, past studies have employed different techniques to achieve reconstitution at cellular scales. One such study showed the synthesis of lipids from cell-free expressed enzymes encapsulated within liposomes[127]. Another work demonstrated communication between and within synthetic cells by employing gene regulatory networks in CFE systems[128]. To explore the possibility of a self-catalyzed enzymatic reaction with RNA, functional ribosomes were synthesized inside synthetic cells[129]. Further extrapolation of similar work led to development of

synthetic cells capable of self-replicating DNA by using encoded proteins[130]. These studies illustrate the potential of CFE to reconstitute complex cell-like molecular interactions *in vitro* through the use of synthetic cell models. Such advanced engineering platforms are exploited in this work to study proteins, with an emphasis on membrane proteins, involved in different cellular phenomena.

1.5 Dissertation outline

While *in vitro* reconstitution studies have been extremely important in unravelling the complexities of cell biology, work with membrane proteins is particularly challenging and limited by the type of proteins that can be reconstituted using conventional approaches. There remains a need for better control over functional reconstitution while extending experimental parameters for probing *in vitro* response of proteins subjected to external stimuli. We explore the potential of cell-free systems to alleviate existing limitations by considering different biologically relevant problems as test cases in the following chapters. The goal of this dissertation is to provide standardized tools for investigating different biological phenomena. In Chapter 2, I will describe the advantages of using a HeLa CFE system for reconstituting membrane proteins with controlled orientation of insertion. By doing so, the components of an important protein complex present in the nuclear membrane, is studied. Next, using an *E. coli* CFE system, a mechanosensitive channel and a fluorescent calcium biosensor are simultaneously reconstituted in liposomes in Chapter 3. This allows the creation of a synthetic cell which can couple calcium sensing to changes in membrane tension. In Chapter 4, I demonstrate the modularity of the same *E. coli* CFE system in building genetic circuits capable of simulating cell-like signaling in synthetic cells. This illustrates the possibility of employing

gene regulatory pathways in CFE systems for time-dependent reconstitution of multiple proteins. Finally, the important findings from each chapter will be summarized and possible applications of these engineered platforms will be presented in Chapter 5 with preliminary data supporting the feasibility of those applications.

Chapter 2: Functional Reconstitution of Cell-Free Expressed Nuclear Membrane Proteins in Supported Lipid Bilayers

* Part of this chapter has been published in Majumder et al. *Journal of Cell Science*, 2019[131]. The author implemented the design platform, carried out the experiments presented and generated all figures in the manuscript. All SUN protein plasmids were provided by G.W. Gant Luxton.

2.1 Introduction

2.1.1 Morphology of the nuclear membrane in eukaryotic cells

Eukaryotic cells are defined by the presence of a genome-containing nucleus, the boundary of which is delineated by the nuclear envelope (NE), a specialized subdomain of the endoplasmic reticulum (ER)[132]. The NE consists of concentric inner and outer nuclear membranes (INM and ONM, respectively) separated by a ~30–50 nm perinuclear space that is contiguous with the ER lumen[133]. While the ONM is an extension of the ER, a unique subset of proteins resides in the INM that interact with the nuclear lamina and chromatin within the nucleoplasm[134]. Fusion between the INM and ONM creates numerous aqueous channels throughout the NE that are occupied by nuclear pore complexes (NPCs), which are the primary sites of molecular exchange between the cytoplasm and nucleoplasm[135,136]. However, mechanical forces generated by the cytoskeleton within the cytoplasm can also be sensed and transmitted across the NE and into the nucleoplasm by LINC complexes[137,138]. These evolutionarily conserved NE-spanning molecular bridges mediate several fundamental cellular processes, including

DNA damage repair, meiotic chromosome pairing, mechanoregulation of gene expression and nuclear positioning[137,139,140]. Consistent with their central role in cellular function is a growing list of genetic mutations in LINC complex proteins associated with human diseases such as aging-related hearing loss, ataxia and muscular dystrophy[141,142].

LINC complexes are formed by the transluminal interactions of the ONM Klarsicht/ANC-1/SYNE homology (KASH) proteins and the INM Sad1/UNC-84 (SUN) proteins[143]. The divergent cytoskeletal-binding cytoplasmic domain of KASH proteins largely consists of spectrin repeats or coiled-coils (CCs)[139,144], while their C-termini contain the conserved nuclear envelope targeting KASH domain composed of a transmembrane domain (TMD) followed by the ~10–32-residue luminal KASH peptide[145]. Within the perinuclear space, the C-terminal SUN domain of SUN proteins interacts with KASH peptides[146], whereas their divergent N-termini reside within the nucleoplasm where they interact with A-type lamins, chromatin, as well as other INM proteins[147]. Mammals encode six KASH proteins [nesprins 1–4 (also known as SYNE1–4) lymphocyte restricted membrane protein and KASH5] and five SUN proteins (SUN1–5)[134,139]. The expression of SUN3–5 is testis specific and their ability to assemble into functional LINC complexes remains unclear[148]. In contrast, SUN1 and SUN2 are both widely expressed in somatic cells and interact with all known KASH proteins[149,150].

2.1.2 Structure of LINC complex and role of SUN proteins

Groundbreaking *in vitro* studies have provided critical insights into the mechanism of LINC complex assembly. In key papers describing its crystal structure, the Kutay, Schwartz and Wang laboratories have shown that SUN2 homo-trimerizes and that a short preceding CC is necessary and sufficient for homo-oligomerization[148,151]. In addition, Kutay and

Schwartz revealed that SUN2 homo-oligomerization was required for KASH peptide binding, which further stabilized the homotrimer[148]. In an extension of this earlier work, the Feng laboratory suggested that the CC-containing region of the SUN2 luminal domain should be viewed as a pair of CCs that potentially influence the monomer-trimer equilibrium of SUN2[152]. Using fluorescence fluctuation spectroscopy, an imaging-based technique that enables the quantification of protein oligomerization *in vivo*[153], it was recently confirmed that the luminal domain of SUN2 homo-trimerizes within the NE of living cells[154]. While SUN2 and SUN1 share a high level of sequence similarity (~65% identity between mouse SUN2 and SUN1), display similar affinity for the nesprin-2 KASH peptide[150] and are involved in several redundant cellular functions (i.e. DNA damage repair[155] and sub-synaptic nuclear anchorage in skeletal muscle[156]), we found that the homo-oligomerization of the SUN1 luminal domain within the NE was not limited to the formation of a homo-trimer[154].

Taken together, these results suggest that LINC complexes containing SUN1 assemble via a distinct mechanism from those containing SUN2, which may explain the specific requirement for SUN1 during meiotic chromosome pairing[141,157] as well as in the assembly of NPCs and their distribution throughout the NE[158–160]. To date, our understanding of the mechanisms underlying the differential assembly and function of SUN1- and SUN2-containing LINC complexes remains limited by the fact that the results described above were all generated using soluble fragments of the luminal domains of SUN1 and SUN2, not full-length SUN proteins within the context of a lipid bilayer. This was primarily due to the difficulty of probing SUN protein interactions in the perinuclear space and isolating membrane embedded proteins for structural studies. To begin to overcome this limitation, I describe here the development of artificial nuclear membranes

(ANMs) using a mammalian cell-free expression (CFE) in the presence of supported lipid bilayers with excess membrane reservoirs (SUPER templates). SUPER templates were previously demonstrated to contain lipid bilayer membranes on silica beads which are loosely bound and can shed off in response to shear or contact forces[161]. Such supported bilayers are ideal for the reconstitution of integral membrane proteins given the significant spacing between the bilayer and the silica substrate. Multiple membrane tethers can be pulled from these SUPER templates demonstrating the flexibility and weak membrane-substrate coupling of these supported lipid bilayers. The combination of CFE and SUPER templates serve as a simple bottom-up synthetic biology platform for the rapid reconstitution and mechanistic dissection of LINC complex assembly using full-length SUN proteins.

2.2 Materials and Methods

2.2.1 Reagents

Restriction enzymes were either purchased from New England Biolabs (NEB, Ipswich, MA) or Promega (Madison, WI). Phusion DNA polymerase, T4 DNA ligase, and PNK were also purchased from NEB. All other chemicals were from Sigma-Aldrich (St Louis, MI) unless otherwise specified. Wizard SV Gel and PCR Clean-Up System was from Promega. All lipids were purchased from Avanti Polar Lipids Inc. (Alabaster, AL) in chloroform stock solutions. Anti-EGFP antibody (ab6556) was purchased from Abcam (Cambridge, MA) and used at 1:500 for western blotting. DiI was purchased from Thermo Fisher Scientific (Waltham, MA) and used at 1:20. Anti-Penta-His-AF647 antibody was purchased from QIAGEN (cat. no. 35310, Hilden, Germany) and used at 1:60 for immunofluorescence. Cell culture HeLa S3 cells obtained from the ATCC (Manassas, VA)

were cultured using standard sterile technique in SMEM supplemented with 5% bovine calf serum (Sigma-Aldrich), 0.5% penicillin/streptomycin, 10 mM HEPES (pH 7.4) and 0.5% glutamax (ThermoFischer Scientific).

2.2.2 CFE lysate generation

HeLa S3 cells were cultured in a flat bottom bell jar with rotating flaps using a magnetic stirrer until reaching a density of ~6×106 cells/ml. Harvested cells were washed three times with washing buffer (35 mM HEPES pH 7.5, 140 mM NaCl and 11 mM glucose) and once with extraction buffer (20 mM HEPES pH 7.5, 45 mM potassium acetate, 45 mM potassium chloride, 1.8 mM magnesium acetate, 1 mM DTT). The washed cells were then resuspended in 1 ml of extraction buffer before being lysed in a BeadBug Homogenizer (Benchmark Scientific, Edison, NJ) using 2 ml tubes filled partially with 0.1 mm titanium beads. To remove debris, nuclei, and most organelles, the resulting lysate was centrifuged three times at 16,000 g, after which 50 µl aliquots of the cleared lysate were flash-frozen in liquid nitrogen and stored at -80°C for future use. CFE reactions CFE reactions were performed by mixing 9 µl of the CFE lysate, 2.25 µl Mix 1 (27.6 mM magnesium acetate, 168 mM HEPES pH 7.5) and 2.7 µl GADD34 (final concentration of 310 nM) in a 1.5 ml microcentrifuge tube, which was then incubated at 32°C for 10 min. Thereafter, 2.25 µl Mix 2 (12.5 mM ATP, 8.36 mM GTP, 8.36 mM CTP, 8.36 mM UTP, 200 mM creatine phosphate, 7.8 mM HEPES pH 7.5, 0.6 mg/ml creatine kinase, 0.3 mM amino acid mixture, 5 mM spermidine, and 44.4 mM DTT), 5 nM of plasmid DNA and 1.8 µl T7 RNA polymerase (final concentration of 450 nM) were added to the CFE reaction followed by vortexing. All supplements for the CFE reaction were stored at -80°C for future use.

2.2.3 ANM generation

SUPER templates were generated as previously described (Neumann et al., 2013). Briefly, SUVs composed of 45% 1,2-dioleoyl-sn-glycero-3-phosphatidylcholine (DOPC), 27% 1,2-dioleoyl-sn-glycero-3-phosphoethanolamine (DOPE), 9% 1,2-dioleoyl-sn-glycero-3-phospho-Lserine (sodium salt) (DOPS), 2.2% L-α-phosphatidic acid (egg, chicken) (sodium salt) (Egg-PA), and 16.8% cholesterol were prepared by extrusion in milli-Q water through a 100 nm extruder (T&T Scientific, Knoxville, TN) and then fused with 5 μm silica beads (Bangs Laboratories, Fischers, IN) in the presence of 1 M NaCl. The resulting SUPER template beads were washed with milli-Q water twice and then resuspended in 30 μl of milli-Q water at a final concentration of ~9.6×106 beads/ml, 2 μl of which were then added to a CFE reaction and incubated for 8 h at 32°C.

2.2.4 Ultracentrifugation of microsomes

Microsomes were observed using a glibencamide based ER tracker with BODIPY probe (Thermo Fisher Scientific) (Ex:561 nm). To visualize microsomes in HeLa lysate, 1 μM dye was directly added to the cell-free reaction mixture and incubated at room temperature for 10 minutes. A benchtop airfuge (Beckman Coulter) with 175 μL open top plastic tubes was used to spin down the microsomes from the lysate. 20 μL reaction was diluted to 30μL with the buffer used for extracting the HeLa lysate[162] and 1M Urea. The diluted sample was spun at 120,000-130,000 g for 10 minutes. 20 μL of the supernatant was pipetted out and imaged or used for western blot analysis. The pellet was resuspended in the remaining 10 μL buffer for further analysis.

2.2.5 DNA constructs

The His_6–GST–EGFP pET28 construct was a kind gift from Michael Jewet (Northwestern University, Evanston, IL). A previously described EGFP tagged mouse SUN1FL construct (EGFP–SUN1FL)[150,163] was used as a template for the generation of the SUN1 constructs used in this study. Initially, SUN1FL was PCR amplified from EGFP–SUN1FL using the primers SUN1FL-Forward (F) and SUN1FL-Reverse (R), which contain 5′ EcoRI and SalI cut sites, respectively (primer sequences are available in the SI section on journal page [REF]). The PCR product was purified and digested alongside pT7CFE1-Chis (ThermoFischer Scientific) with EcoRI and SalI. Following gel purification, the digested PCR product and plasmid were ligated together to create SUN1FL–His_6. Unfortunately, an unwanted stop codon was found between SUN1FL and the His_6 tag. We removed this stop codon by PCR using the primers SUN1FL/ΔSTOP-F and SUN1FL/ΔSTOP-R and subsequent kinase, ligase, DpnI (KLD) treatment where 2 µl of the PCR product was treated with T4 ligase, T4 polynucleotide kinase (PNK) and DpnI in T4 ligase buffer in a 20 µl reaction for 20 min at room temperature. To generate EGFP–SUN1FL–His_6, EGFP was PCR amplified from EGFP–SUN1FL using the primers EGFP-F and EGFP-R, both of which contain 5′ EcoRI cut sites. Following digestion with EcoRI, both the PCR product and SUN1FL–His_6 were gel purified and ligated together to create EGFP–SUN1FL-His_6. EGFP–SUN1ND–His_6 was made by PCR amplifying the SUN1ND using the primers EGFP-SUN1ND-F and EGFP-SUN1ND-F, which contain 5′ HindIII and KpnI cut sites, respectively.

The resulting PCR product was purified and digested alongside pT7CFE1-Chis with HindIII and KpnI, both of which were gel purified, and ligated together to create EGFP–SUN1ND–His_6. EGFP–SUN1LD–His_6 was generated by PCR amplification using the primers EGFP-SUN1LD-His_6-F and EGFP-SUN1LD-His_6-R followed by purification

and KLD treatment. EGFP–SUN11-364–His_6 and EGFP–SUN11-232–His_6 were generated similarly. While the same F primer, SUN1FL/ΔSTOP-F, was used for both constructs, the R primers used to create EGFP–SUN11-364–His_6 and EGFP–SUN11-232–His_6 were EGFPSUN11-364-His_6-R and EGFP-SUN11-364-His_6-R, respectively. A previously described EGFP-tagged mouse SUN2FL construct (EGFP–SUN2FL) (Luxton et al., 2010; Östlund et al., 2009) was used as a template for the generation of the SUN2 constructs used in this study. EGFP–SUN2FL–His_6 was created in an analogous manner to EGFP–SUN1FL–His_6. We first made SUN2FL–His_6 using the primers SUN2FL-F and SUN2FL-R, which respectively contain 5′ EcoRI and XhoI cut sites, to PCR amplify SUN2FL from EGFP–SUN2FL.

The resulting PCR product and pT7CFEC-His_6 were both digested with EcoRI and XhoI, subsequently gel purified, and then ligated together to create SUN2FL–His_6. Again, an unwanted stop codon was found between SUN2FL and the His_6 tag, which was removed by PCR using the primers SUN2FL/ΔSTOP-F and SUN2FL/ΔSTOP-R and subsequent KLD treatment. As described above, EGFP was PCR amplified from EGFP–SUN1FL using the primers EGFP-F and EGFP-R and EcoRI digested alongside SUN2FL–His_6, both of which were gel purified and ligated together to form EGFP–SUN2FL–His_6. EGFP–SUN2ND–His_6 and EGFP–SUN2LD–His_6 were made by PCR amplification using the respective primer pairs EGFP-SUN2ND-His_6-F/EGFP-SUN2ND-His_6-R and EGFP-SUN2LD-His_6-/EGFP-SUN2LD-His_6-R followed by purification and KLD treatment. EGFP–SUN21-131–His_6 was made by PCR amplification using the primers SUN2FL/ΔSTOP-F and EGFP-SUN21-131-His_6-R, the product of which was purified and subjected to KLD treatment.

2.2.6 Protein purification

GST-tagged T7 RNA polymerase and truncated GADD34 were expressed in BL21 DE3 strain *E. coli* and purified using standard glutathione-based affinity chromatography as previously described[164]. The His_6–GST–EGFP construct was transformed into a BL21 DE3 *E. coli* strain. A 1 l liquid culture was inoculated with a single colony and induced with IPTG when the bacteria reached a concentration of an optical density at 600 nm of 0.6. Following 4 h of growth at 37°C, cells were harvested at 10,000 g for 15 min. The resulting cell pellet was then resuspended in 40 ml lysis buffer (20 mM HEPES pH 7.5, 200 mM NaCl, 1 mM DTT, 5% glycerol, 5 mM EDTA) supplemented with a complete Protease Inhibitor Cocktail tablet (Roche, Basel, Switzerland). Next, cells were lysed by sonication (50% duty cycle for 5 min with a 1-min on/off cycle) and subsequently centrifuged at 92,400 g using a Ti70 rotor (Beckman Coulter Life Sciences, Indianapolis, IN) for 45 min at 4°C. Afterwards, the supernatant was loaded onto an Acta HPLC system (General Electric, Schenectady, NY) with a 1 ml nickel column for affinity chromatography. The bound protein was then eluted with elution buffer [20 mM HEPES (pH 7.5), 200 mM NaCl and 300 mM imidazole]. The concentration of imidazole was reduced 40,000× by consecutive dialysis using an Invitrogen 3 ml dialysis cassette (ThermoFisher Scientific) in 20 mM HEPES (pH 7.5) and 200 mM NaCl solution. The remaining volume was concentrated to 1.5 ml using an Amicon Ultra cellulose 10,000 MWCO filtration unit (Millipore Sigma). The final protein concentration was quantified with a Pierce BCA assay (ThermoFisher Scientific) to be 2 mg/ml. Finally, 10% glycerol was added for storage at -80°C.

2.2.7 Pronase digestion assay

Lyophilized S. griseus pronase (Roche) was dissolved in milli-Q water to make a stock concentration of 6 mg/ml, which was then stored at 4°C for up to 3 days. Following ANM generation, beads were pelleted by centrifugation at 300 g for 5 min at 4°C. The supernatant was then carefully removed without disturbing the bead pellet, which was subsequently washed twice in 1 ml PBS (Ca2+ and Mg2+-free, pH 7.5) followed by resuspension in 30 µl PBS. Next, 18 µl of sample was loaded via capillary action into an imaging flow chamber made from a glass coverslip adhered to a glass slide, both of which were purchased from ThermoFischer Scientific, and separated by two strips of double-sided tape. Finally, 9 µl of pronase stock solution was added to the chamber containing the ANMs resulting in a final pronase concentration of 2 mg/ml. For the digestion of His_6–GST–EGFP, purified protein was added to SUPER templates containing 60% DOPC, 30% cholesterol, and 10% Ni-NTA lipids at a final concentration of 1 µM, incubated at room temperature for 15 min, washed twice with PBS, and then resuspended in 30 µl PBS. Confocal images were acquired before and 15 min after the addition of pronase.

2.2.8 KASH-binding assay

TRITC–KASH2WT (SEDDYSCQANNFARSFYPMLRYTNGPPPT) and TRITC–KASH2ΔPPPT (SEDDYSCQANNFARSFYPMLRYTNG) were purchased from Genscript Biotech (Piscataway, NJ). The lyophilized peptides were dissolved in DMSO to give a final stock concentration of 10 µM each. Similar to the pronase digestion assay, the ANMs were washed and resuspended in 30 µl PBS and then 10 µl aliquots were made for TRITC–KASH2 peptide-binding tests. To each aliquot of washed ANMs, we added 0.5 µl of TRITC–KASHWT or KASH2ΔPPPT peptides as well as 0.5 µl milli-Q water, resulting in a final peptide concentration of 450 nM. To each aliquot of washed SUPER templates,

which were resuspended completely before being equally distributed in different tubes, we added 1.0 µl of TRITC–KASHWT peptide resulting in a final peptide concentration of 1 µM. The binding reactions were then incubated for 15 min at room temperature prior to imaging.

2.2.9 Microscopy

All images were acquired using an oil immersion 100×/1.4 NA Plan Apochromat objective with an Olympus IX-81 inverted fluorescence microscope (Olympus Corporation, Tokyo, Japan) controlled by MetaMorph software (Molecular Devices, San Jose, CA) equipped with a CSU-X1 spinning disc confocal head (Yokogawa Electric Corporation, Tokyo, Japan), AOTF-controlled solid-state lasers (Andor Technology, Belfast, UK), and an iXON3 EMCCD camera (Andor Technology, Belfast, UK). Images of EGFP fluorescence images were acquired with 488 nm laser excitation at an exposure of 500 ms for all experimental conditions. TRITC fluorescence images were acquired with 561 nm laser excitation at an exposure of 100 ms. A Semrock 25 nm quad-band band-pass filter (FF01-440/521/607/700-25, IDEX Health and Science LLC, Rochester, NY) centered at 440, 521, 607 and 700 nm was used as the emission filter. Each acquired image contained ~3–5 beads, SUPER templates or ANMs that had settled down on a coverslip. For an individual experiment, four images were taken at different locations across a coverslip. Each experiment was repeated three independent times using the same imaging procedure. Samples were always freshly prepared before each experiment and were never reused.

2.2.10 Image analysis

All images were analyzed using FIJI software (https://fiji.sc). We did not exclude any data from our analyses, nor did we utilize blinding. Since the fluorescent rings corresponding to all membrane associating proteins were not homogenous in intensity, 8–10 line-scans were performed through the center of each bead at multiple angles and the maximum intensities of those scans were recorded. These values were averaged over each bead to generate one data point in the box plots (marking the first and third quartile with the box and the median) shown. Averaged background intensity measurements were performed for each image, which were subsequently subtracted from the individual fluorescence intensities of all beads present in that image. Normalization was carried out with respect to the maximum background subtracted intensity of beads in a given channel corresponding to the cell-free expression of a given protein in the absence of pronase. For the plots quantifying KASH peptide binding, normalization was carried out with respect to the maximum intensity of the beads incubated with TRITC–KASH2WT peptides. Since the fluorescence intensities measured for each sample displayed very little variation, the ~16–20 beads, SUPER templates, or ANMs analyzed per condition were sufficient to enable the detection of statistically significant effect of particular experimental manipulation. Statistical analysis was performed using a two-tailed t-test with a significance level of 0.05, as the data shown in this work meets its assumptions for statistical significance. The variance is conserved between the individual groups of data that were compared using this statistical test.

2.3 Results

2.3.1 Synthesis of SUN1 and SUN2 using mammalian CFE

CFE systems enable the synthesis of proteins of interest encoded by cDNA constructs in a one-pot transcription–translation reaction[165,166]. Recent studies demonstrate the successful reconstitution of membrane proteins in ER-derived microsomes and supported lipid bilayers following CFE in eukaryotic cell extracts[109,167]. The use of CFE for mechanistic structure/function-based studies of membrane proteins offers several important advantages over more conventional cell-based methods where membrane proteins are overexpressed in and purified from heterologous systems[168,169]. Specifically, CFE systems significantly reduce the risk of membrane protein denaturation, as newly

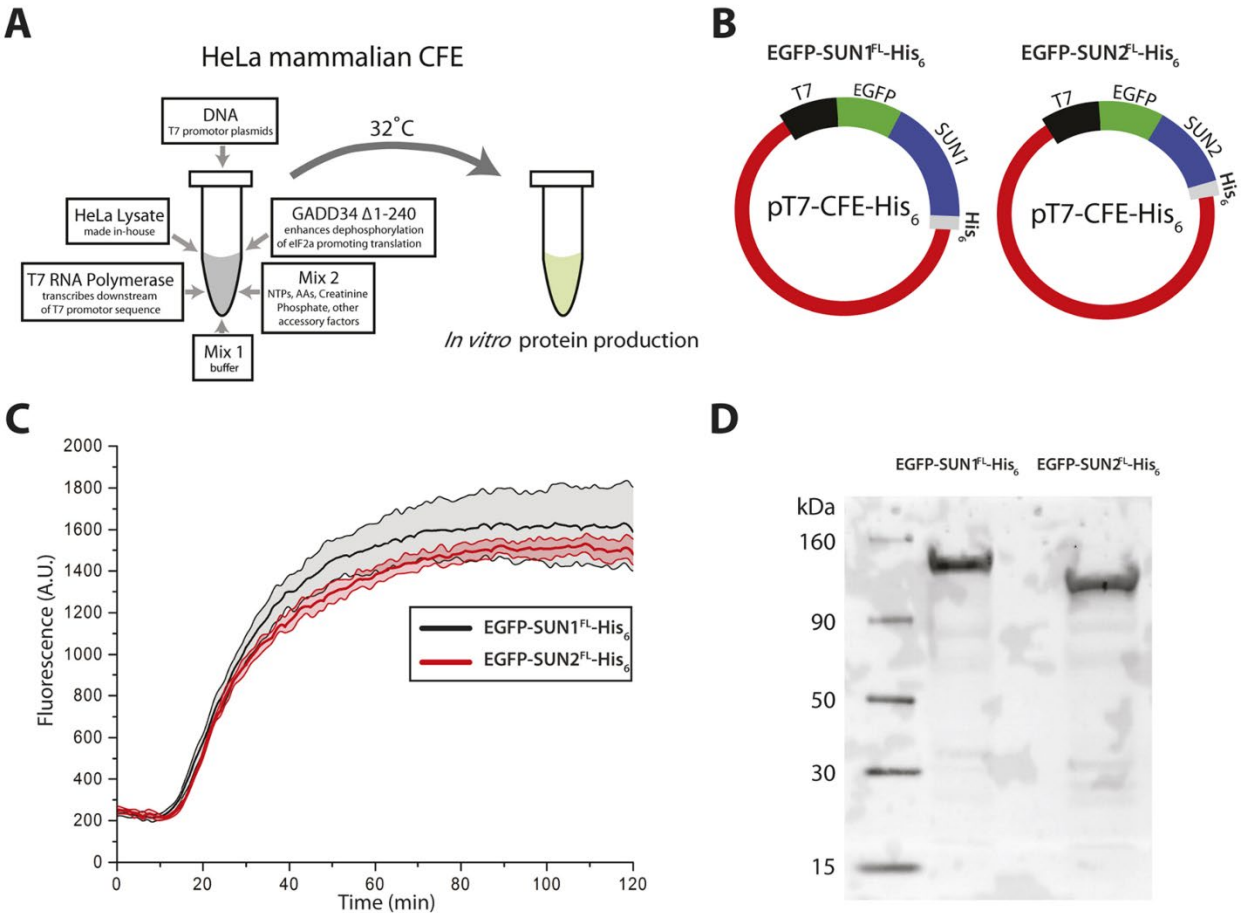

Figure 2.1: **Synthesis of FL SUN1 and SUN2 using a mammalian CFE system**. (A) Schematic of the HeLa CFE system used in this work. (B) Illustration of the pT7-CFE-His_6 constructs encoding EGFP–SUN1FL–His_6 and EGFP–SUN2FL–His_6. (C) Plot of the kinetics of EGFP–SUN1FL–His6 and EGFP–SUN2FL–His_6 synthesis in HeLa CFE reactions as a read-out of EGFP fluorescence over time. Error bands indicate the standard deviation calculated from three independent experiments. (D) Western blot of CFE-synthesized EGFP–SUN1FL–His_6 and EGFP–SUN2FL–His_6 probed with an anti-EGFP antibody.

synthesized membrane proteins are directly inserted into natural ER-based lipid bilayers in the absence of detergents, thus allowing for their proper folding. In addition, CFE is significantly more robust and efficient than the time-consuming process of cell-based expression followed by purification and reconstitution.

To investigate the feasibility of using CFE to reconstitute LINC complexes, we tested the ability of our previously described CFE system, generated using lysates prepared from HeLa S3 cells grown in suspension[162], to synthesize full-length (FL) mouse SUN1 and SUN2 in the absence of exogenously supplied artificial membranes (Figure 2.1A). To do this, we sub-cloned previously characterized cDNA constructs encoding EGFP tagged SUN1FL and SUN2FL[150,163] behind the T7 promoter in the pT7CFE1-CHis vector for mammalian CFE to generate EGFP–SUN1FL–His_6 and EGFP–SUN2FL–His_6, respectively (Figure 2.1B). These constructs were then added separately to CFE reactions containing T7 RNA polymerase and incubated at 32°C in a 96-well plate. Protein production was monitored in a plate reader by quantifying bulk EGFP fluorescence for 2 h, which revealed robust synthesis of both EGFP–SUN1FL–His_6 and EGFP-SUN2FL–His_6 above background levels (Figure 2.1C). Western blot analysis of these CFE reactions using anti-EGFP antibodies demonstrated single bands at molecular masses consistent with the synthesis of FL of EGFP–SUN1FL–His_6 (~131 kDa) and EGFP–SUN2FL–His_6 (~110 kDa) (Figure 2.1D).

To determine whether EGFP–SUN1FL–His_6 and EGFP–SUN2FL–His_6 were membrane associated, we stained microsomes in CFE reactions expressing either protein with the lipophilic membrane stain (1,1′- dioctadecyl-3,3,3′,3′-tetramethylindocarbocyanine perchlorate; DiI). Confocal images of the stained CFE

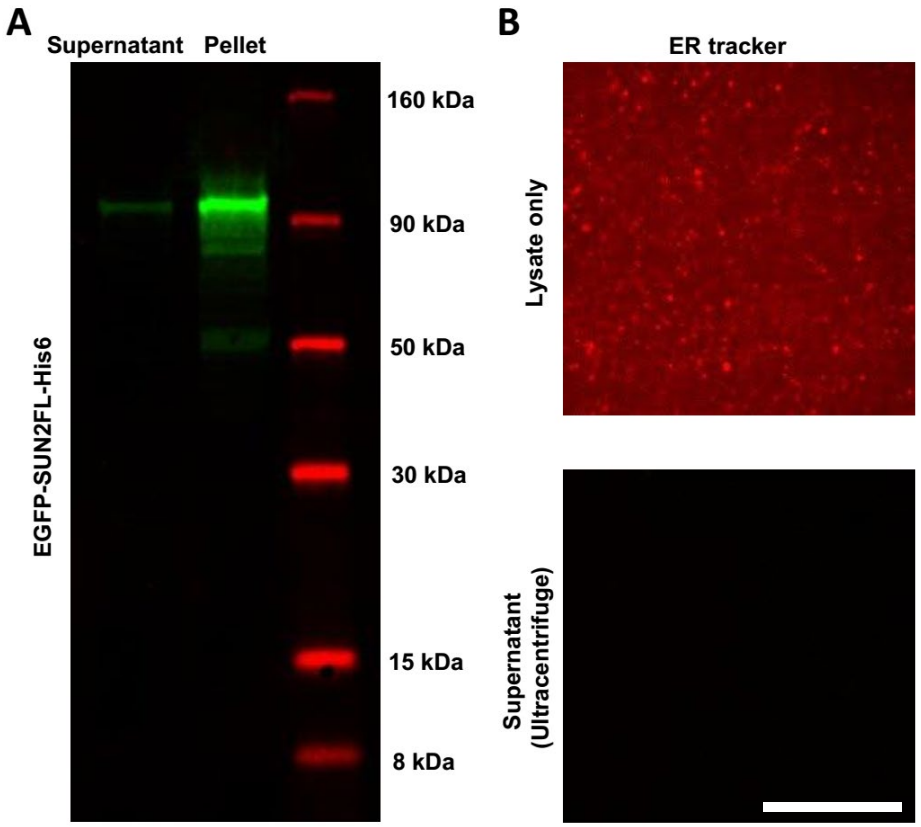

Figure 2.2: **Microsome mediated protein reconstitution in HeLa CFE.** (A) Western blot showing localization of SUN2 FL protein in microsomal fraction of CFE after ultracentrifugation. (B) Labelled microsomes with ER tracker before (top) and after ultracentrifugation (bottom), supernatant fraction. Scale bar: 10 μm

reactions revealed puncta of EGFP and DiI fluorescence; however, we were unable to observe a clear colocalization between these puncta owing to the speed of their diffusion and the temporal limitation of our microscope set-up (Fig. S1A in published manuscript[131]). Nevertheless, colocalization between EGFP and DiI was observed in puncta that had settled down onto the coverslip suggesting that EGFP–SUN1FL–His_6 and EGFP–SUN2FL–His_6 may be inserted into the ER-derived microsomes present within the HeLa S3 cell extracts used for their CFE (Fig. S1B in published manuscript[131]). Further analysis was carried out by ultracentrifugation and EGFP–SUN1FL–His_6 and EGFP–SUN2FL–His_6 were present in the microsome pellet as confirmed by Western blot (Figure 2.2A). Images of the HeLa lysate before and after ultracentrifugation (supernatant)

confirmed removal of microsomes by ultracentrifugation (Figure 2.2B). Taken together, these results show that our mammalian CFE system can be used for the efficient synthesis of FL SUN1 and SUN2 proteins.

2.3.2 Insertion of CFE-generated SUN1 and SUN2 into ANMs

Our next step towards LINC complex reconstitution was to determine whether our CFE-synthesized SUN proteins could be inserted into exogenously provided artificial lipid bilayer membranes. Here, we used supported lipid bilayer with excess membrane

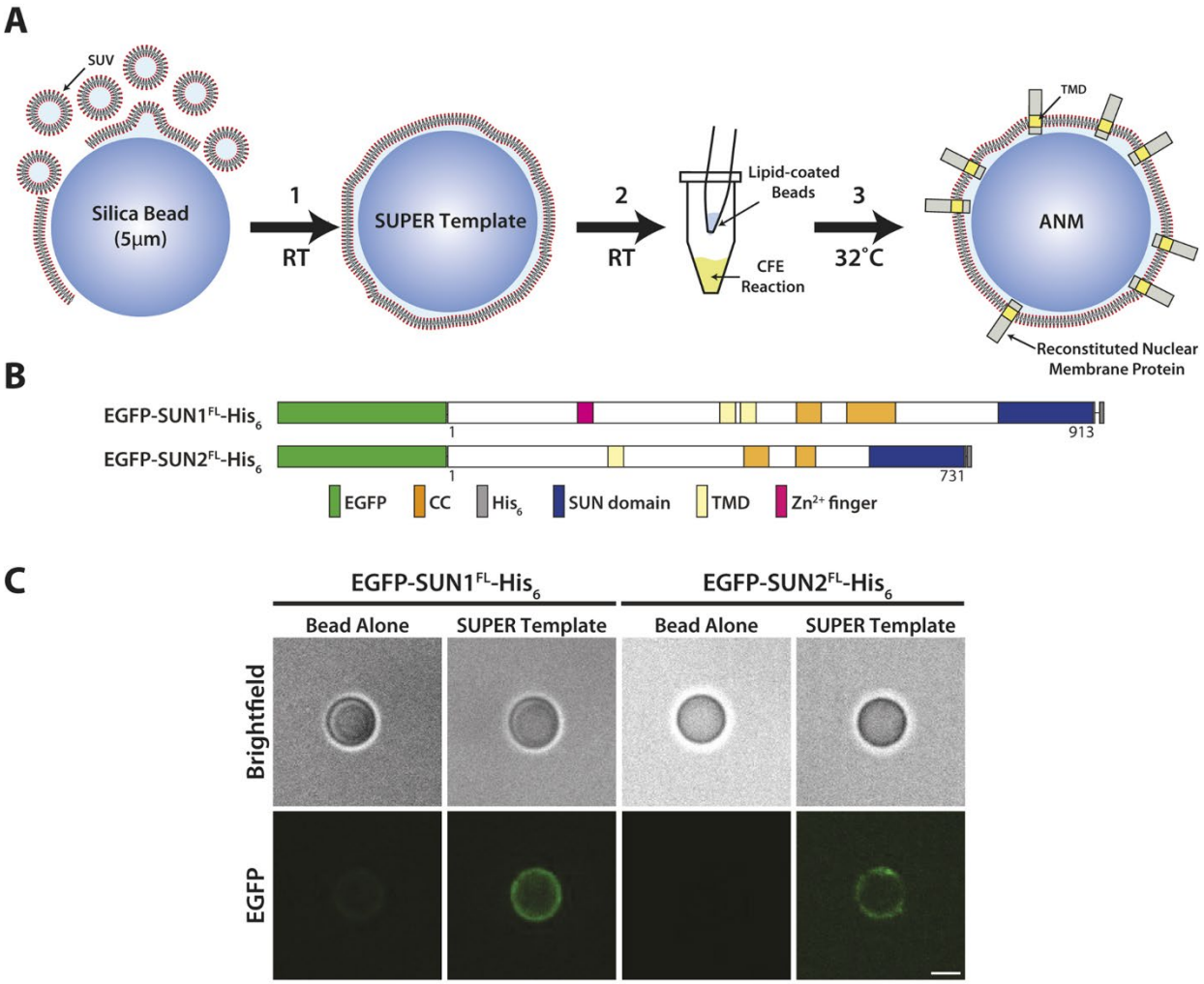

Figure 2.3: **Reconstitution of CFE-synthesized FL SUN1 and SUN2 in ANMs**. (A) Schematic of the process of generating ANMs with inserted CFE-synthesized membrane proteins. (B) Illustrations of the constructs used in this figure. (C) Representative images of silica beads or SUPER templates incubated in CFE reactions for the indicated constructs. Scale bar: 5 µm.

reservoir (SUPER) templates to facilitate the isolation of functional SUN protein inserted into artificial lipid bilayer membranes. Initially developed for *in vitro* studies of protein-mediated membrane fission[161], SUPER templates allow for the reconstitution of excess lipid bilayer membranes on 5 μm diameter silica beads due to the fusion of small unilamellar vesicles (SUVs) containing negatively charged lipids under conditions of high-ionic strength (Figure 2.3A). The lipid composition used for the SUVs in this study was designed to closely mimic that of the INM[170].

Following their assembly, the SUPER templates were added to a CFE reaction containing synthesized SUN proteins. We observed the successful association of both EGFP–SUN1FL–His_6 and EGFP–SUN2FL–His_6 with SUPER templates incubated in their CFE reactions (Figure 2.3B,C). Analysis of the protein domain architectures of SUN1FL and SUN2FL using the simple modular architecture research tool (SMART)[171] predicted the existence of one and two TMDs, respectively. Importantly, neither construct associated with silica beads in the absence of SUPER template, strongly suggesting the specific insertion of EGFP–SUN1FL–His_6 and EGFP–SUN2FL–His_6 into the lipid bilayer membrane of the SUPER template and the assembly of SUN protein-containing ANMs. Although we limit our use of ANMs in this work to reconstitute INM proteins, they could easily be used to reconstitute ONM proteins, such as nesprins.

2.3.3 The C-termini of SUN1 and SUN2 inserted into ANMs remain solvent-exposed

Since the LINC complex assembly is driven by the direct interaction of the C-terminal SUN domain of SUN proteins with the C-terminal KASH peptide of KASH proteins within

the perinuclear space, we next needed to determine the orientation of EGFP–SUN1FL–

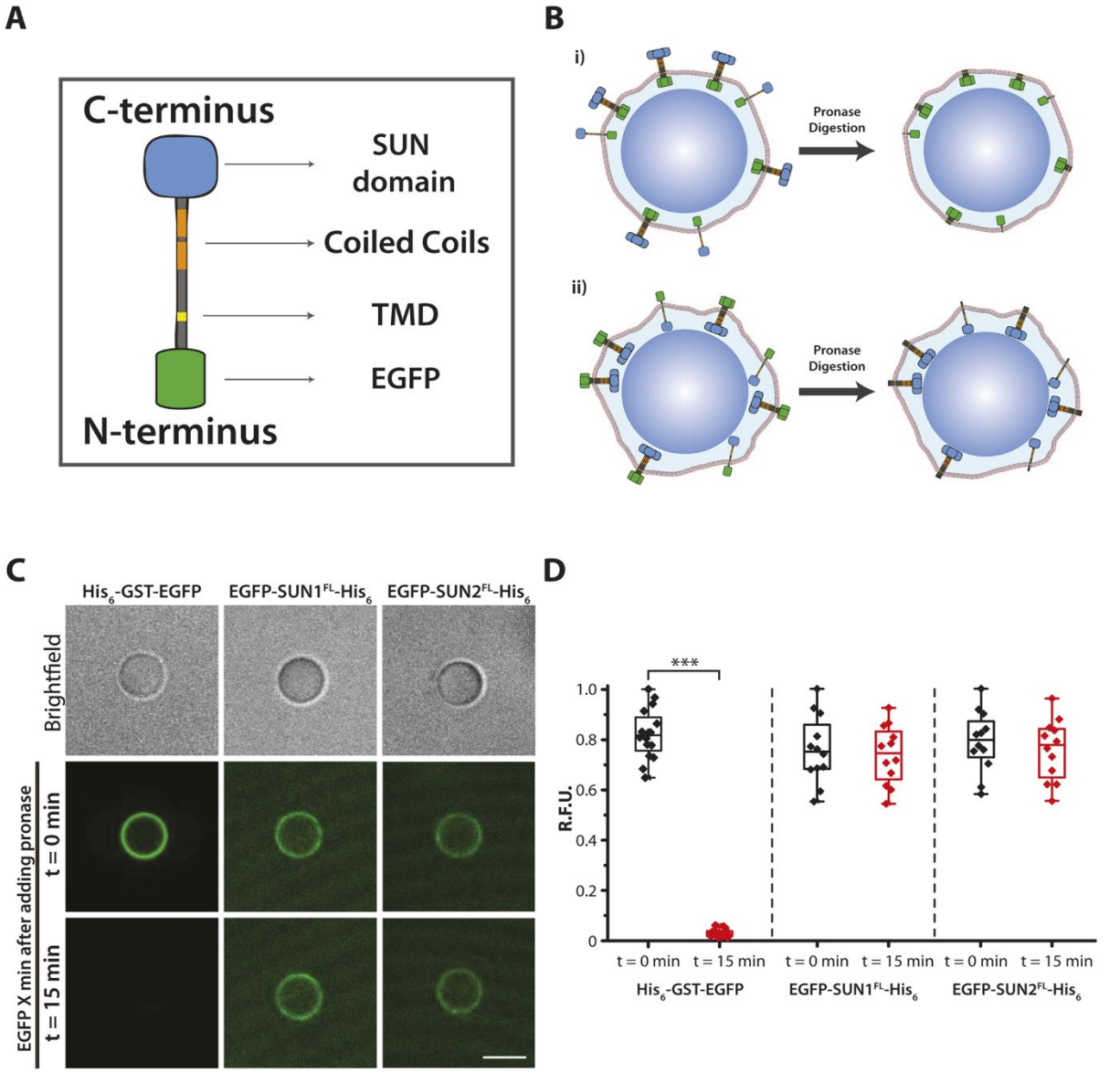

Figure 2.4: **Orientation of CFE-synthesized FL SUN1 and SUN2 inserted in ANMs**. (A) Illustration of a FL SUN protein with EGFP fused to its N-terminus. (B) Schematic of the pronase digestion assay used to determine the topology of ANM-inserted FL SUN proteins synthesized by CFE. If the SUN proteins were oriented with their N-termini protruding away from the ANM into the solution and their C-termini inserted in between the lipid bilayer and the silica bead, EGFP would be protected from pronase-mediated degradation (i). If SUN proteins were oriented in the opposite direction, EGFP would be degraded by pronase (ii). (C) Representative images of SUPER templates incubated in CFE reactions expressing the indicated FL SUN protein constructs before (t=0 min) or after (t=15 min) the addition of pronase. As a positive control for pronase digestion, purified His_6–GST–EGFP was incubated with SUPER templates containing 10% DOGS-NTA-Ni prior to the addition of pronase. Scale bar: 5 µm. (D) Box plots depicting the relative fluorescence units (RFU) of EGFP quantified on ANMs before (t=0 min) and after (t=15 min) the addition of pronase for the indicated constructs from three independent experiments (n=24–30 beads). The box represents the 25–75th percentiles, and the median is indicated. The whiskers show the minimum and maximum data points. ***P<0.001. R.F.U., relative fluorescence units.

His_6 and EGFP–SUN2FL–His_6 in reconstituted ANMs. To do this, we developed an imaging-based protease protection assay using the Streptomyces griseus-derived pronase[172], which was added to reconstituted ANMs on beads after 8 h of incubation followed by a washing step. As EGFP is fused to the N-termini of our SUN protein constructs (Figure 2.4A), the loss of fluorescence following pronase addition would indicate that their N-termini are exposed to solvent. Alternatively, if the EGFP fluorescence were detected in the presence of pronase, we would conclude that the N-termini of our constructs was found within the space between the supported lipid bilayer of the SUPER template and the silica bead (Figure 2.4B).

To control for protease activity, we tested the ability of pronase to efficiently

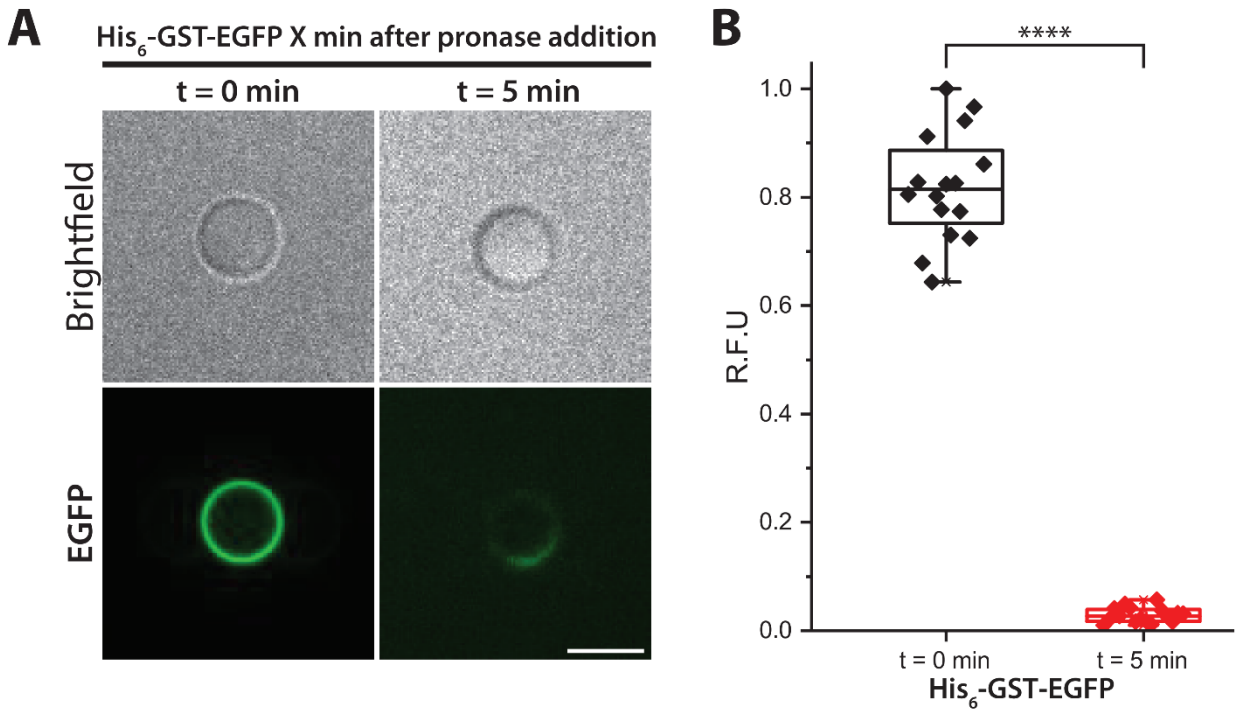

Figure 2.5: **Rapid reduction of EGFP fluorescence on SUPER templates by pronase.** A) Representative images of purified His_6-GST-EGFP incubated with SUPER templates containing 10% DOGS-NTA-Ni before (t = 0 min) or after (t = 5 min) the addition of pronase. Scale bar: 5 µm. **B)** Box plots depicting the relative fluorescence units (RFU) of EGFP quantified on ANMs before (t = 0 min) and after (t = 5 min) the addition of pronase for His_6-GST-EGFP from 3 independent experiments (n = 16 beads per condition). The box represents the 25–75th percentiles, and the median is indicated. The whiskers show the minimum and the maximum data points. **** $p < 0.0001$. R.F.U., relative fluorescence units.

degrade His6-tagged glutathione-S-transferase (GST) EGFP (His6–GST–EGFP), the membrane association of which was promoted by the incorporation of 10% 1,2-dioleoyl-sn-glycero-3-[(N-(5-amino-1-carboxypentyl)iminodiacetic acid)succinyl] (nickel salt) (DOGS-NTA-Ni) into the SUPER templates incubated in the CFE reaction (Figure 2.4B). As expected, the addition of pronase reduced the levels of EGFP fluorescence detected on the surface of His_6–GST–EGFP-bound ANMs to negligible levels after 5–15 min (Figure 2.4C; Figure 2.5). In contrast, no significant difference in EGFP fluorescence was detected on ANMs containing either EGFP–SUN1FL–His_6 or EGFP–SUN2FL–His_6 before or 15 min after the addition of pronase (Figure 2.4C,D). To further examine the orientation of EGFP–SUN1FL–His_6 and EGFP–SUN2FL–His_6 in ANMs, we performed the pronase protection assay on ANMs containing these reconstituted SUN proteins, which were labeled with an anti-His monoclonal antibody directly conjugated to the fluorescent dye Alexa Fluor 647 (anti-Penta-His–AF647 antibody) (Figure 2.6). Confocal images of these labeled SUN protein-containing ANMs prior to the addition of pronase revealed clear ANM-associated EGFP and AF647 fluorescence, while only EGFP

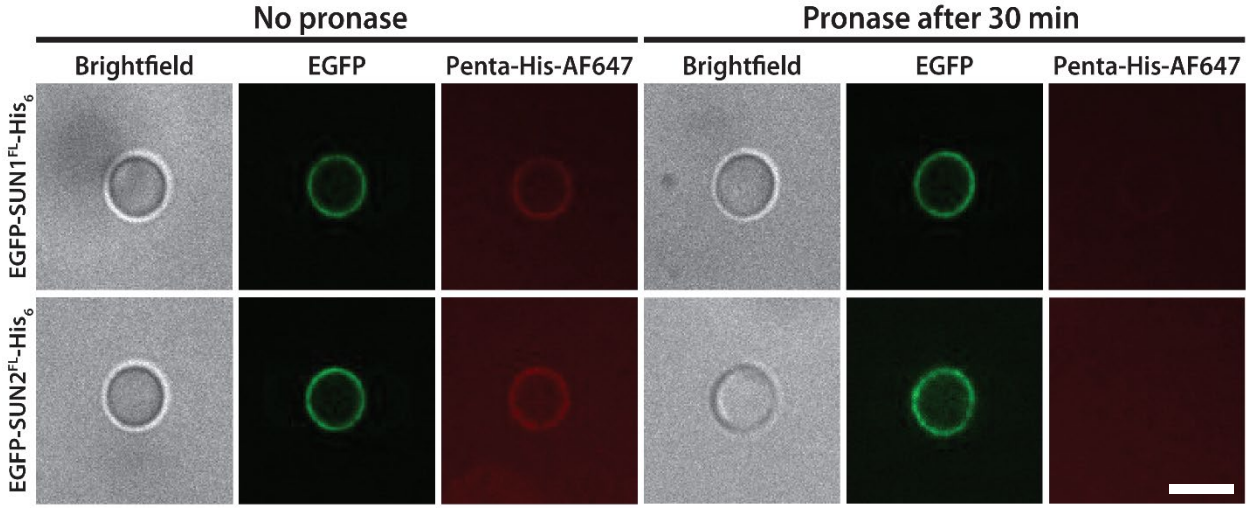

Figure 2.6: **Topology of Penta-His-AF647-labeled EGFP-SUN1FL-His_6 and EGFP-SUN2FL-His_6 inserted into ANMs determined by pronase protection assay.** Representative images of Penta-His-AF647-labeled EGFPSUN1FL-His_6 and EGFP-SUN2FL-His_6 inserted into ANMs taken before and 30 minutes after the addition of pronase. Scale bar: 5 μm.

fluorescence was detected on the ANMs after exposure to pronase. Thus, these results suggest that the N-termini of EGFP–SUN1FL–His_6 and EGFP–SUN2FL–His_6 reside within the space in between the supported lipid bilayer and the silica bead of the ANM.

2.3.4 SUN1 contains three TMDs

Several lines of experimental evidence in the literature support a model where the SUN proteins are single-pass type II membrane proteins with nucleoplasmic N-termini and luminal C-termini[148,173]. However, earlier studies demonstrated the presence of additional hydrophobic regions (HRs) in the nucleoplasmic domains (NDs) of both SUN1 and SUN2[158,174,175]. To begin to assess whether or not additional TMDs exist in SUN1, we generated EGFP- and His_6-tagged constructs encoding the amino acids N- and C-terminal of the previously identified TMD, which were referred to as the ND and luminal domain (LD), respectively (Figure 2.7A). Whereas CFE-synthesized EGFP–SUN1LD–His_6 remained soluble, EGFP–SUN1ND–His_6 strongly associated with SUPER templates incubated in CFE reactions (Figure 2.7B). These results clearly suggest that additional TMDs and/or HRs within the ND of SUN1. Computational analysis of the solvent accessibilities of the amino acid residues present in the ND of SUN1 using the SABLE server (http://sable.cchmc.org/sable_doc.html)[176] revealed the presence of two additional HRs in the SUN1ND (Figure 2.7C). To test the role of these HRs in promoting the association of SUN1ND with ANMs, we generated a panel of EGFP- and His_6-tagged constructs encoding SUN1ND truncations (Figure 2.7C). The single HR-containing EGFP–SUN1(1-364)–His_6 construct still associated with ANMs, whereas the HR-devoid EGFP–SUN1(1-232)–His_6 construct did not (Figure 2.7D). Based on these results, we conclude that the HRs present in SUN1ND mediates its ability to associate with the ANM.

While the SUN1ND also contains an enigmatic C2H2 Zn^{2+} finger[158,177], it is not sufficient

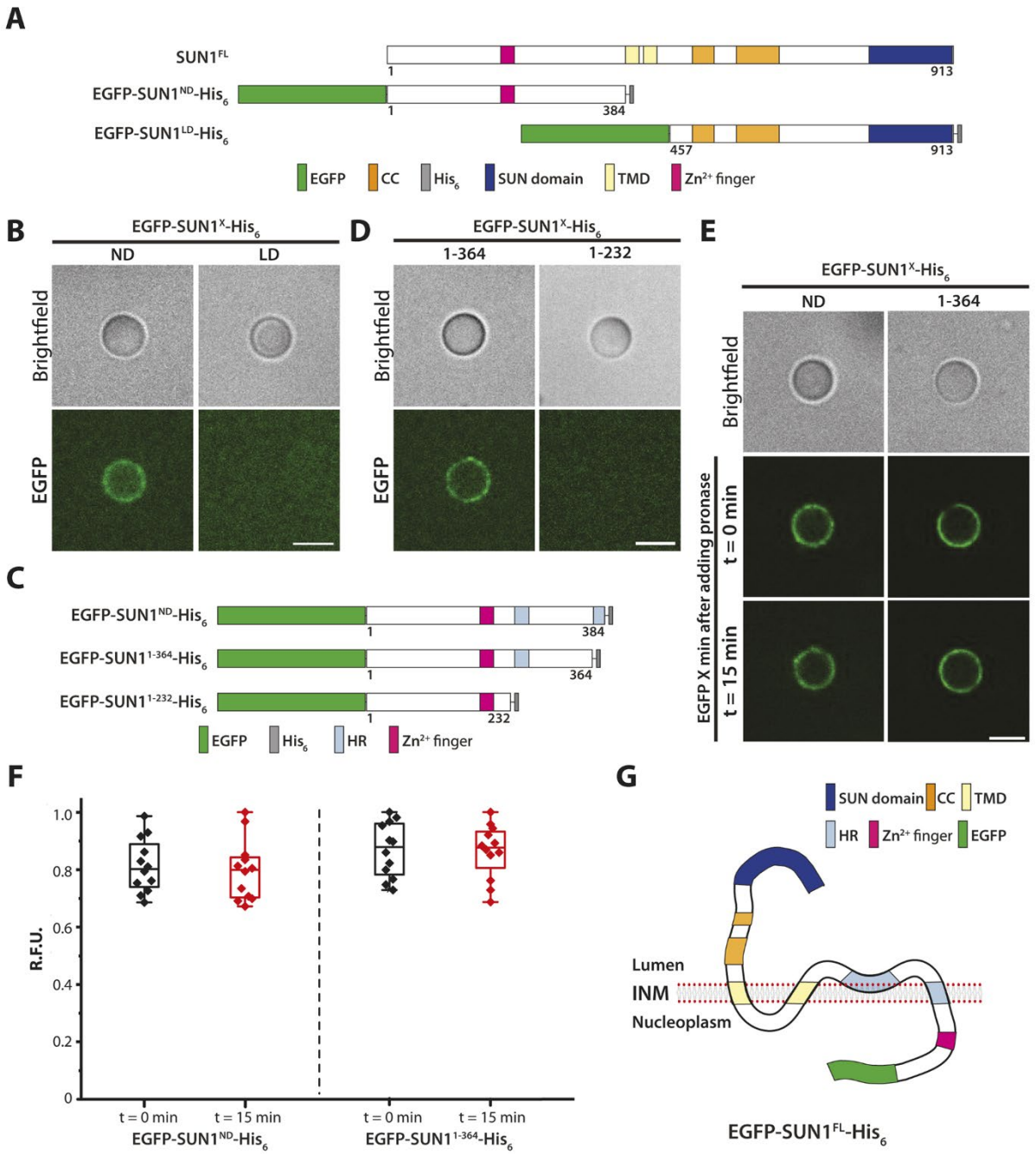

Figure 2.7: **Topology of SUN1 inserted in ANMs.** (A,C) Illustration of the constructs used in this figure. (B,D) Representative images of silica beads or SUPER templates incubated in CFE reactions for the indicated constructs. (E) Representative images of SUPER templates incubated in CFE reactions expressing the indicated constructs before (t=0 min) or after (t=15 min) the addition of pronase. (F) Box plots depicting the RFU of EGFP quantified on ANMs before (t=0 min) and after (t=15 min) the addition of pronase for the indicated constructs from three independent experiments (n=12 beads per condition). The box represents the 25–75th percentiles, and the median is indicated. The whiskers show the minimum and maximum data points. (G) Working model for the topology of EGFP–SUN1FL–His6 inserted into the INM. Scale bars: 5 μm. R.F.U., relative fluorescence units.

for ANM association.

To determine whether the HRs found within SUN1ND are TMDs or peripherally associated with membrane, we again turned to the pronase protection assay described above. Treatment of EGFP–SUN1ND–His_6 or EGFP–SUN1(1-364)–His_6-associated ANMs with pronase for 15 min did not significantly decrease the levels of ANM-associated EGFP fluorescence (Figure 2.7E,F). In addition, we performed pronase protection assays on ANMs containing either EGFP–SUN1ND–His6 or EGFP–SUN1(1-364)–His6, which were also labeled with anti-Penta-His-AF647 antibody (Fig. S3 in published manuscript[131]). Similar to what was observed with ANMs containing either EGFP–SUN1FL–His_6 or EGFP–SUN1FL–His_6, confocal images of these labeled SUN protein-containing ANMs prior to the addition of pronase revealed clear ANM-associated EGFP and AF647 fluorescence, while only EGFP fluorescence was detected on the ANMs after exposure to pronase. Thus, we propose that one of the two additional HRs in the SUN1ND is a TMD. Based on these results and the possibility of a membrane-associating HR in SUN1ND, a potential model of SUN1 topology in the INM is shown (Figure 2.7G), which would preserve the luminal orientation of the C-terminus while maintaining the nucleoplasmic orientation of the N terminus.

2.3.5 SUN2 contains a single TMD and a membrane-associated HR

We next asked whether SUN2 also possessed more than one TMD by testing the ability of EGFP- and His_6-tagged constructs encoding the SUN2ND and SUN2LD to associate with membranes (Figure 2.8A). Similar to SUN1, EGFP–SUN2LD–His_6 remained soluble, while EGFP–SUN2ND–His_6 strongly associated with SUPER templates incubated in CFE reactions (Figure 2.8B). Computational analysis using the SABLE server revealed the

presence of a single HR within the ND of SUN2 (Figure 2.8C), which was found to be

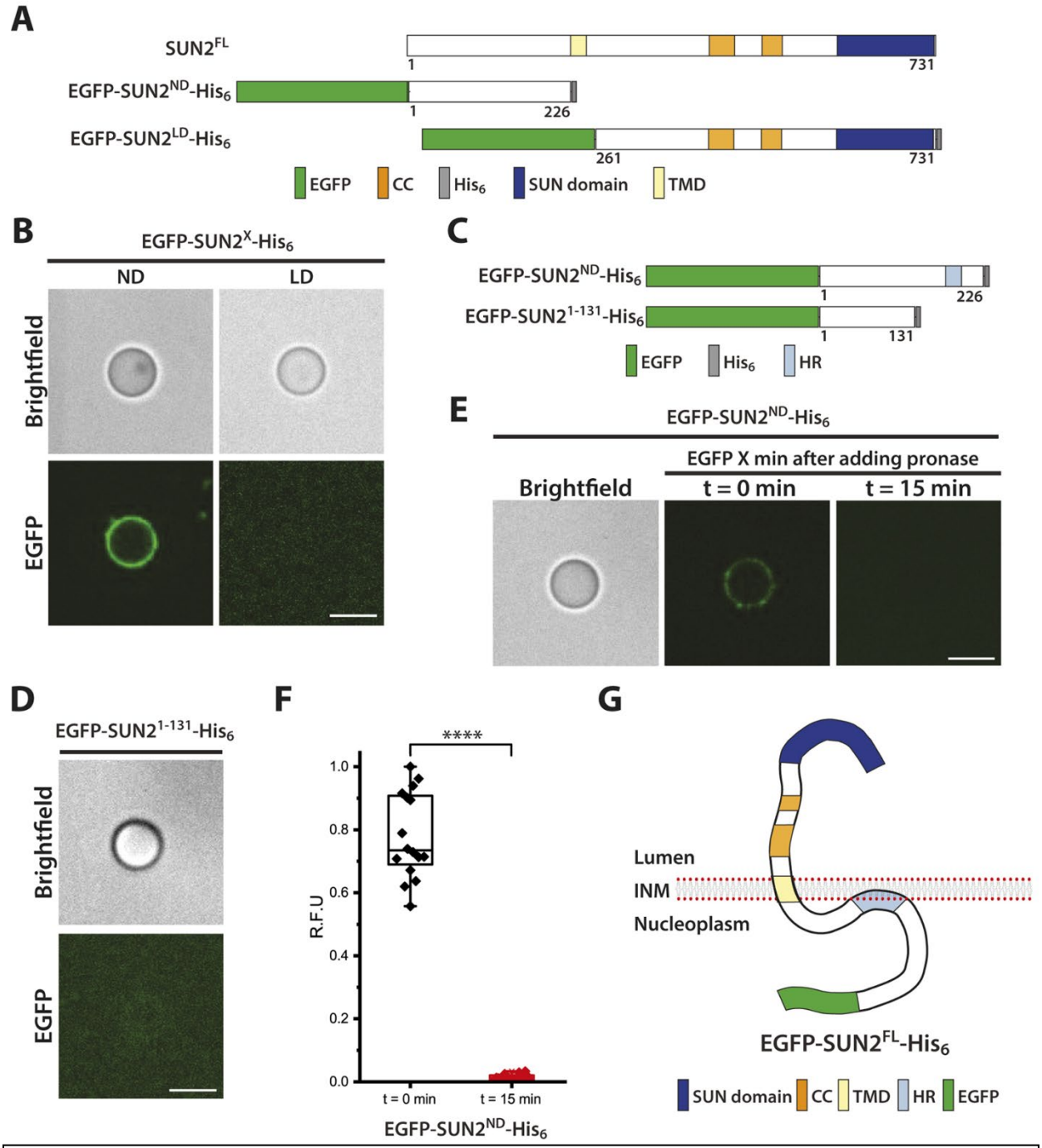

Figure 2.8: **Topology of SUN2 inserted in ANMs.** (A,C) Illustration of the constructs used in this figure. (B,D) Representative images of SUPER templates incubated in CFE reactions for the indicated constructs. (E) Representative images of SUPER templates incubated in CFE reactions expressing the indicated constructs before (t=0 min) or after (t=15 min) the addition of pronase. (F) Box plots depicting the RFU of EGFP quantified on ANMs before (t=0 min) and after (t=15 min) the addition of pronase for the indicated constructs from three independent experiments (n=12 beads per condition). The box represents the 25–75th percentiles, and the median is indicated. The whiskers show the minimum and maximum data points. ****P<0.0001. (G) Working model for the topology of EGFP–SUN2FL–His6 inserted into the INM. Scale bars: 5 μm. R.F.U., relative fluorescence units.

critical for SUN2ND to associate with membranes, as a construct lacking this HR, EGFP–SUN2(1-131)–His_6, remained soluble (Figure 2.8D). However, the addition of pronase to EGFP–SUN2ND–His_6-associated SUPER templates reduced EGFP fluorescence to background levels (Figure 2.8E,F). Consequently, we propose that the SUN2ND peripherally associates with the nucleoplasmic leaflet of the INM, thereby maintaining the type II membrane protein topology of SUN2 (Figure 2.8G).

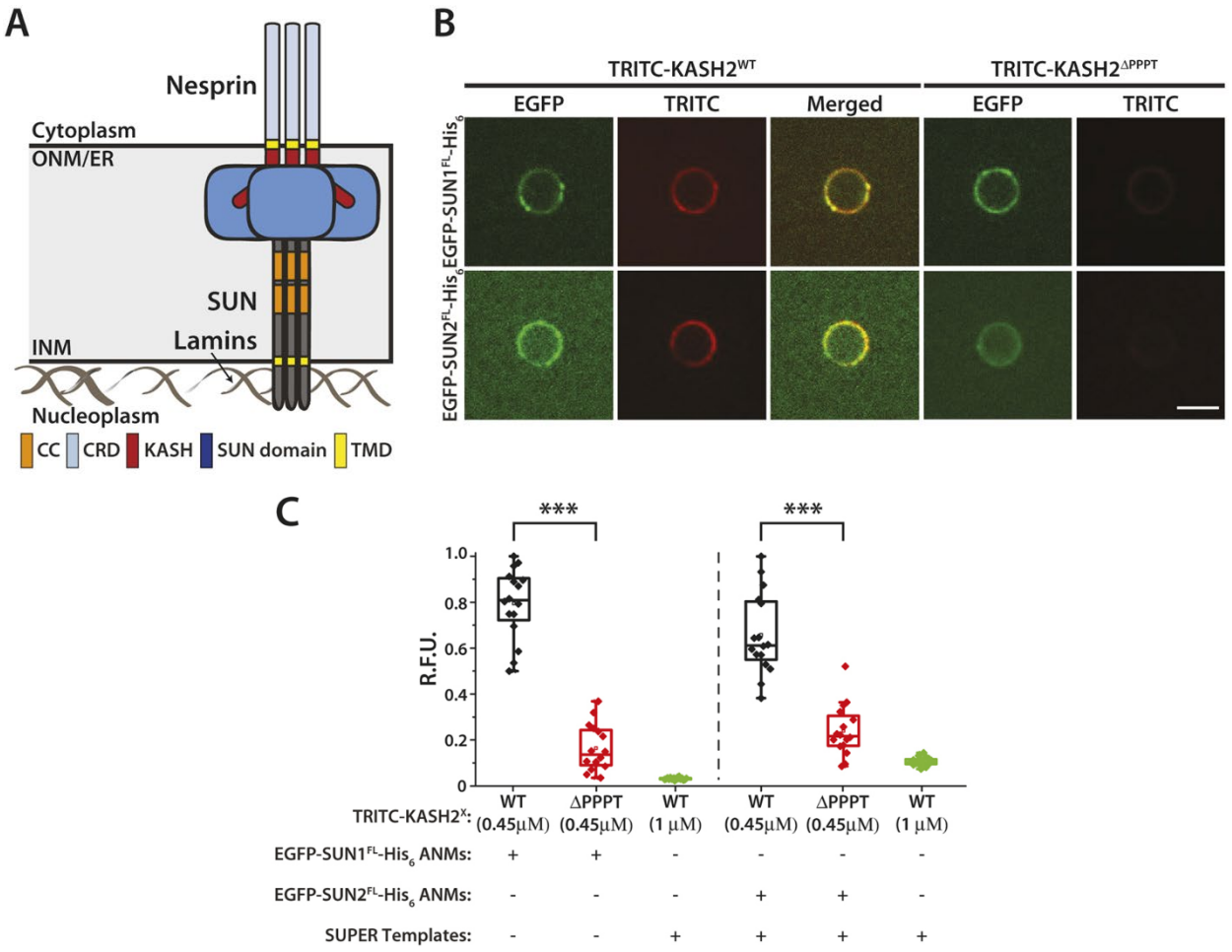

Figure 2.9: **Reconstitution of KASH-binding SUN1FL and SUN2FL complexes using CFE and ANMs.** (A) Schematic depicting an assembled LINC complex based on previously published structural and computational modeling studies (Jahed et al., 2018; Sosa et al., 2012). CRD, central rod domain. (B) Representative images of ANMs containing the indicated inserted SUN protein as well as SUPER templates incubated together with the indicated KASH2 peptide. Scale bar: 5 μm. (C) Box plots depicting the quantified RFUs from the indicated KASH2 peptides recruited to ANMs containing the inserted indicated SUN protein as well as to SUPER templates, which were not incubated in CFE reactions from three independent experiments (n=12 beads per condition). The box represents the 25–75th percentiles, and the median is indicated. The whiskers show the minimum and maximum data points. ***P<0.001. R.F.U., relative fluorescence units.

2.3.6 Reconstitution of KASH-binding FL SUN1 and SUN2 in ANMs

Having demonstrated that we could successfully use CFE to generate supported artificial lipid bilayers containing FL SUN1 and SUN2 oriented such that their C-termini were exposed to solvent, we finally ask whether or not we could use these ANMs to reconstitute LINC complex assembly in vitro. Since the core of the LINC complex is formed by the direct interaction between the LD of SUN proteins and the KASH peptide of KASH proteins[148] (Figure 2.9A), we tested the ability of EGFP–SUN1FL–His_6- and EGFP–SUN2FL–His_6-containing ANMs to recruit wild-type (WT) KASH peptides from the KASH protein nesprin-2 with tetramethylrhodamine (TRITC) attached to their N-termini (TRITC–KASH2WT). ANMs containing EGFP- SUN1FL–His_6 or EGFP–SUN2FL–His_6 displayed an efficient recruitment of TRITC–KASH2WT. Importantly, neither ANM was able to recruit TRITC labeled KASH peptides lacking the four C-terminal amino acids that are required for the SUN–KASH interaction to occur normally[177] (TRITC-KASH2ΔPPPT) to levels similar to those observed with TRITC–KASH2WT (Figure 2.9B,C). However, the recruitment of TRITC–KASH2ΔPPPT to ANMs containing EGFP–SUN1FL–His_6 or EGFP–SUN2FL–His_6 was slightly elevated relative to its recruitment to SUPER templates, which were not incubated in CFE reactions. Therefore, TRITC–KASH2ΔPPPT appears to maintain some ability to interact with FL SUN proteins. Because LINC complex assembly is critically dependent upon the ability of SUN proteins to directly interact with KASH peptides, these results strongly suggest that we have successfully reconstituted the SUN–KASH interaction using CFE and ANMs.

2.4 Conclusion

Here, we describe ANMs as a bottom-up synthetic biology platform for the reconstitution and mechanistic dissection of LINC complex assembly. We show that we can reconstitute FL SUN1 and SUN2 proteins into ANMs with their N-terminal NDs oriented in between the lipid bilayer and the silica bead while their C-terminal LDs extend away from the ANM and into the solution. We also use ANMs to determine that SUN2 possesses a single transmembrane domain, while SUN1 possesses three. Finally, we demonstrate that ANM-inserted FL SUN proteins are capable of recruiting the KASH peptide of nesprin-2, suggesting that we have successfully reconstituted the SUN–KASH interaction, which is the core of the LINC complex. The minimal ability of TRITC–KASH2ΔPPPT to interact with FL SUN proteins inserted into ANMs suggests that the PPPT motif is not the only binding interface between the KASH2 peptide and SUN proteins. In fact, KASH2 interacts with SUN2 through two additional binding interfaces[178,179]. The first interface consists of residues -4 to -14 (numbering relative to the C-terminus) of the KASH peptide, which insert into a groove formed between two SUN2 protomers, with the conserved hydrophobic residues at -7 and -9 being oriented towards the groove. The third interface, residues -15 to -23, fits along the surface of the adjacent SUN2 protomer. A conserved cysteine residue at position -23 of the KASH peptide is oriented to form an intermolecular disulfide bond with a conserved cysteine residue in the SUN domain of SUN2. Future experiments will be aimed at testing the role of these other binding interfaces on the residual recruitment of TRITC–KASH2ΔPPPT to reconstituted SUN protein containing ANMs.

The orientation of SUN proteins reconstituted in ANMs is not random, presumably because the CFE reaction lysates contain ER derived microsomes, which contain the cellular machinery necessary for the co-translational translocation of membrane

proteins[111]. Since the interior of ER-derived microsomes is equivalent to the ER lumen and the contiguous perinuclear space of the nuclear envelope, the C-terminal LD of SUN proteins will be co-translationally translocated into the interior while the N-terminal ND will remain on the outside of the ER-derived microsomes in the CFE reaction. Thus, when the SUPER templates are introduced into the SUN protein-expressing CFE reactions, the SUN protein-containing ER-derived microsomes fuse with the supported lipid bilayer surrounding the silica bead of the SUPER template. Consequently, the N-terminal ND can now be found in the space between the lipid bilayer and the silica bead, while the C-terminal LD is oriented away from the ANM and is solvent exposed. However, this case does not hold for EGFP–SUN2ND, which contains a membrane-associated HR, because the protein is likely synthesized outside of the ER derived microsomes and is only present on the solvent-exposed side of the ANM.

Chapter 3: Development of a Mechanosensitive Synthetic Cell capable of Calcium Biosensing

* Part of this chapter has been published in Majumder, Garamella et al. *Chemical Communications*, 2017[180]. The author designed and carried out all encapsulation experiments in liposomes for Figures 3.4 and 3.5. The *E. coli* TXTL system and MscL and deGFP plasmids were provided by Vincent Noireaux.

3.1 Introduction

3.1.1 Protein synthesis with cell-free expression

Cell-free expression (CFE) has been recently reshaped into a highly versatile technology applicable to an increasing number of research areas[181]. The new generation of DNA-dependent cell-free transcription–translation systems (TXTL) has been engineered to address applications over a broad spectrum of engineering and fundamental disciplines, from synthetic biology to biophysics and chemistry[182,183]. Modern TXTL platforms are used for medicine and biomolecular manufacturing, such as the production of vaccine and therapeutics[184,185]. By performing non-natural chemistries[186–188], the TXTL technology has been improved to expand the molecular repertoire of biological systems. Because the time for design-build-test cycle is dramatically reduced, TXTL has become a powerful platform to rapidly prototype genetic programs *in vitro*, from testing single regulatory elements to recapitulating metabolic pathways[189]. Remarkably, the new TXTL systems have also been prepared so as to work at many different scales and in different experimental settings. As such, TXTL reactions can be carried out in volumes spanning

more than twelve orders of magnitudes, from bulk reactions to microfluidics and synthetic cell systems[129,183,190].

3.1.2 Synthetic cells as an experimental system

The bottom-up construction of synthetic cells that recapitulates gene expression has become an effective means to characterize biological functions in isolation and to prototype cell-sized compartments as chemical bioreactors for applications in biotechnology[191,192]. In particular, engineering synthetic cells integrating active membrane functions is critical to develop mechanically robust compartments capable of sensing the physical and chemical environment. Such undertaking, however, remains challenging as only a few synthetic cell systems loaded with executable genetic information and harboring membrane sensors have been achieved[121]. In this work, we construct synthetic cells capable of responding to osmotic pressure by expressing the *E. coli* mechanosensitive membrane protein MscL using a TXTL system encapsulated into synthetic liposomes. Using the calcium sensitive reporter G-GECO, we demonstrate that the osmotic pressure and calcium intake can be detected simultaneously, at different concentrations of the divalent ion. TXTL is carried out with a highly versatile all *E. coli* cell-free toolbox based on the endogenous transcription machinery (*E. coli* core RNA polymerase and sigma factor 70, σ70). We characterize the channel function by monitoring the fluorescence of G-GECO and the leak of polymers of various sizes. Our novel approach expands the functional capabilities of encapsulated cell-free TXTL reactions and demonstrates, for the first time, that synthetic cell systems with biosensing interfaces can be achieved by directly expressing membrane proteins inside liposomes.

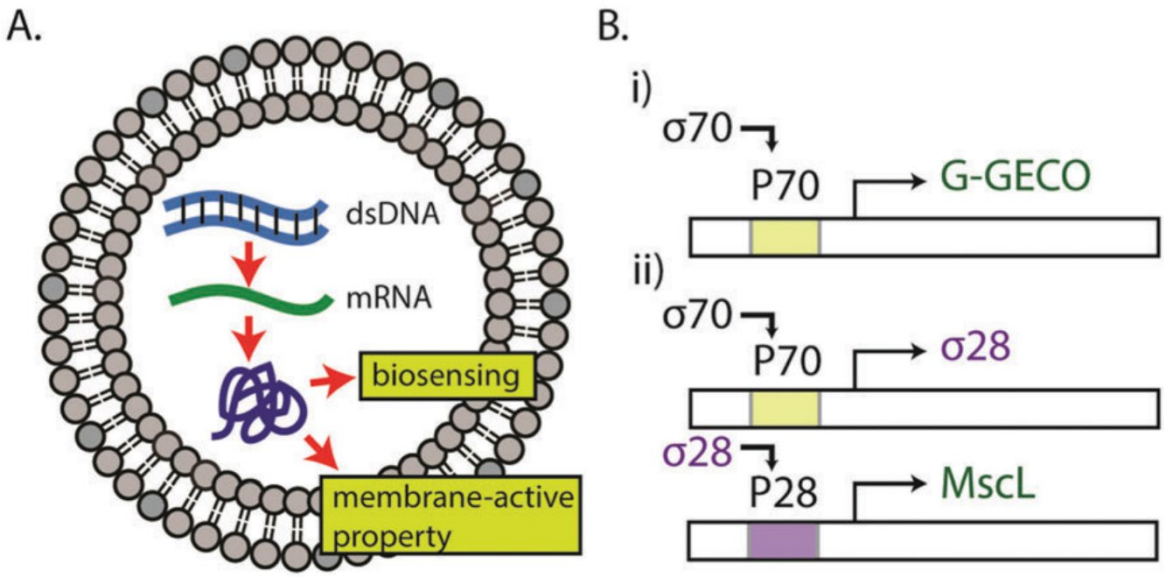

Figure 3.1: **Schematics of protein synthesis in liposomes and gene circuits.** (A) dsDNA is transcribed into mRNA, which is then translated to a biosensing fluorescent reporter protein (G-GECO) and a mechanosensitive membrane-active protein (MscL). (B) Gene circuits used in this work. (i) The *E. coli* housekeeping transcription factor σ70 activates the promoter P70a. (ii) The σ28 cascade requires the expression of σ28 protein, expressed through the P70a promoter. The σ28 transcription factor activates the corresponding promoter P28a.

Our general methodology is to encapsulate TXTL reactions within phospholipid vesicles as a versatile platform that recapitulates *in vitro* transcription–translation for producing proteins that endow biosensing and molecular transport properties to the vesicles (Figure 3.1A). DNA-based cell-free protein synthesis inside liposomes links the information contained in the DNA to the phenotype of synthetic cells in a reduced environment suitable for isolation and characterization of cellular functions. Like a complex chemical reaction that can be broken down to elementary processes, biochemical reactions based on genetic circuits can also be constructed to control rates of protein production. Such settings are conveniently adjusted in TXTL by either choosing the appropriate plasmids stoichiometry and circuit architectures, or by calibrating the strength of promoters and ribosome binding sites[183].

3.2 Materials and Methods:

3.2.1 DNA constructs

The plasmids P70a-deGFP, P70a-σ28, and P28a-deGFP have been described previously[183]. P28a-MscL and P28a-MscL-eGFP were obtained by first cloning MscL from *E. coli* K12 into a P28a backbone and then adding eGFP as a fusion protein. The pcDNA3-G-GECO construct was obtained from Takanari Inoue (Johns Hopkins University) and the calcium-sensing function was verified by monitoring G-GECO activity from external calcium flux through ionophore A23187 (Sigma Aldrich). G-GECO was then cloned into the pT7-CFE backbone for use in a mammalian cell-free expression system. Specifically, G-GECO was PCR amplified from of the pcDNA backbone and a 5' Kozak sequence and 3' CAAX sequence (in frame) added. The resulting PCR amplicon was cloned into the pT7-CFE empty vector between the plasmid IRES and poly-A tail sequence using BamHI and NotI. pT7-G-GECO DNA sequence was confirmed by sanger sequencing and its function was verified in bulk mammalian cell-free expression assays with and without calcium. Subsequently, restriction enzyme cloning from the pT7 construct into P70a-deGFP was carried out to obtain the P70a-G-GECO plasmid used in the present study. Due to lack of appropriate restriction cut sites, the gene for G-GECO was PCR amplified along with the 3' CAAX motif, and inserted by restriction enzyme cloning using PspXI and NcoI, in between the ribosome binding site and the T500 terminator sequences of the P70a-deGFP vector.

3.2.2 TXTL preparation and reactions

TXTL reactions are composed of the *E. coli* lysate, an amino acid mixture, and an energy buffer. Transcription and translation are performed by the endogenous molecular components provided by the *E. coli* cytoplasmic extract. A detailed description of the

standard TXTL preparation has been reported previously in several articles[126,183]. The energy buffer is composed of: 50 mM HEPES pH 8, 1.5 mM ATP and GTP, 0.9 mM CTP and UTP, 0.2 mg/ml tRNA, 0.26 mM coenzyme A, 0.33 mM NAD, 0.75 mM cAMP, 0.068 mM folinic acid, 1 mM spermidine, 30 mM 3-PGA, 2% PEG8000, either 10-15 mM maltose or 20-40 mM maltodextrin. A typical cell-free reaction is composed of 33% (volume) of *E. coli* crude extract. The other 66% of the reaction volume are composed of the energy mixture, the amino acids and plasmids. The amino acid concentration was adjusted between 1.5 mM and 3 mM of each of the 20 amino acids (always equimolar for the 20 amino acids). Mg-glutamate and K-glutamate concentrations were adjusted according to the plasmids used (typically 90 mM K-glutamate and 4 mM Mg-glutamate for P70a-deGFP). Cell-free TXTL reactions were carried out in a volume of 5 µl to 20 µl at 29-30°C.

3.2.3 Measurement of TXTL gene expression in bulk reactions

Quantitative measurements were carried out with the reporter protein deGFP (25.4 kDa, 1 mg/ml = 39.37 µM). deGFP is a variant of the reporter eGFP that is more translatable in cell-free systems. The excitation and emission spectra as well as fluorescence properties of deGFP and eGFP are identical, as previously reported[183]. The fluorescence of deGFP produced in batch mode reactions was measured on an H1m plate reader (Biotek Instruments, V-bottom 96-well plate, interval of three minutes, Ex/Em 488/525 nm). End-point measurements were carried out after 8-12 h of incubation. Pure recombinant eGFP (from either Cell Biolabs Inc. or purified in the lab) was used to make a linear calibration of intensity versus eGFP concentration for quantification on plate readers. Error bars are the standard deviations from at least three repeats. The measurements in batch more reactions for G-GECO were similar to deGFP.

Measurements were recorded with a Synergy H1 plate reader (Biotek Instruments) in 96 V-bottom Nunc polypropylene plates. The temperature was set at 29°C for all conditions and kinetic measurements were carried out with an interval of one minute. The excitation and emission wavelengths were set at 488 nm and 525 nm respectively. The measurement run was stopped at a given time and restarted after externally adding calcium to the bulk reaction. This led to a delay of 1-2 minutes indicating the loss of at most two data points at the instant of calcium addition in the supplementary figures.

3.2.4 Liposome preparation

Liposomes were prepared using the water-in-oil emulsion transfer method. Lipids (Egg PC, Avanti Polar Lipids) were dissolved in mineral oil (Sigma-Aldrich) at 2 mg/ml. 2-8 µl reactions were added to 500 µl oil and vortexed to create an emulsion. This emulsion was added atop 10-20 µl of a feeding solution. The biphasic solution was centrifuged for 10 minutes at 1500 g to form liposomes. Single emulsion droplets were created by vortexing 6 µL of TXTL reaction in 30 µL of 2% Span 80 surfactant in mineral oil.

Double emulsion templated vesicles were generated by a glass capillary device as described in previous works[162,193]. DOPC, cholesterol and Liss-Rhod PE (Avanti Polar Lipids) were mixed in a glass test tube and Argon gas was used to remove the solvent. The lipids were then placed in a dessicator for an hour following which they were resuspended in a 36:64 chloroform-hexane solution by volume. The final concentration of the lipids was kept constant at 6 mg/ml for all experiments when using this device. The inner solution was prepared by adding 1.5% polyvinyl alcohol (PVA) and 1 mM EGTA (final concentrations) to a standard TXTL cell-free reaction. The cell-free solution was then incubated at 29C for an hour before encapsulation. Outer solution composition was

20 mM K-HEPES, 80 mM KCl, 1.3% glycerol, 10% PVA, and 280 mM glucose (final osmolarity is 770 mOsm). The outer solution osmolarity was matched with the inner phase by adding appropriate concentration of glucose just before encapsulation. 10 mM CaCl2 (final conc.) was added to this outer solution for resuspending the collected double emulsions. 50 µl of double emulsion collection was then added to 100 µl of the outer solution containing calcium for all experimental conditions except the hypo-osmotic shock with two plasmids, in which case 50 µl double emulsions was added to 100 µl of the hypo-osmotic solution. The hypo-osmotic solution composition was 20 mM K-HEPES, 80 mM KCl, 10% PVA, 400 mM glucose and 10 mM CaCl2 (final osmolarity is 660mOsm). All osmolarities were measured on a Vapro-Osmometer (by vapor pressure) with 10 µl of sample. Following resuspension in calcium-containing solutions, the double emulsions were incubated on a slide. Oil dewetting and lipid bilayer formation was observed within a short duration after double emulsion generation.

3.2.5 Measurement of TXTL gene expression in liposomes

The phospholipid vesicles were observed using an inverted microscope (Olympus, IX-81) equipped with Metamorph Advanced software. Liposomes expressing deGFP/eGFP were imaged with a GFP filter set (excitation 473 nm, emission 520 nm). To image the TRITC-dextran dye (Sigma-Aldrich) and BSA-TRITC dye (Sigma-Aldrich), a Texas Red filter set was used (excitation 556 nm, emission 617 nm). At least 40 lipid vesicles were monitored to generate the standard deviation shown in the error bars. The method used to quantify the deGFP protein expression has been described previously.1 deGFP was expressed and quantified using the Biotek H1m plate reader. Then, deGFP protein at different, known concentrations was encapsulated in liposomes and standard curves of

area vs intensity were created. By comparing the leading coefficients of these curves, we verify the scaling is linear. The CCD camera used was also verified to scale linearly with varying exposure times.

The double emulsion templated vesicles were imaged with Olympus IX-81 spinning disk confocal microscope connected to an Andor iXOn 3 CCD camera, and operated with the Metamorph Advanced software. G-GECO and deGFP images were captured with a GFP filter set (excitation 488 nm, emission 525 nm) under constant exposure of 500 ms for all experimental conditions. A TRITC filter set (excitation 560 nm/emission 607 nm) was used to capture the fluorescent lipid images. The exposure was kept constant at 100 ms for lipid imaging. All images were background subtracted and their contrasts were matched for visual comparison. For the quantitative analysis of calcium detection under different concentrations, integrated density (ID) measurement was carried out in ImageJ. For each image, a box was drawn based on the size of a vesicle and the ID was calculated three times by shifting the box within the lumen of the vesicle. Next, using the same box, the background ID was calculated at three different positions in the image. The relative fluorescence intensity was then calculated by subtracting the average background ID from the average luminal ID and normalizing the result with the area of the box.

3.3 Results

3.3.1 Development of gene circuits for simultaneous expression of MscL and G-GECO

In this work, we used two different genetic circuit schemes to produce proteins of interests (Figure 3.1B). In the first scheme, the endogenous *E. coli* core RNA polymerase σ70 drives the transcription of downstream coding sequence through the constitutive promoter

P70a[183]. Our second scheme is a transcriptional activation cascade where P70a/σ70 drives the expression of sigma factor 28 (σ28) that is required for subsequent expression from a P28a promoter sequence specific to σ28. We first used the reporter protein deGFP to characterize the circuit functions and features[183]. deGFP is a slightly modified version of eGFP with identical fluorescence properties. Both schemes were then used to express G-GECO, a genetically encoded green fluorescence protein whose fluorescence depends on calcium concentration[194], and the *E. coli* mechanosensitive channel of large conductance (MscL) for biosensing and incorporating a membrane-active property, respectively. We first performed bulk reactions (10 ml reactions) and compared deGFP expression kinetics of the single-step circuit vs. the transcriptional activation cascade circuit. As expected, the requirement for σ28 to drive expression of deGFP in the transcriptional activation resulted in a delay in deGFP expression compared to the single-step circuit (Figure 3.2A). The delay observed for the cascade, on the order of 15 minutes, corresponded to the amount of time necessary for the synthesis of σ28. The bulk reaction persisted for many hours and deGFP production began to slow down after 8 hours and reached a plateau after 10 hours. The time course observed in these experiments is typical for TXTL reactions where protein synthesis ceases due to resource limitation (depletion of nucleotides and amino acids), change in the biochemical environment (pH) and accumulation of reaction byproducts. We next asked whether compartmentalization could preserve the delay in deGFP production that we observed in the bulk reactions. Using a single-step emulsion approach by vortexing aqueous TXTL reactions in 2% Span 80 dissolved in mineral oil, we produced emulsion droplets with a wide range of sizes encapsulating the TXTL reactions. As clearly evident, we observed deGFP expression as early as 45 minutes for the single-step circuit compared to relatively weak fluorescence

after 1 hour for the transcriptional activation cascade (Figure S1 in published manuscript[180]). Fluorescence intensity reached maximum after approximately 2 hours in both cases. The shorter protein production time in single emulsions is consistent with a faster rate of resource depletion in a compartmentalized system as compared to a bulk system[129], as well as to the limited supply of oxygen necessary for cell-free TXTL.

3.3.2 MscL activation with osmotic shock causes dye leakage in liposomes

We next created synthetic cells by encapsulating TXTL reactions into phospholipid vesicles that have a physical boundary comparable to real living cells. We used a reverse emulsion technique for generating liposomes[183] and we accounted for the delay in imaging start time due to preparation (estimated to be around 15 min). Because of the initial low protein production in vesicles, we acquired images at a high exposure time during the first hour (100 ms compared to 5 ms after 75 minutes of incubation) so that some fluorescence signals were observable at the earlier time points. Consistent with the experiments carried out under bulk conditions and in single emulsions, there was a clear delay in deGFP production in the transcriptional activation cascade in liposomes (Figure 3.2B). deGFP production leveled off after about 10 hours. The longer lasting expression compared to single emulsion is likely due to the availability of oxygen from the outer aqueous solution. Together, these experiments demonstrate that a cascaded circuit can delay reporter expression and that we can achieve robust protein expression by compartmentalizing CFE reactions. Phospholipid vesicles are particularly useful for encapsulating TXTL reaction in cell-sized compartments because lipid bilayers are the

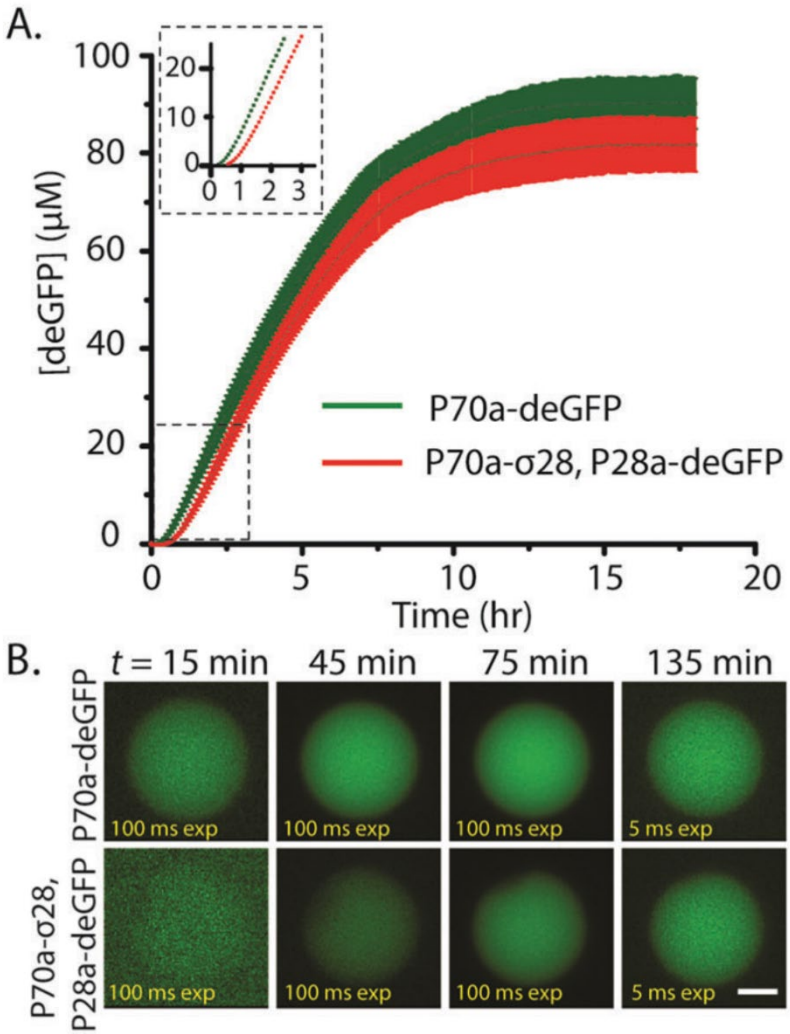

Figure 3.2: **deGFP synthesis in bulk reactions and in liposomes.** (A) Kinetics of expression. Plasmid P70a-deGFP fixed at 5 nM, P70a-S28 fixed at 0.2 nM, and P28a-deGFP fixed at 5 nM. Inset: 0–3 hours magnified. (B) deGFP synthesis in liposomes using both the P70a plasmid and P28a cascade. Scale bar: 5 μm.

natural substrates for membrane proteins such as channels and receptors. Expressing membrane proteins is a critical step towards constructing synthetic cells with functional interfaces to provide, for instance, transport or catalytic capabilities to a vesicle. In this regard, only a few of such artificial systems with membrane protein channels and sensors have been achieved so far[121,195]. As a model system, we expressed MscL using the cascaded transcriptional activation circuit. MscL is a bacterial membrane protein that senses an increase in membrane tension and opens a pore of 2.5 nm diameter to allow influx/efflux of molecules down the concentration gradient. It is thought to serve as the

emergency release valve during osmotic downshock without which bacteria can lyse due to elevated osmotic pressure.

We and others have shown that an increase in osmotic pressure or membrane tension can directly gate MscL[72,196,197]. Integrating active MscL into the membrane of synthetic cells by CFE is important for several reasons. First, it provides increased mechanical robustness to the vesicles against bursting by equilibrating osmotic pressure. It is a necessary step towards constructing synthetic cells robust enough to be used outside laboratory conditions. Second, the channel diameter is ideal to pass small nutrients molecules and feed the synthetic cells, while keeping the TXTL machineries inside. Third, it demonstrates that TXTL supports the expression of mechanosensitive membrane proteins that could be used as a means to test MscL mutants. When expressing MscL using the transcriptional activation cascade, the delay in MscL expression (about 15 minutes) is advantageous because it corresponds to the amount of time needed to prepare the liposomes. We first expressed MscL-eGFP to visualize MscL localization. We observed the accumulation of MscL-eGFP at the membrane over time as expected (Figure S2 in published manuscript[180]). In order to test MscL function, we developed a simple dye-leakage assay where TRITC-labeled dextrans of different molecular weights (3, 10, and 70 kDa) and TXTL reaction producing wild type MscL were co-encapsulated using the emulsion method to make liposomes (Figure 3.3A). We expressed the native MscL without a fluorescent protein tag as MscL fusion proteins have a higher activation tension threshold[72].

In our experiments, we relied on the osmotic pressure from a hypo-osmotic feeding solution (630 mOsm) relative to the encapsulated TXTL reaction (700 mOsm). In the absence of MscL expression, 5 mM of 3000 Da TRITC-dextran remained encapsulated

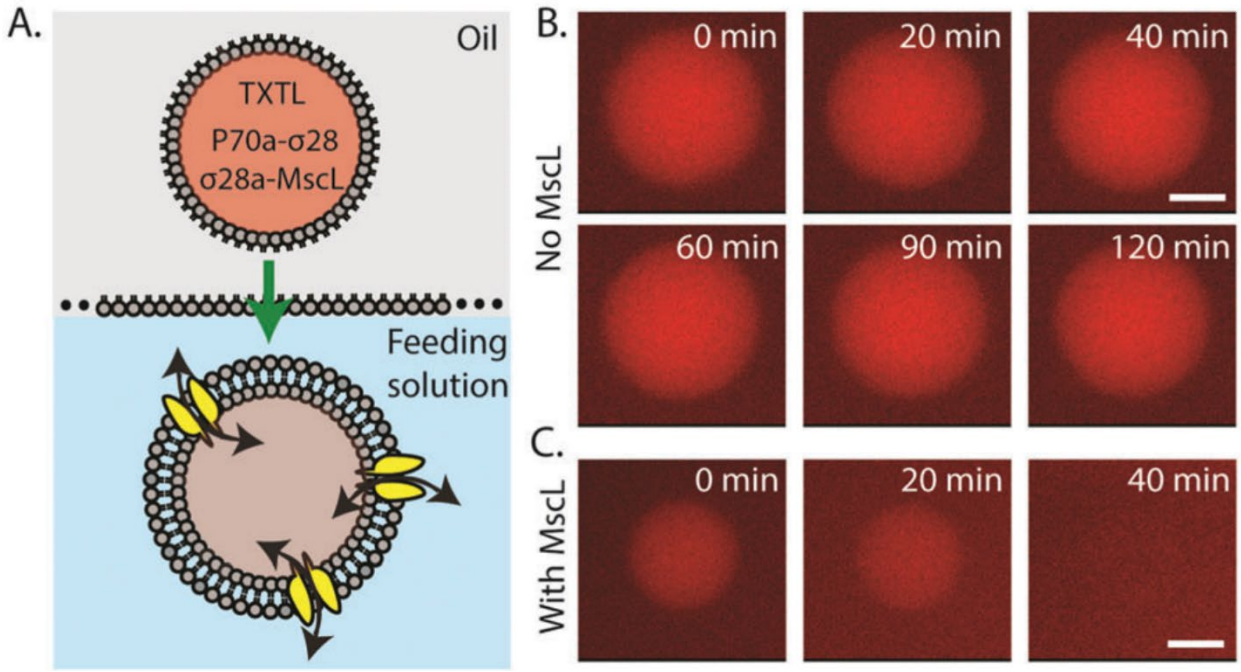

Figure 3.3: **Leakage of a 3 kDa TRITC-dextran in liposomes in the absence or presence of MscL.** (A) Schematic of the encapsulation of a cell-free reaction containing 3 kDa TRITC-dextran (5 mM), P70a-S28 (0.2 nM), and P28a-MscL (5 nM) into liposomes via the water-in-oil emulsion transfer method. (B) Fluorescence images of liposomes containing 3 kDa TRITC-dextran over a 2-hour period with only P70a-S28 added to the cell-free reaction. (C) Fluorescence images of liposomes containing 3 kDa TRITC-dextran over a 40-minute period with P70a-S28 and P28a-MscL added to the cell-free reaction. Scale bar: 5 μm.

in the vesicle after 2 hours (Figure 3.3B). In contrast, MscL expression led to dye-leakage after 20–30 minutes (Figure 3.3C). When a larger 10000 Da TRITC-dextran was used, we observed complete dye-leakage after 60 minutes in MscL-expressing vesicles (Figures S3A and S3B in published manuscript[180]). Larger dextran molecules at 70000 Da were completely retained after 120 minutes with or without MscL expression (Figure S3C in published manuscript[180]), with no leakage observed after 12 hours of incubation (data not shown). We also tested the leakage of two proteins, deGFP (27 kDa) and BSA-TRITC (60 kDa). Both were also completely retained inside the liposomes in MscL-expressing vesicles after 2 hours of incubation (Figure S3D in published manuscript[180]). No leakage was observed after overnight incubation (data not shown).

3.3.3 Co-expression of G-GECO and MscL enables calcium detection upon osmotic shock

Our next challenge was to use a genetically-encoded reporter and demonstrate that we can couple a mechanical input to biosensing. We cloned the genetically-encoded calcium ion (Ca2+) biosensor G-GECO that is composed of a circularly permuted GFP fused to the calmodulin (CaM)-binding region of myosin light chain kinase M13 at its N-terminus and CaM at its C-terminus[198]. G-GECO is dim in the absence of Ca^{2+} and bright when bound to Ca^{2+} with a Ca^{2+}-dependent fluorescence increase of 23–26 fold (Figure 3.4A)[187]. We cloned G-GECO under the P70a promoter and verified that it can sense Ca^{2+} in a plate reader assay (Figure S4A in published manusript[180]). To eliminate traces of Ca^{2+} present in TXTL reactions estimated to be up to 1 mM Ca^{2+}, we added 1 mM EGTA to the TXTL reactions so that G-GECO can report an increase in calcium level when externally added to the reactions. Both G-GECO and MscL-eGFP can be produced together in a single TXTL reaction, as shown by the increased fluorescence level by G-GECO after adding 1 mM Ca^{2+} at 120 minutes after TXTL started (Figure S4B in published manuscript[180]). To create mechanosensitive-biosensing vesicles, we employed double emulsion templated vesicles generated by droplet microfluidics[162,199]. We have previously used this approach and showed that small molecules from the feeding solution can enter encapsulated vesicles containing integrated synthesis, assembly, and translation (iSAT) reactions[129]. We have also shown that Ca^{2+} can enter a double emulsion droplet with an ultrathin oil layer as the middle phase when the droplet is under hypo-osmotic shock[200]. However, Ca^{2+} as a charged ion cannot across a lipid bilayer. When G-GECO was

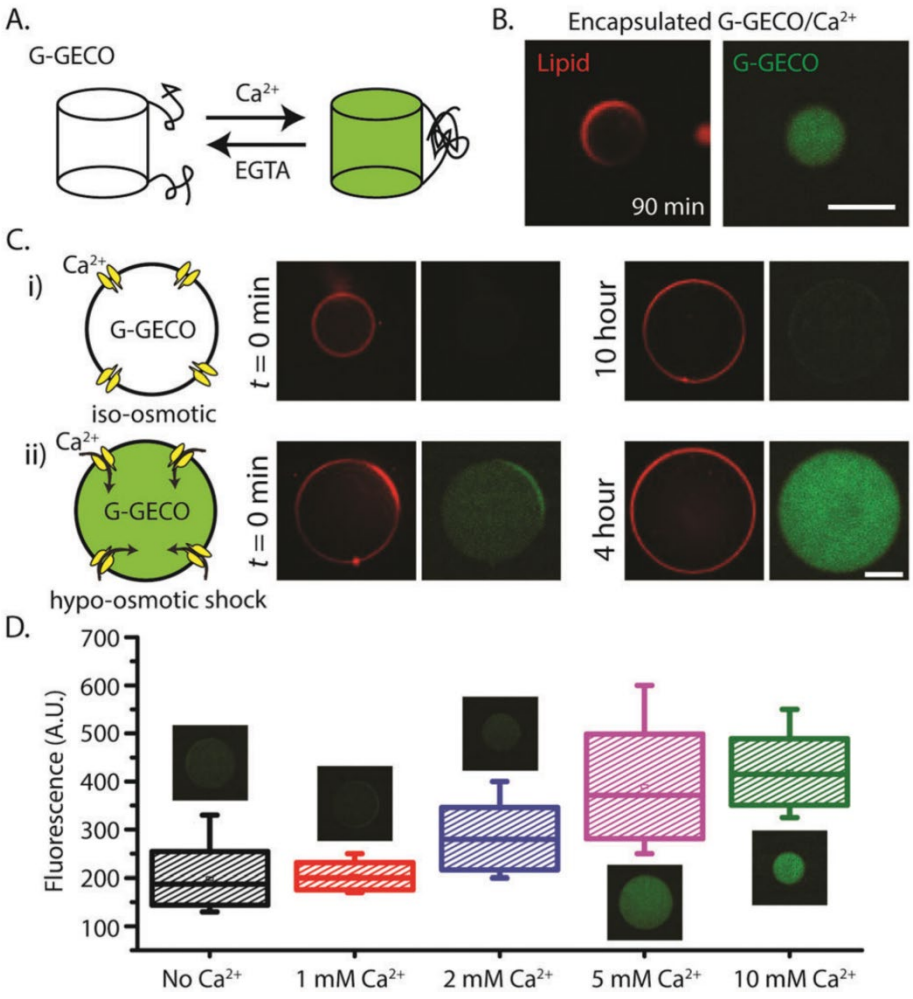

Figure 3.4: Mechanosensitive and biosensing synthetic cell system. (A) Schematic depicting the reversible transformation between the fluorescent and nonfluorescent states of G-GECO protein in presence of calcium and EGTA. (B) Fluorescence images of G-GECO expression with calcium addition inside vesicles (1 nM P70a-G-GECO, 1.5 mM calcium chloride was added to TXTL reaction after 1.5-hour incubation prior to encapsulation). (C) (i and ii) Three plasmid expression under different external conditions. Concentrations of P70a-S28, P28a-MscL and P70a-G-GECO in cell-free reaction were fixed at 0.2 nM, 1.4 nM and 0.6 nM respectively. The outer solutions for all conditions contained 10 mM calcium chloride. (D) Box plot showing the relative fluorescence intensities from vesicles in hypo osmotic media with different external calcium concentrations. Each box corresponds to intensity values from ten vesicles. Plasmid concentrations of P70a-S28, P28a-MscL and P70a-G-GECO were 0.4 nM, 1.3 nM and 1 nM respectively. For both (C) and (D), the lipid vesicles were introduced into hypo-osmotic solution immediately after encapsulation following a 1.5-hour incubation period. EGTA was used at a concentration of 1 mM in all cell-free reactions. Imaging for (D) was carried out after 2-hour incubation in the hypo-smotic medium. The osmolarity difference between iso-osmotic and hypo-osmotic solutions was measured at 100 mOsm. All experiments were repeated three times under identical conditions. Scale bars: 50 μm.

expressed in the presence of 1.5 mM Ca^{2+} inside a vesicle, fluorescence was readily detected after 90 minutes, demonstrating that G-GECO can be used to detect increased calcium concentration in a synthetic cell (Figure 3.4B). As expected, if Ca^{2+} is added to

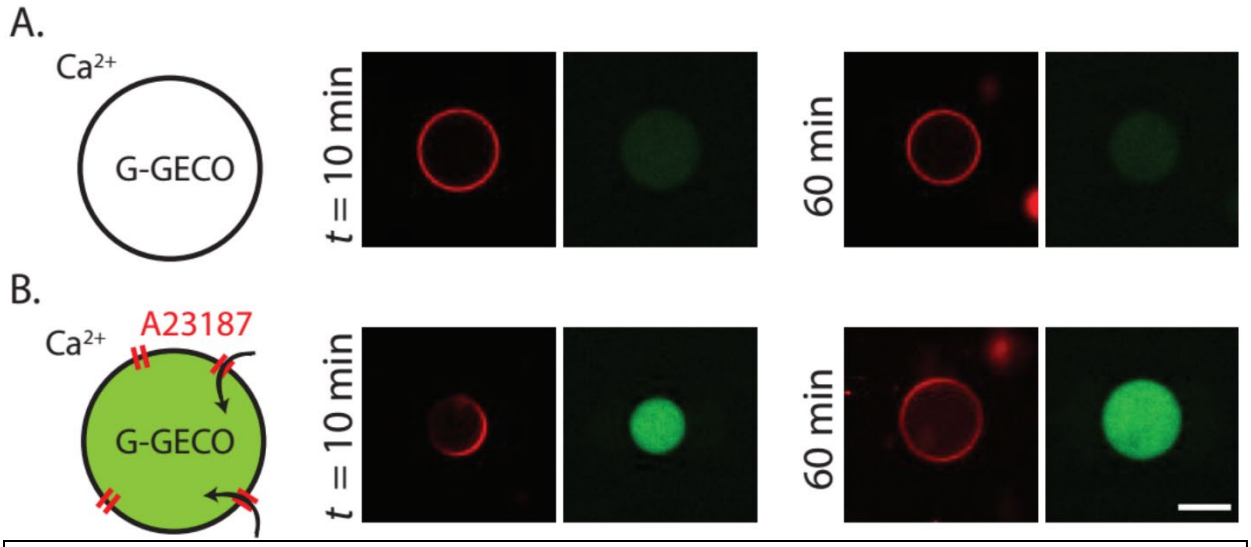

Figure 3.5: Calcium-dependent increase in G-GECO fluorescence inside lipid vesicles. (A) Images showing the native fluorescence of cell-free expressed G-GECO after 3 hours of incubation. (B) Increase in fluorescence as observed upon addition of 1 μM A23187 (calcium ionophore). The time points indicate incubation of vesicles after the addition of A23187 and the simultaneous control experiment without the ionophore. All cell-free reactions contained 1 mM EGTA. The calcium concentration in the outer solution was 10 mM. P70a-G-GECO plasmid was added at a concentration of 1.5 nM. Scale bar: 50 μm.

the outside (at 10 mM) of G-GECO expressing vesicle, no G-GECO fluorescence was observed because Ca^{2+} is impermeable to phospholipid membrane (Figure 3.5A). However, addition of a calcium ionophore A23187 allowed rapid entry of Ca^{2+} and G-GECO fluorescence was readily observed in as little as 10-minute post A23187 addition (Figure 3.5B). To couple mechanical input to sensing the external environment, we co-expressed G-GECO (under P70a promoter) and MscL (under P28a promoter) in TXTL for 2 or 3 hours and then encapsulated the reaction into double emulsion templated vesicles. Under iso-osmotic condition, we did not observe G-GECO fluorescence for over 10 hours, our longest observation time point (Figure 3.4C(i)). In contrast, hypo-osmotic condition of 100 mOsm osmotic difference between inside and outside the vesicle robustly led to an increase in G-GECO fluorescence as Ca^{2+} was able to enter the lipid bilayer membrane through MscL (Figure 3.4C(ii)). To our knowledge, this is the first demonstration of an AND-gate composed of a mechanical input (i.e. hypo-osmotic

pressure) and an external chemical input (i.e. Ca^{2+}) that lead to a specific fluorescence response. The synthetic cell system is also sensitive to the concentration of calcium added to the external solution (Figure 3.4D and Figure S6 in published manuscript[180]). The detection time for calcium intake was as short as 20 minutes when hypo-osmotic shock was applied post synthesis of MscL and G-GECO inside liposomes for one hour in iso-osmotic solution.

3.4 Conclusion

In summary, we have generated a DNA-programmed cell-sized synthetic cell that senses osmotic pressure and external calcium concentration. We demonstrated two different circuit architectures for TXTL that exhibit different reaction kinetics that are preserved across length scale from bulk reactions to micron-sized encapsulated droplets or vesicles. The ability to endow synthetic cells with mechanosensitive functions to sense external small molecules using genetically-encoded biosensors allows for rapid sensing, rather than relying on fluorescence reporter synthesis using chemical inducers that most studies have used[201,202]. Recapitulating TXTL for synthetic cell engineering can be used for reconstituting cellular processes and functions[3]. It can also serve as a powerful platform for chemical applications, such as biosensing and novel synthetic pathways for chemicals.

Chapter 4: Reconstitution of a Membrane-Associated Protein using Inducible Gene Circuits in Mechanosensitive Synthetic Cells

* Part of this chapter has been published in Garamella, Majumder et al. *ACS Synthetic Biology*, 2019[203]. The author in collaboration with co-first author of the manuscript came up with the design of the final genetic circuit used in Figures 4.6, 4.7 and 4.8. All encapsulation experiments in liposomes shown in Figures 4.3-4.8 were carried out by the author. The author generated all figures used in the manuscript. All plasmids were provided by Vincent Noireaux.

4.1 Introduction

4.1.1 Adaptive synthetic cell for mechanically activated reconstitution of membrane-associated protein

Building genetically encoded microscopic compartments capable of mimicking functions of real living cells has become a conceivable, yet challenging, goal of synthetic biology[126,204,205]. While the top-down approach consists of stripping down a living cell to a minimum set of components[206], the bottom-up approach attempts to build a functioning cell by assembling components from scratch[3,195,207–209]. Bottom-up synthetic cells are micron-sized compartments, programmed with elementary gene networks or purified proteins, that recapitulate specific cellular functions in isolation. In such settings, fundamental questions can be addressed by quantitative molecular construction. Apart from being at the cutting edge of biological engineering, synthetic biology, and biophysics, bottom-up synthetic cells are also particularly interesting for developing applications geared toward biotechnologies and medicine[210]. Integrating components into truly active

cell analogues remains, however, a major bottleneck in synthetic cell research[126]. A major approach to bottom-up synthetic cells consists of encapsulating a cell-free expression system into cell-sized liposomes[162,211–213]. Such systems can be programmed with gene networks to isolate and engineer single biological functions[180,195,209]. Transcription-translation (TXTL) has become a versatile and effective tool for prototyping biomolecular systems over a broad range of physical scales, from gene circuits to synthetic cells[214]. The major advantage of TXTL is to dramatically reduce the design-build-test cycle from days or weeks, for in vivo experiments, to hours. The all *E. coli* TXTL used in this work is highly programmable, having access to the full set of *E. coli* sigma factors, allowing the construction of complex gene circuits from both plasmid and linear DNA[183]. Our goal is to demonstrate that TXTL-based synthetic cells can cooperatively link, like in real living cells, DNA information, metabolism, and self-assembly.

Herein, we describe results that build upon the work presented in Chapter 3 involving the *E. coli* mechanosensitive channel of large conductance (MscL) and a calcium sensing recombinant protein, G-GECO[180]. We advance beyond biosensing by developing a synthetic cell capable of responding to environmental stimuli and subsequently synthesizing proteins responsible for cell mechanical robustness, specifically the production of the *E. coli* cytoskeleton protein MreB. The synthesis of GFP or MreB is controlled by the lac repressor and a Lac01/σ28 amplifier, creating an AND gate consisting of the IPTG inducer and the hypo-osmotic conditions. We further show that when MreB is expressed, it readily associates with the inner membrane of the liposomes, forming a cortex-like structure. The pattern of the structure changes based on the extent of induction which is mediated by the amount of plasmid used in the TXTL reactions. Our overall experimental design is to encapsulate, in phospholipid vesicles,

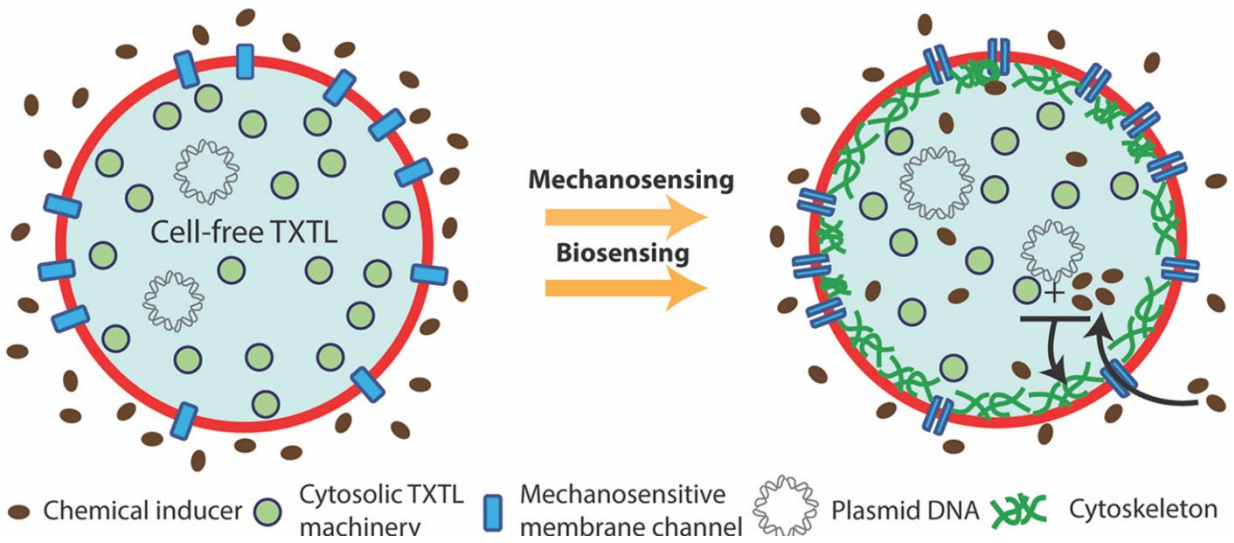

Figure 4.1: **Schematic depicting the proposed synthetic cell.** Transition of synthetic cell from its native state to an active state (development of cell-like cytoskeletal cortex) in response to mechanical and chemical stimuli.

TXTL reactions expressing MscL and couple its mechanosensitivity in response to hypo-osmotic conditions to the influx of chemical inducers which, in turn, change the phenotype of synthetic cells (Figure 4.1). The TXTL system supplies both a cytosolic environment and the machinery to express proteins from plasmid DNA. While we made a mechanosensitive vesicle as described in Chapter 3[180], in this work, we explored ways to couple mechanosensitivity with gene expression. This is desirable to look into the effect of protein-protein interaction with temporal control through an external stimulus. Since protein production in CFE is governed by the complexity of the gene circuit, effect of changing concentration of the expressed protein can be monitored over time. Given known interaction of MreB with cell membranes and its role in maintaining rod like shapes in bacteria, the choice of protein is suited to be studied in a mechanosensitive synthetic cell.

4.1.2 Design of synthetic cell with inducible gene circuit

The interior of the liposome contains a TXTL reaction and plasmid DNA, while the exterior feeding solution contains a chemical inducer that regulates gene expression by either binding mRNA or sequestering a repressor. When this liposome is in an iso-osmotic environment, the inducer cannot cross the bilayer membrane. However, upon hypo-osmotic conditions, the channels open and the membrane becomes permeable to the inducer. Subsequently, the *E. coli* cytoskeleton protein MreB is expressed and associates with the inner membrane of the liposome. Such synthetic cell system has not been achieved previously because it requires engineering and coordinating several processes in micron-sized compartments. First, tight and inducible genetic regulation has to be achieved in liposomes. Second, the bilayer has to be functionalized with stress-responsive membrane proteins to enable selective and adaptive permeability. Third, the output of the circuit has to be specific to the applied stress. In our pursuit of this goal, we designed and tested three synthetic cell prototypes. We describe our motivations for each iteration. All the DNA circuits were first tested in batch mode TXTL reactions to optimize and characterize plasmid stoichiometry before encapsulation in cell-sized liposomes.

4.2 Materials and Methods

4.2.1 Materials

All reagents unless otherwise mentioned were purchased from Sigma-Aldrich (St. Louis, MO). Lipids were purchased from Avanti Polar Lipids Inc. (Alabaster, AL). Synthetic DNA was purchased from Integrated DNA Technologies (Coralville, IA).

4.2.2 DNA Constructs

The plasmids P70a-σ28, P28a-deGFP, P70a-T7RNAP, and T7p14-deGFP have been described previously[183]. P28a-Venus-MreB was obtained by inserting Venus-MreB28 into

a P28a backbone between SalI and BamHI. T7p14-MscL was obtained by cloning MscL into a backbone. Specifically, MscL was obtained via PCR from *E. coli* K12 and inserted into a T7p14 backbone between restriction sites XbaI and XhoI. The switch/trigger pair used was first described by Green et al. as toehold switch number 10 in their set of forward-engineered toehold switches in Table S3.20[215]. The plasmid P70a-switch-σ28 was constructed by inserting a gBlock gene fragment (IDT) into the plasmid P70a-σ28 between NheI and BamHI. The plasmid T7p14-trigger was cloned by inserting a gBlock gene fragment (IDT) of the trigger sequence into T7p14-deGFP between BglII and XhoI. T7p14-switch-deGFP was obtained by inserting a gBlock gene fragment (IDT) of the switch-deGFP sequence into T7p14-deGFP between XbaI and XhoI. The single stranded trigger DNA (ssDNA) fragment was ordered from IDT and resuspended in water at 500 μM. The LacO1 and TetO1 plasmids were constructed using synthetic regulatory parts[216].

4.2.3 TXTL Reactions

The myTXTL kit (Arbor Biosciences) was used. TXTL reactions are composed of an *E. coli* lysate, an amino acid mixture, an energy buffer, and the desired DNA templates. The preparation of the lysate used for TXTL has been extensively described in prior works[183,217]. The lysate represents roughly one-third of the total reaction volume and contains the endogenous machinery required for both transcription and translation. The amino acid mixture is an equimolar blend of the 20 canonical amino acids, with the total amino acid concentration in the final reaction fixed between 2 and 4 mM. When linear DNA was used, Chi6 was added to the reaction at 2 μM to prevent degradation[218].

4.2.4 Bulk Expression Assay

Fluorescence from batch mode TXTL reactions was measured using the reporter protein deGFP (25.4 kDa, 1 mg/mL = 39.4 μM), a more translatable version of GFP in TXTL[219]. Fluorescence was measured at 3 min intervals using monochromators (Ex/Em 488/525 nm) on Biotek Syngery H1 plate readers in Nunc polypropylene 96-well, V-bottom plates. End point reactions were measured after 8-12 h of incubation. To measure protein concentration, a linear calibration curve of fluorescence intensity versus eGFP concentration was generated using purified recombinant eGFP obtained from Cell Biolabs, Inc. or purified in the lab. All reactions were incubated at 29 °C in either a benchtop incubator, for end-point measurements, or in the plate readers, for kinetic measurements.

4.2.5 Liposome preparation

Liposomes were prepared using a microfluidic device suitable for encapsulating complex biochemical solutions as illustrated in detail in a previous publication[162]. Briefly, W/O/W double emulsions were made using the cell-free solution as the inner phase and a buffer solution (20 mM K-HEPES pH 7.5, 70 mM potassium chloride, 1.3% glycerol, 10% poly(vinyl alcohol), 1% Pluronic F-68, 10 mM magnesium chloride and 170 mM glucose) as the outer aqueous phase. A mixture of DOPC, DOPE, cholesterol and Liss-Rhod PE in the ratio of 60:9.9:30:0.1 by mole was prepared in a glass vial which was then subjected to a steady stream of argon gas to remove residual chloroform from the mixture and generate a pseudo dry lipid film on the glass surface. The glass vial was then placed under vacuum for 2 h at room temperature to ensure minimal traces of residual chloroform before resuspending in 1 mL of oil phase (hexane and chloroform in a ratio of 64:36 by volume). 750 μL of formed double emulsion solution was collected in an epi tube and

incubated at 29 °C for 1 h following which 250 µL of buffer containing 20 mM K-HEPES pH 7.5, 10% PVA and 10 mM IPTG or 100 µM trigger DNA was added to get a final outer solution with osmolality ~100 mOsm/kg less than the inner cell-free solution. This osmotic difference was chosen as we had previously observed the MscL activation at similar osmolarity differences. The osmolarities were measured prior to liposome encapsulation using a vapor pressure osmometer (Vapro, Wescor). The osmolality of the cell-free reaction was previously measured to increase with time by about 1.5-2% depending on the type of protein being expressed. Following the incubation for 1 h and subsequent addition of buffer containing IPTG or trigger DNA, the now formed liposomes were gently filled into imaging chambers on a glass slide, sealed and allowed to incubate at 29 °C for 6 hours.

4.2.6 Imaging

All images of liposomes were taken with an inverted spinning disk confocal microscope setup. An Olympus IX-81 scope connected to an Andor iXon3 CCD camera were used to image the liposomes. Solid state lasers with ALC tuning (488 nm for deGFP and 561 nm for Liss-Rhod PE) were used to excite the liposomes, respectively. All image analysis was carried out in ImageJ. In order to quantify fluorescence intensities when using the fluorescent trigger or following IPTG induction of deGFP synthesis, three large rectangular regions of interest were randomly made inside the lumen of each liposome and the average intensity calculated. Thereafter the same three regions were translated to the outside of the liposomes to record the average background intensities. The final background corrected intensities as calculated were normalized and plotted in Origin Pro. For the line scan plot, three lines of equal length were drawn across a single liposome

and the average values of the intensities were calculated after background subtraction. The intensity values for the liposome corresponding to the positive control scenario was normalized with respect to its maximum value while the other two liposome intensities were normalized by dividing by the maximum value of the liposome under hypo-osmotic condition subjected to IPTG induction. In order to normalize the line plot intensities with respect to the diameter of each liposome, the smallest liposome diameter was chosen as the reference line. The intensities for all the liposomes were then parsed into the total number of data points available for this reference liposome. A MATLAB code was written to carry out the above procedure. The plots for the Supplementary Figures were generated in Origin Pro. All error bars indicate the standard deviation of all data collected for each condition.

4.3 Results

4.3.1 Prototype I: using riboswitches to regulate protein synthesis

Toehold switches are a class of synthetic riboregulators that have been developed to have both a high degree of orthogonality and a high dynamic range[215]. They typically function using the secondary structures available to mRNA, with the ribosome binding site (RBS) and start codon masked in an RNA hairpin. Upstream of this hairpin is a “switch” sequence, which can be bound by a “trigger” transcript. When bound by the trigger, the hairpin unfolds and the RBS becomes available for translation initiation. These switches can be engineered to work with arbitrary sequences, allowing for the creation of a large set of toehold switches in a potential synthetic cell[184]. Given their versatility and ability to be used as regulators in simultaneous translation of orthogonally expressed proteins, we aimed to implement toehold switches in our first generation of

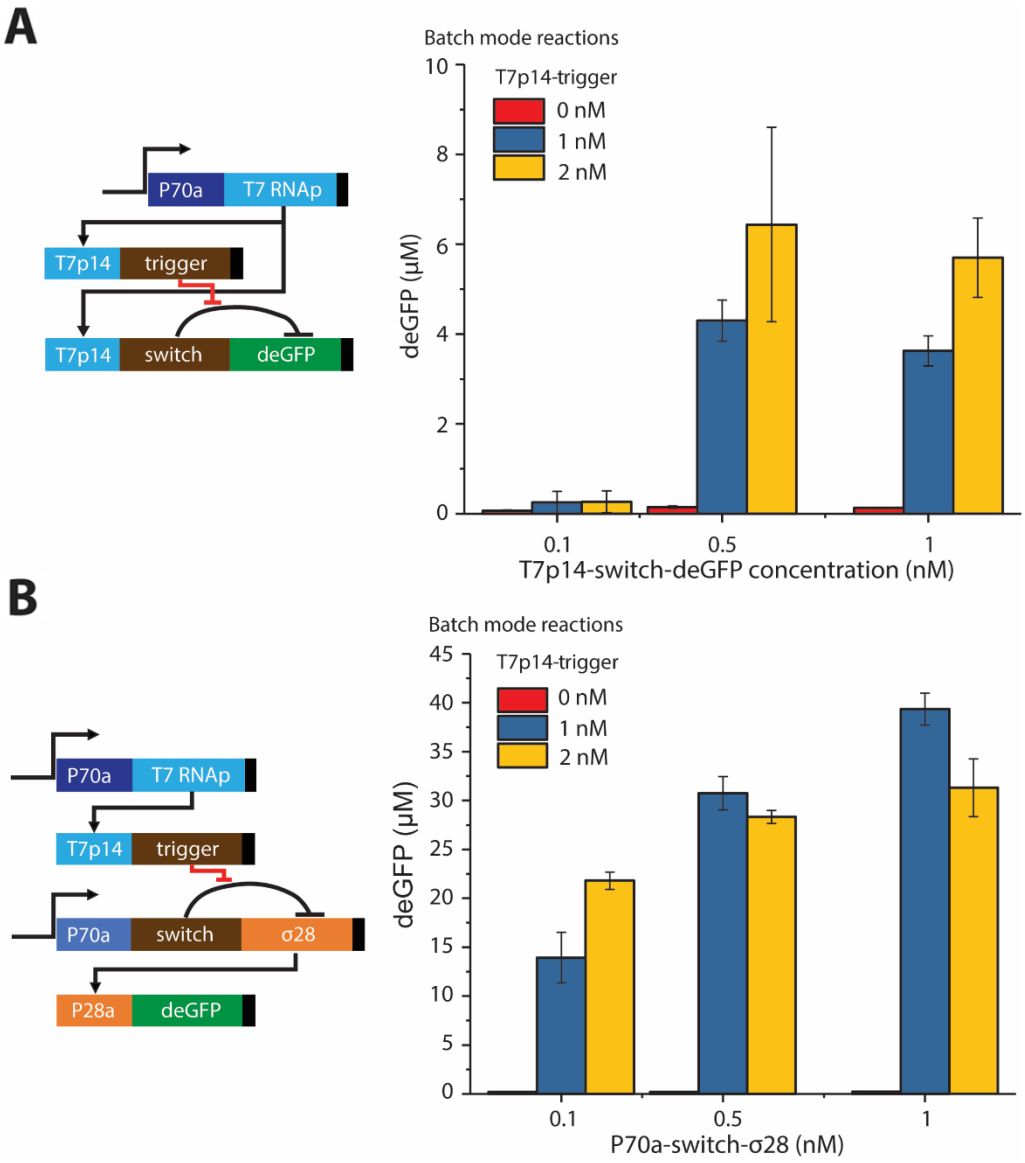

Figure 4.2: Kinetics of toehold switch-mediated deGFP expression with two different gene circuits. (A) deGFP expression via the toehold switch cascade using the T7 promotor to express both switch and trigger sequences from plasmid DNA. (B) deGFP expression via an amplified toehold switch cascade in which the P70a promoter is used to express switch-σ28, and deGFP is expressed via the P28a promoter. Concentrations of switch and trigger plasmids were kept the same as a) and the concentration of P28a-deGFP plasmid was fixed at 5 nM.

mechanosensitive, genetically adaptive synthetic cell prototype. Using the strong T7 promoter, we cloned toehold switch and trigger sequences previously tested[215] into separate plasmids, T7p14-switch-deGFP, which uses the switch to control the expression of deGFP, and T7p14-trigger, which expresses the 30-nucleotide trigger sequence corresponding to the specific switch. In bulk TXTL reactions (2 μL) expressing T7 RNAP

from the P70aT7RNAP plasmid, this switch gave an ON/OFF ratio of 75-80 while expressing 5-6 μM active deGFP protein (Figure 4.2A).

To improve the ON/OFF ratio and to increase protein expression, we designed an amplified toehold switch using sigma factor 28 (σ28) from *E. coli*. The promoter corresponding to σ28, P28a, has a high affinity for the *E. coli* RNAP/σ28 holoenzyme characterized by a high protein expression with relatively low levels of σ28 as only 1-2 μM σ28 is needed for optimal expression. Using such a strong sigma factor also minimizes the load on the system such that other proteins can be produced. Instead of using the trigger sequence to allow translation of deGFP, we placed σ28 under the control of the switch using a P70a-switch-σ28 plasmid and expressed deGFP using the P28a-deGFP plasmid[183]. In doing this, we do not waste TXTL resources expressing large quantities of switch-σ28 mRNA, since only a small amount is needed to drive expression via P28a. The trigger RNA was still produced using a T7 cascade. With this scheme, the ON/OFF ratio increased over 2-fold, up to a ratio of 176, while deGFP expression increased by a factor of 6 to 39 μM (Figure 4.2B). Our next step was to demonstrate that this amplified toehold switch functioned without expressing the trigger RNA from a plasmid, but by adding to the reaction an oligonucleotide that could be used as an inducer. Testing the amplifier with ssDNA in batch mode TXTL reactions, we searched for a stoichiometric regime where we could observe a strong and specific induction. We found the optimal concentrations to be 50 μM trigger ssDNA and 1 nM P70a-switch-σ28 plasmid (Figure 4.3A). Using 5 nM P28a-deGFP plasmid along with the afore-mentioned concentrations of trigger ssDNA and P70aswitch-σ28, we expressed 31 μM deGFP while maintaining an ON/OFF ratio of 140. Although protein expression increased when the concentration of P70a-switch-σ28 was set to 4 nM, control over the amplified toehold

dramatically decreased, with the circuit active even in the absence of trigger ssDNA. This leak resulting in the production of σ28, though small, is enough to drive moderate TXTL expression through the P28a promoter.

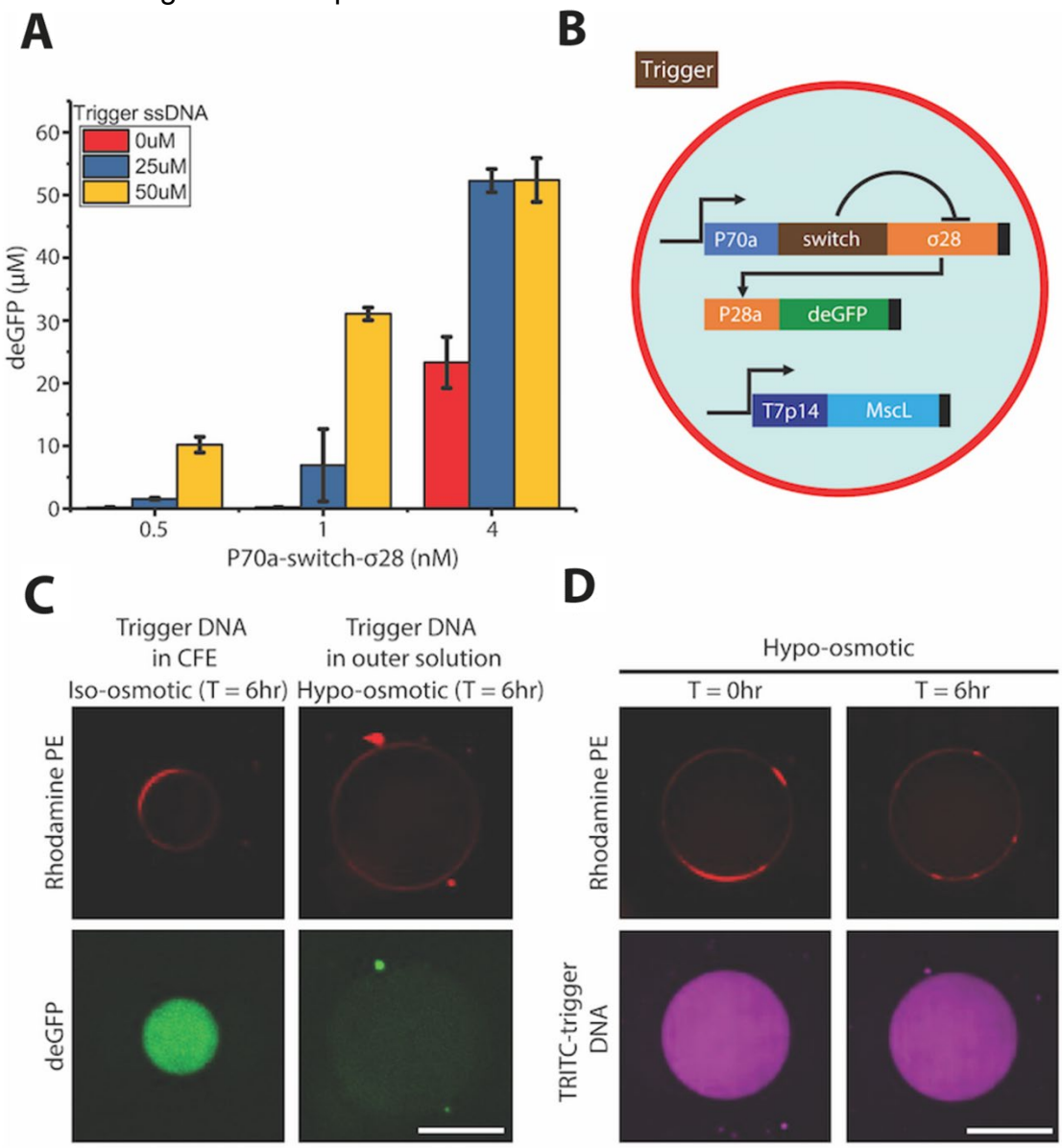

Figure 4.3: **Gene expression using toehold switch triggered by ssDNA in mechanosensitive liposomes** (A) Plot showing the end point deGFP expression of the toehold switch cascade with different concentrations of switch plasmid and the trigger ssDNA in TXTL reactions performed in batch mode reactions. (B) Schematic representing the first minimal cell model where the toehold switch cascade is encapsulated along with a TXTL reaction inside liposomes, orthogonally programmed to express MscL through the T7 promoter, which are then exposed to an outer solution containing the trigger ssDNA. (C) Images of liposomes expressing deGFP with the trigger ssDNA inside (iso-osmotic conditions) or outside (hypo-osmotic conditions) the liposomes, respectively. (D) Images of liposomes expressing MscL containing 50 μM TRITC-labeled trigger ssDNA that are exposed to a hypo-osmotic solution for 6 h. Rhodamine labeled PE lipids were used to visualize liposomal membranes. Scale bar: 50 μm.

On the basis of our findings from batch mode toehold reactions, we proceeded to engineer our first synthetic cell prototype by encapsulating TXTL reactions in double emulsion templated cell-sized phospholipid bilayer vesicles. The TXTL reactions contained an amplified toehold switch with its activation dependent on the influx of trigger ssDNA through MscL generated by a T7 cascade (Figure 4.3B). As a positive control, the trigger ssDNA was encapsulated inside the vesicles under iso-osmotic conditions and compared with adding the trigger sequence to the exterior solution under hypo-osmotic conditions. The reaction output was measured by the fluorescence of deGFP in the lumen of the vesicles. After 6 h, the reactions with the trigger ssDNA inside produced 9-10 times more deGFP than those with the trigger in the external solution under hypo-osmotic condition (Figures 4.3C and 4.4A). This suggests that the trigger ssDNA might not be able

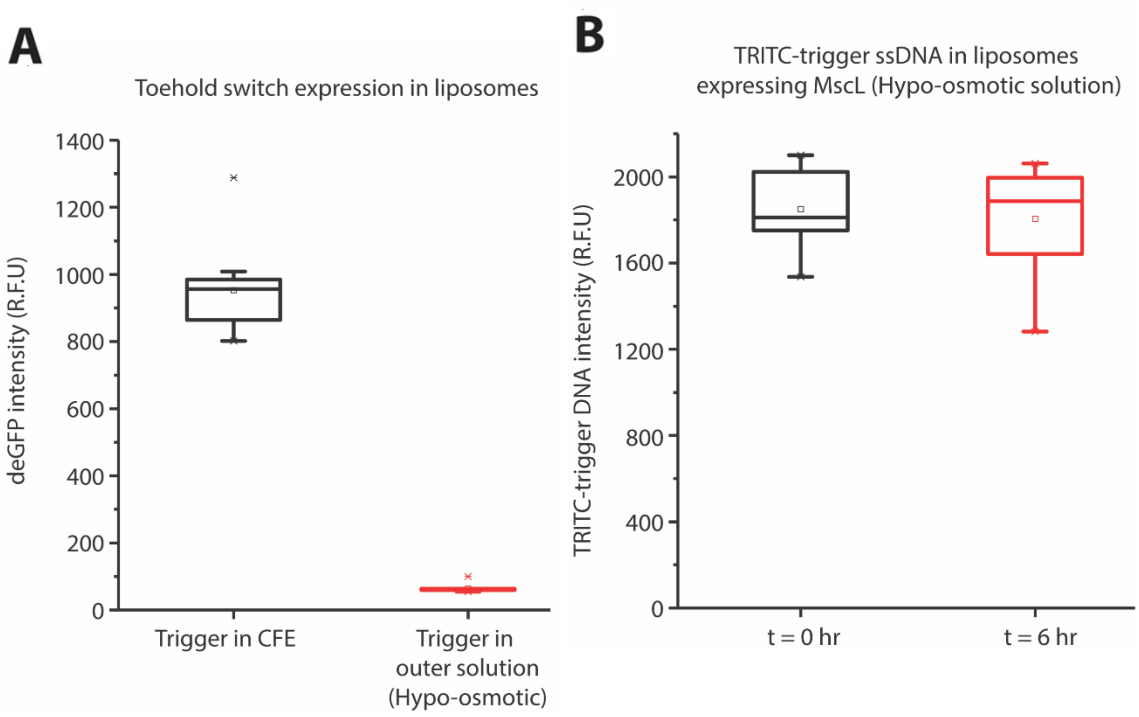

Figure 4.4: Trigger DNA is unable to pass through MscL within relevant time scales for CFE. (A) Boxplot of deGFP fluorescence in the vesicle lumen when 50 μM trigger ssDNA is either inside the vesicle or in the external solution. (B) Boxplot of TRITC-conjugated trigger ssDNA fluorescence in the vesicle lumen at 0 and 6 h after encapsulation and exposure to hypo-osmotic solution. MscL is expressed using the T7 promoter. 10 liposomes observed were analyzed for each condition. Boxes indicate 20th and 80th percentile values for each condition.

to enter the vesicles through MscL under hypo-osmotic conditions.

To confirm this, fluorescently labeled trigger ssDNA was encapsulated and the leakage through MscL was monitored under hypo-osmotic conditions (Figure 4.3D). No statistically significant change in the fluorescence intensities after 6 h was observed, confirming that the 30-nt trigger ssDNA is too large to pass through the ~2.5 nm diameter pore[220] (Figure 4.4B). Given the ionic strength of the buffer in which the liposomes were incubated in, we assumed the persistence length of ssDNA to be between 2-5 nm[221,222]. This suggests that the trigger sequence could potentially pass through the pore in hypo-osmotic conditions without considering reptation, which would require much longer time scales.

4.3.2 Prototype II: Simulating bacterial induction in TXTL with lac operon

The second synthetic cell prototype was based upon one of the most studied genetic signaling pathways in bacteria: the lac operon. Generally, this pathway regulates *E. coli*'s ability to consume lactose in the absence of glucose. We used the synthetic regulatory part, PL-LacO1, consisting of a strong σ70 promoter and two lac operators[216]. The lac repressor gene lacI and the reporter gene deGFP were cloned under the synthetic promoters PL-TetO1 and PL-LacO1, respectively; synthesis of MscL remained under the control of the T7 promoter. TXTL reactions containing these plasmids were encapsulated inside liposomes while IPTG, which inhibits repression by LacI, was added to the external feeding solution (Figure 4.5A). Initially, no deGFP fluorescence was observed inside the vesicles. After 6 h, there was a 5-fold increase in fluorescence intensities of vesicles exposed to hypo-osmotic conditions, while an increase of less than a factor of 2 was observed in vesicles kept at iso-osmotic conditions (Figure 4.5B). These data suggest

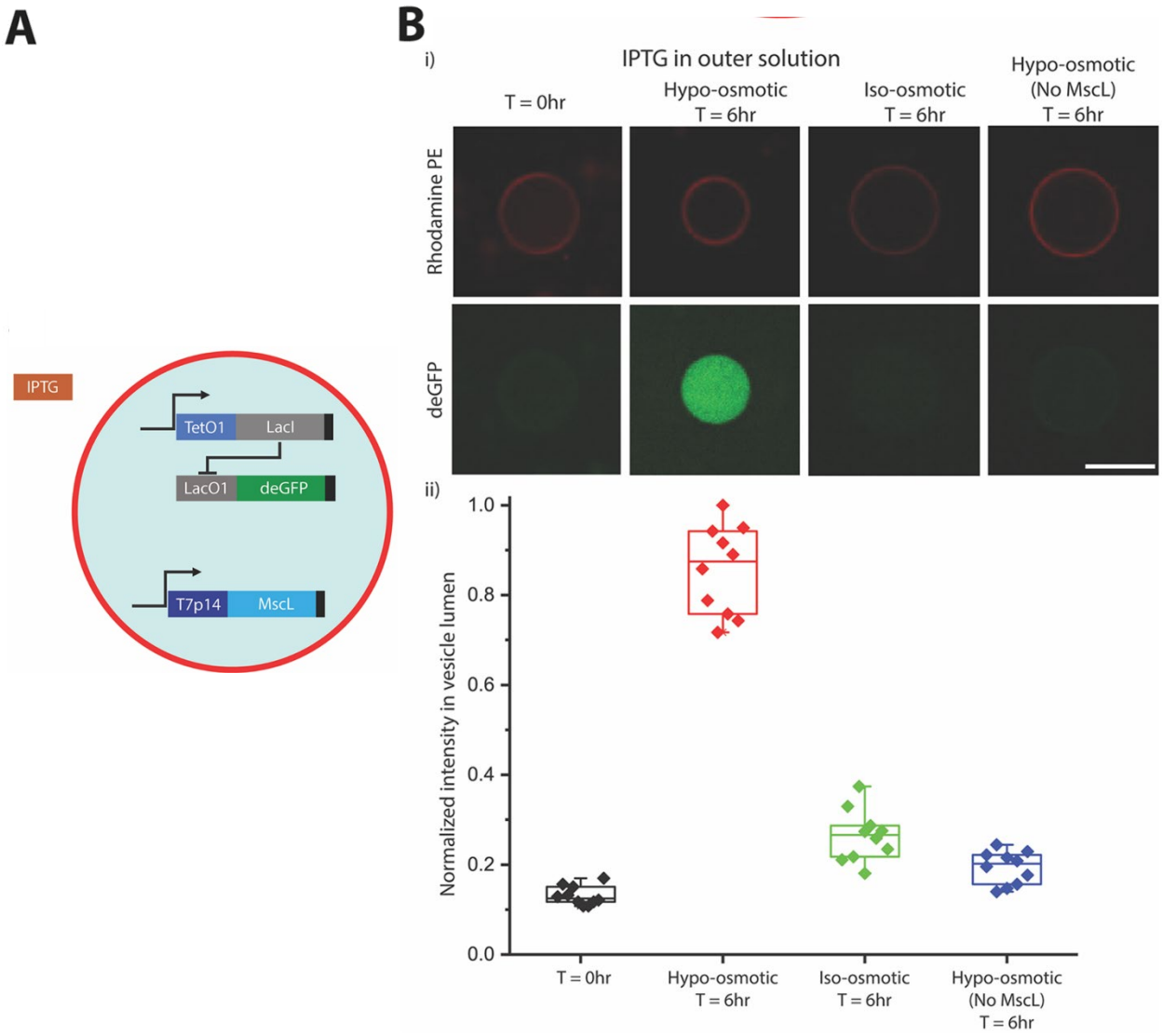

Figure 4.5: **IPTG induction of deGFP in response to hypo-osmotic shock.** (A) Schematic depicting the second model of the proposed synthetic cell co-expressing an inducible gene circuit and MscL constitutively. IPTG, the inducer, is in the outer solution. (B) (i) Fluorescence images showing expression of deGFP inside liposomes exposed to outer solutions with IPTG and different osmotic conditions at 0 and 6 h. (ii) Box plot of deGFP fluorescence in the vesicle lumen under the different osmotic conditions. Ten liposomes were measured for each condition. Rhodamine labeled PE lipids were used to visualize liposomal membranes. Boxes indicate 20th and 80th percentile values for each condition. Scale bar: 50 μm.

that gene expression is induced by IPTG entering the vesicles through MscL and this predominantly occurs in response to osmotic pressure differences between the internal and external solutions.

In the absence of MscL and in hypo-osmotic conditions, a slight induction close to background level was observed when IPTG was added in the external solution (Figure

4.5B). In the absence of IPTG, a slight leak of the PL-LacO1 induction system was observed (Figure S3 in published manuscript[203]). Both tests suggest that the leak observed in the iso-osmotic condition (Figure 4.5B(ii)) is primarily due to the construct design and not due to the small amount of IPTG influx under iso-osmotic conditions. The PL-LacO1 promoter offers strong gene repression but is too weak in TXTL. As is, however, the magnitude of the circuit output is too weak to induce the expression of MreB at a concentration sufficiently high to assemble at the inner membrane of liposomes because the critical concentration for polymerization of MreB is estimated to be around 1.5 μM[223] (Figure 4.6A).

4.3.3 Prototype III: Combining IPTG induction with gene amplifier circuit

To overcome the problem of low rate of protein synthesis post induction with IPTG, we developed an amplifier, again using the σ28 cascade. The σ28 gene was cloned under the PL-Lac01 promoter and deGFP was placed under the control of the P28a promoter. LacI now repressed the production of σ28, without which deGFP could not be expressed. The standard PL-Lac01 promoter showed linear protein expression in bulk reactions 30 minutes after the beginning of the reaction when 200 μM IPTG was added from the start (Figure 4.6A,B). The case where the reaction was allowed to incubate for 1 h before the addition of IPTG was also tested to ensure that the circuit can indeed be induced when LacI is already blocking the promoter site. This was important to simulate delayed induction of the proposed cell-like liposomes post assembly due to an externally triggered osmotic shock. When this was done, protein expression was identical to a reaction without IPTG for 90 min, when deGFP fluorescence could be measured. Once protein expression began, the synthesis rates in both cases were the same, around 0.1 μM/h. In the amplified

PL-Lac01 circuit with IPTG present from the start, there was a greater delay (60 min as opposed to 30 min) between the onset of the reaction and the measurement of deGFP fluorescence as σ28 needs to be expressed prior to deGFP. The delay in reactions induced after 60 min was likewise longer than in the unamplified circuit, with protein production not evident until 60 min from induction.

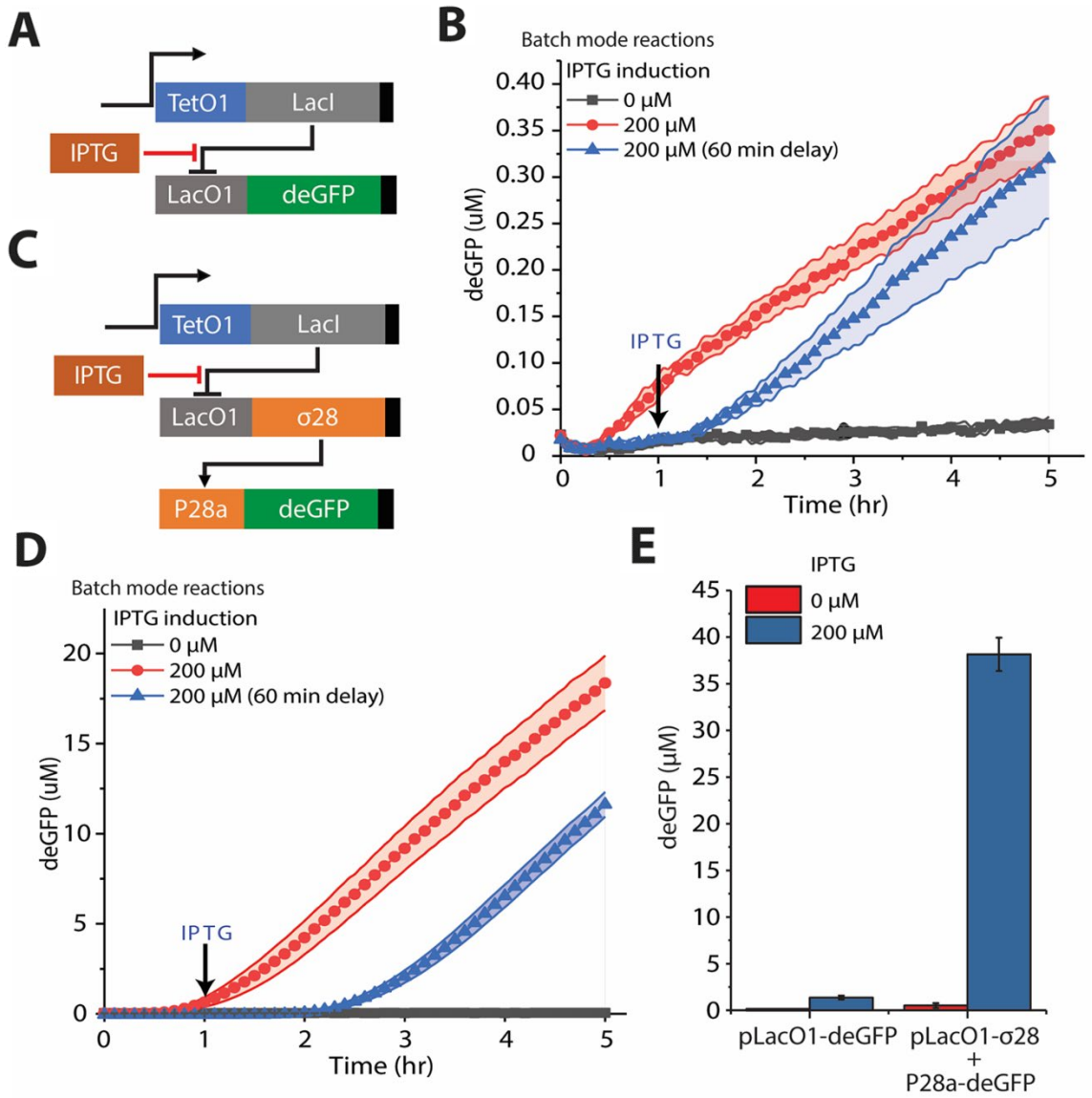

Figure 4.6: **Amplifier circuit allows higher sensitivity to IPTG and increase in final yield of deGFP.** (A) Schematic of the unamplified inducible gene circuit. (B) Kinetics of deGFP expression in batch mode TXTL reactions using the circuit shown in (A) with no IPTG; induction at time T = 0 h; and delayed induction at time T = 1 h. (C) Schematic of an amplified inducible circuit using the σ28 cascade. (D) Kinetics of deGFP expression in batch mode TXTL reactions using the circuit shown in (C) with no IPTG; induction at time T = 0 h; and delayed induction at time T = 1 h. (E) Plot of end point deGFP expression with and without IPTG induction after 14 h for the gene circuits shown in (A) and (C).

Again, the rates of protein expression were the same in this linear regime, around 5 μM/h (Figure 4.6C,D). After both circuits were incubated until completion (>12 h), the amplified circuit produced 38.5 μM deGFP compared to 1.3 μM for the unamplified circuit. The amplified inducible circuit also gave a large ON/OFF ratio (presence vs absence of 200 μM IPTG) of 298 compared to 11 for the unamplified circuit, making it ideal for the purposes of this work (Figure 4.6E). We have shown thus far that gene expression can be regulated via mechanosensing and biosensing.

4.3.4 Induction of MreB synthesis using hypo-osmotic shock results in membrane association in liposomes

Given the overarching goal of designing a functional minimal cell, we aimed to advance beyond expressing a reporter protein in the third prototype of synthetic cells. A fluorescent MreB fusion protein (Venus-MreB) was placed under the control of P28a which, in turn, was placed under the control of PL-LacO1. Thus, Venus-MreB would only be expressed in the presence of IPTG (Figure 4.7A). After 6 h of incubation under hypo-osmotic conditions, vesicles containing the T7p14-MscL plasmid showed fluorescence at the lipid bilayer while those not expressing MscL did not (Figure 4.7B). The positive control, in which IPTG was encapsulated along with the TXTL reaction in iso-osmotic conditions, showed the same localization of MreB at the membrane, confirming that the observation made in hypo-osmotic conditions with IPTG outside was caused by the influx of inducer through the transiently opened MscL. The concentration of fluorescence at the membrane suggests that MreB is associated with the inner membrane and forms a strikingly different fluorescence pattern than that of deGFP only (Figure 4.7C).

MreB is known to localize at phospholipid bilayers when expressed *in vitro*[224,225]. In hypo-osmotic condition, we did not observe polymerization of MreB in the case without MscL as any leaky expression is likely below the critical concentration for MreB to polymerize. In contrast, in MscL-expressing vesicles, the formation of a ring-like structure

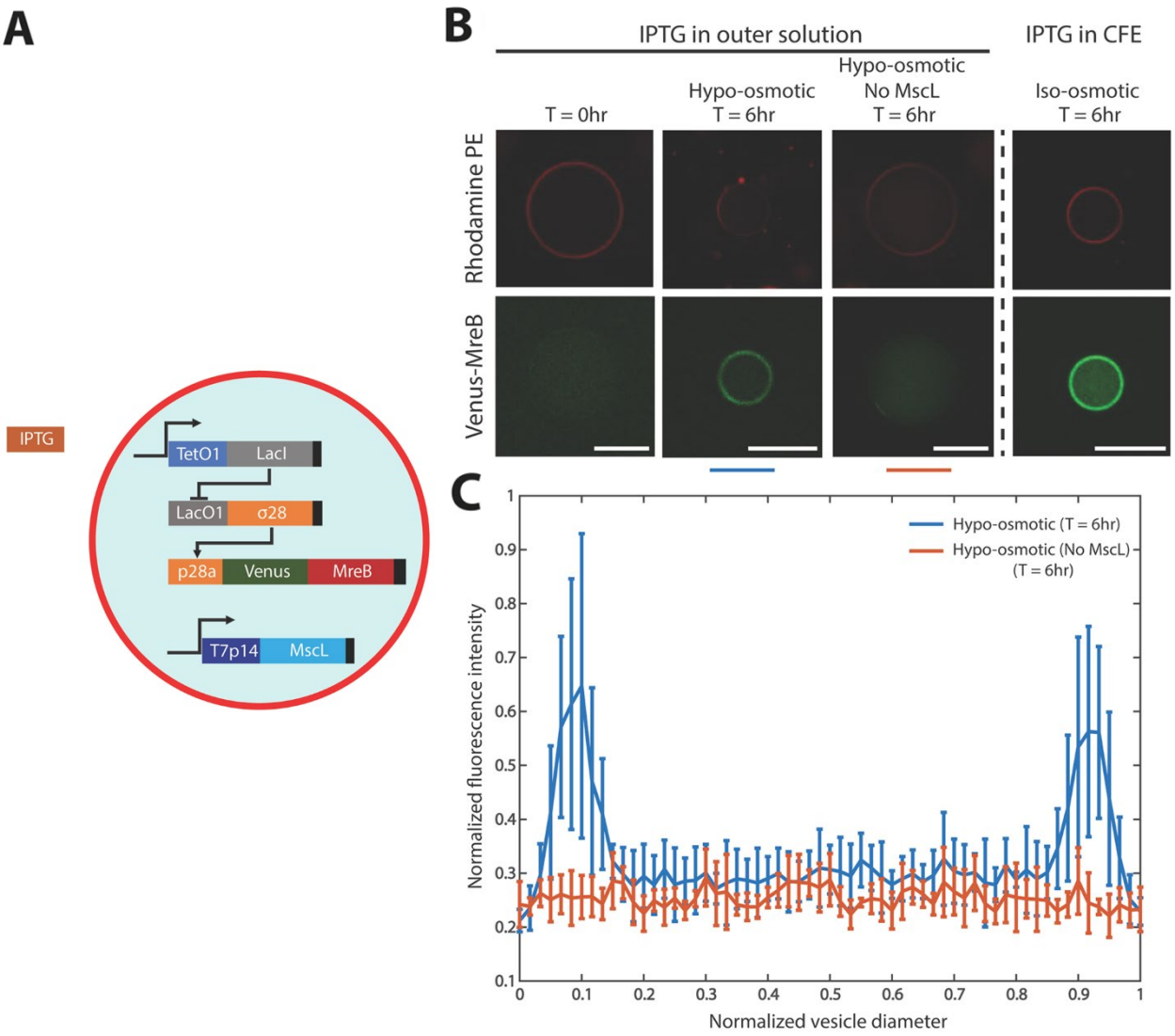

Figure 4.7: **MreB synthesis and pattern formation in liposome membranes in response to hypo-osmotic shock.** (A) Schematic depicting the third proposed synthetic cell system co-expressing an amplified gene circuit encoding the gene for VenusMreB and MscL constitutively. The liposomes were placed in a feeding solution containing 200 μM IPTG, except for the control experiment (IPTG inside liposomes). (B) IPTG induction of synthetic cells in outer solutions containing IPTG and different osmotic conditions over a time duration of 6 h and a positive control experiment with IPTG inside the liposomes. (C) Line scans of liposomes normalized with respect to their diameters and the maximum intensity among all liposomes observed. Five liposomes for each condition reported were analyzed. Error bars indicate standard deviation of the normalized data. Rhodamine labeled PE lipids were used to visualize liposomal membranes. Scale bars: 50 μm.

was prominent in ~90% of the liposomes exposed to the hypo-osmotic shock post synthesis. While the intensities varied owing to different levels of induction and IPTG influx, they were always slightly lower than the control scenario with IPTG encapsulated inside liposomes which can be attributed to delayed influx of IPTG though MscL and depletion of resources while incubating in iso-osmotic conditions prior to the hypo-osmotic shock. No physical deformation of the membrane was observed supposedly because the tension at the membrane is too high. Nevertheless, the assembly of a cortex-like MreB structure would presumably provide the vesicles with stronger mechanical resistance to external mechanical stresses, similar to the effect of what an actin cortex has in a mammalian cell[226]. On further investigation, we found interesting patterns for MreB association with the liposomal membrane based on the concentration and quality of plasmids used for cell-free expression. Previous studies have demonstrated variability in protein expression with single gene studies within a population of liposomes. Additionally, we found that the quality of plasmid (whether extracted with mini-prep or midi-prep) also affects the expression dynamics of MreB. At high concentrations of Venus-MreB plasmid (15 nM), we observed the formation of curved filaments homogenously associated with the membrane post induction (Figure 4.8). In contrast, low plasmid concentration results

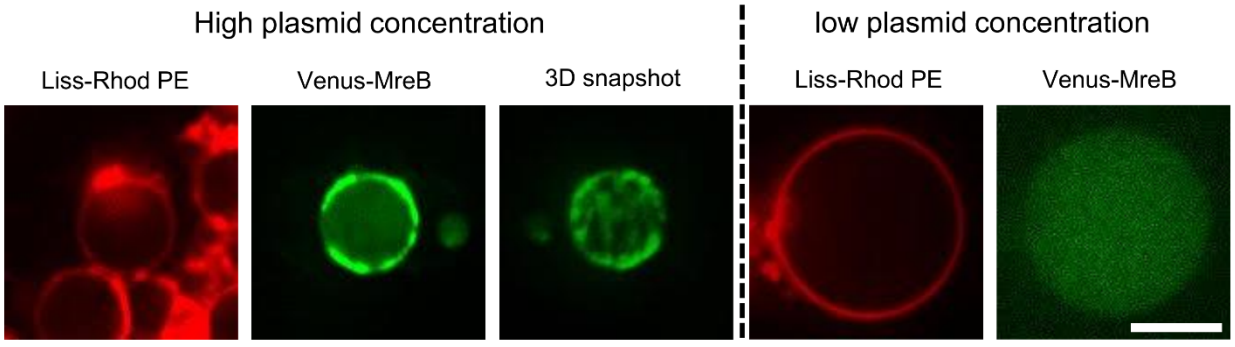

Figure 4.8: **Formation of ring-like networks on liposomal membranes**. Left, image of liposome with high plasmid concentration of Venus-MreB (15 nM) post induction. Right, liposome image with 5 nM plasmid after induction. Scale bar: 25 μm

in uniform fluorescence in the vesicle lumen confirming the concentration dependent kinetics of MreB polymerization and association with the membrane.

4.4 Conclusion

While generating a synthetic cell model capable of expressing multiple proteins with temporal and spatial variation is desirable to better understand and mimic cellular processes, it is important to reconstitute intercellular and extracellular interactions toward enabling the synthetic cells to respond to external, time-varying stimuli. The synthetic cell developed here is one such example and can be expanded further by leveraging orthogonal TXTL reactions to mediate simultaneous or sequential induction with different membrane impermeable molecules, thus providing modularity in the number of different systems that can be reconstituted within the same compartment. Prior to this work, liposomes were programmed with DNA to execute inducible gene circuits[128,201,209], express cytoskeleton proteins from *E. coli*[225] and, in separate experiments by these authors, to generate mechanosensitive biosensors[180]. To our knowledge, the work described here is the first work that couples an external stimulus to inducible gene expression by way of mechanosensitivity. Our experiments provide information on how to integrate multiple biological mechanisms into a synthetic cell system involving membrane properties and inducible gene expression. The experimental approach presented in this work could be used to learn the dynamics of multi-protein interactions or step-by-step assembly in order to better understand the complexities of real cells.

Chapter 5: Conclusion and Future Work

5.1 Summary

Recent advances in cell-free expression (CFE) systems and the development of cell membrane models have enabled the studies of a wide variety of membrane proteins. These reconstitution studies are primarily focused on expanding the repertoire of functional proteins that can be expressed using CFE *in vitro.* Through the work carried out in this dissertation, I have developed reconstitution platforms that better simulate the biological context of the proteins of interest at an organelle or cell-like level. I demonstrated the modularity of such platforms to address fundamental questions of organization and protein interactions and coupled reconstituted protein functions to cell-like macroscopic behaviors.

We found that the SUN proteins reconstituted into artificial lipid bilayers with a uniform orientation of insertion. Staining with ER tracker dyes revealed the presence of microsomes in our lysates. Ultracentrifugation and Western blot analyses demonstrated the localization of cell-free expressed SUN proteins in the microsome fraction, consistent with previous studies[111,227]. Using this experimental system, we determined the topology of SUN1 and SUN2 proteins and discovered previously unknown membrane spanning and membrane-associated regions. The reconstituted SUN proteins retained the ability to bind to KASH peptides, hinting at the possibility of homo-oligomerization of the SUN proteins in the membrane (studies have suggested that KASH protein binding promotes oligomerization[154,178]). The SUPER template beads were preferred over liposomes for

their robustness to multiple incubation periods and wash cycles. Overall, this platform in conjunction with simple biochemical assays and fluorescence microscopy can be used to decipher the topologies and functions of other membrane proteins.

In Chapter 3, we used liposomes as model membranes and encapsulated a CFE system instead of carrying out bulk reactions. Like cells, the encapsulated liposomes could be exposed to different solutions for studying functions of reconstituted membrane proteins. By using well characterized gene circuits in *E. coli* CFE, we developed an optical detection technique for monitoring the activity of MscL, a mechanosensitive channel, in response to osmotic stresses. In cells, activation of mechanosensitive channels is dependent on changes in local membrane tension which are affected by interactions with the coupled cytoskeleton. Membrane tension in liposomes can be externally controlled by mechanical stretching or osmotic gradients. Therefore, liposomes serve as ideal models for studying gating properties of mechanosensitive membrane proteins. The so-called synthetic cells were capable of sensing changes in physical and chemical environment. It is important to note that the developed system is modular in its use of CFE. By employing different gene circuits one can envision the production of a set of proteins whose activity could be coupled to a fluorescence-based output. This would allow the screening of a wide range of mutants and other proteins with similar functions without expressing them in cells, on a much shorter time scale.

Finally, in Chapter 4, I attempted to use mechanosensitivity of synthetic cells to mediate cell-like signaling culminating in induced gene expression. This was motivated by the necessity to reconstitute multiple proteins with temporal and spatial control. MreB is a well-studied actin-like protein in bacteria and its effect at different concentrations on

membranes was previously demonstrated[223,224]. By monitoring induced gene expression of MreB in response to osmotic shock, we found direct association of MreB with liposomal membranes. Further, different geometric patterns like rings and cortex-like structures on liposome membranes were observed based on the concentrations of the MreB plasmid encapsulated along with CFE. Through this study, we developed synthetic cells with gene circuits capable of inducing gene expression in response to osmotic stress. Such platforms can be used to study physical and chemical changes in liposomes as a result of multi-protein interactions in a time-dependent manner.

In summary, in this dissertation, I have exploited the potential of CFE in studying nuclear membrane proteins and carried out bottom-up *in vitro* reconstitution at a cellular scale with mechanosensitive and membrane-associated proteins. The knowledge gained through this investigation can help in the development of new assays with CFE for complementing cell biology studies and extend the paradigm for reconstitution of complex cellular pathways through construction of synthetic cells.

5.2 Future work and perspectives

5.2.1 Study of SUN-SUN and SUN-KASH interactions.

Our finding that SUN1 possesses three transmembrane domains (TMDs) stands in discord with previous reports, which concluded that SUN1 is a type II membrane protein with a single TMD based on *in situ* proteinase K digestions performed in HeLa cells expressing mouse SUN1 tagged with HA at their N-termini and EGFP followed by a Myc epitope at their C-termini[158,177]. The effect of proteinase K was subsequently assessed by Western blot analysis following Myc immunoprecipitation as well as by immunofluorescence microscopy. Even though two of the SUN1 hydrophobic regions

(HRs) could not be ruled out as being membrane-associated in these experiments, the authors concluded that SUN1 was a type II membrane protein with a single TMD. Since EGFP–SUN1$_{1\text{-}364}$–His$_6$ contains this HR and retains EGFP fluorescence in the presence of pronase, our results suggest that the first HR is in fact a TMD. We propose that the second HR peripherally associates with the luminal leaflet of the INM, where it may serve as a docking-site for an as-of-yet unidentified SUN1-binding partner present within the perinuclear space of the NE. The presence of multiple TMDs in SUN1 and not in SUN2 may be relevant during meiosis, when SUN1-containing the linker of nucleoskeleton and cytoskeleton (LINC) complexes associate with the telomeres of meiotic chromosomes to mediate their microtubule-dependent movement during homolog pairing via cytoplasmic dynein[141,157,228]. The additional TMDs may help buffer the shear and tensile forces applied to telomere-associated SUN1-containing LINC complexes by dyneins, which walk along microtubules oriented parallel to the nuclear envelope[229]. It will be interesting to determine whether the additional TMDs in SUN1 are required for this process.

The physiological relevance of the ability of the nucleoplasmid domain (ND) of SUN2 to peripherally associate with the nucleoplasmic leaflet of the inner nuclear membrane (INM) remains unknown. One intriguing possibility is that the peripheral membrane association of SUN2 may regulate its homo-oligomerization, as has been observed with HIV-1 Gag and matrix proteins[230] as well as Ras GTPases[231]. Another may be related to the targeting of SUN proteins to the INM following their synthesis in the ER/outer nuclear membrane (ONM). In order to gain access to the INM, newly synthesized SUN proteins utilize nuclear targeting sequences to move across nuclear pore complexes (NPCs) through a poorly defined mechanism[140,175]. Recently, the size of the ND of SUN proteins was estimated to be less than 10 nm in diameter[232], which is near

the upper size limit for the transport of the NDs of INM proteins through the NPC[233,234]. Thus, the additional TMDs and HR identified in SUN1 and SUN2 may serve to reduce the footprint of their NDs so that they can properly target the INM.

It is worth noting that unlike His_6–GST–EGFP, which evenly coats the surface of the SUPER templates, ANM (artificial nuclear membrane; SUPER template beads with reconstituted SUN proteins)-inserted EGFP–SUN1FL–His_6 and EGFP–SUN2FL–His_6 appear to form clusters within the membranes. These clusters may represent higher-order SUN protein oligomers, such as those previously suggested for SUN1[154,159,229]. Alternatively, these SUN protein clusters may highlight the existence of membrane nanodomains within the ANMs[235], which can be explored by altering the composition of lipids used to generate the SUPER templates. Moreover, the ND SUN constructs appear to be able to form fluorescent patches in ANMs similar to the FL SUN proteins. However, the ability of EGFP–SUN1ND and EGFP–SUN2ND to form these patches is not necessarily mutually exclusive with the previously proposed mechanisms of LD (luminal domain)-mediated higher-order SUN protein clustering[151,154,229].

Based on our results, we suggest that both the LDs and NDs of SUN proteins can separately homo-oligomerize within the perinuclear space of the nuclear envelope and nucleoplasm, respectively. It will be interesting to test this hypothesis experimentally in future studies. ANMs will allow for testing proposed mechanisms for regulating LINC complex assembly and/or disassembly in cells, which have been difficult to address experimentally. For example, the modulation of the oligomeric states of the coiled-coil (CC)-containing regions present within the LDs of SUN proteins was recently proposed as a potential target for the regulation of LINC complex assembly[152] because the homo-

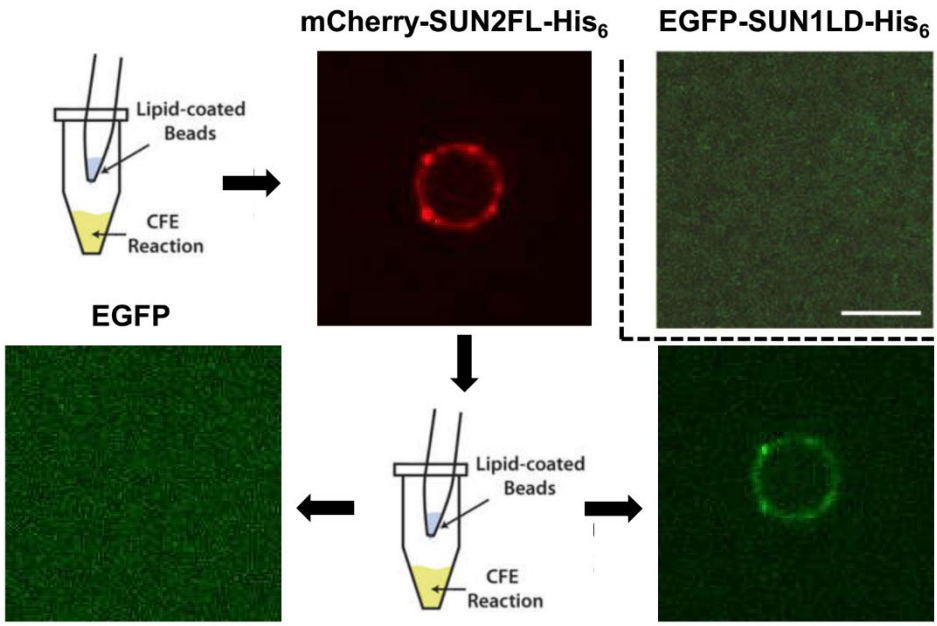

Figure 5.1: Interaction between luminal domains of SUN1 and SUN2 proteins. Image of a bead incubated with CFE expressing SUN1LD only on the right (top). Images of beads reconstituted with SUN2FL first (centre) and then with EGFP on the left or SUN1LD on the right (bottom). Scale bar: 5 µm

oligomerization of the SUN2 LD is essential for KASH peptide-binding[178]. Since these studies were performed using purified fragments of the LD of SUN2, it is essential that they be repeated using FL SUN proteins inserted into ANMs. Further evidence of the interaction of these CC domains among different SUN proteins was found from our ANM studies. When we expressed EGFP-SUN1LD on ANMs already reconstituted with mCherry-SUN2FL, we found association of SUN1LD with the membrane which was quite intriguing. Since SUN1LD does not interact with the SUPER template beads when expressed alone, this result suggests possible heteromeric interaction of the CC domains of SUN1 and SUN2 proteins which has not been reported before (Figure 5.1).

Alteration in the levels of intracellular Ca^{2+} also represents a potential regulator of LINC complex assembly, as the recently identified cation loop present within the SUN domain is required for the SUN–KASH interaction[178]. While deciphering the effects of altered intracellular Ca^{2+} levels on the engagement of SUN and KASH proteins within the

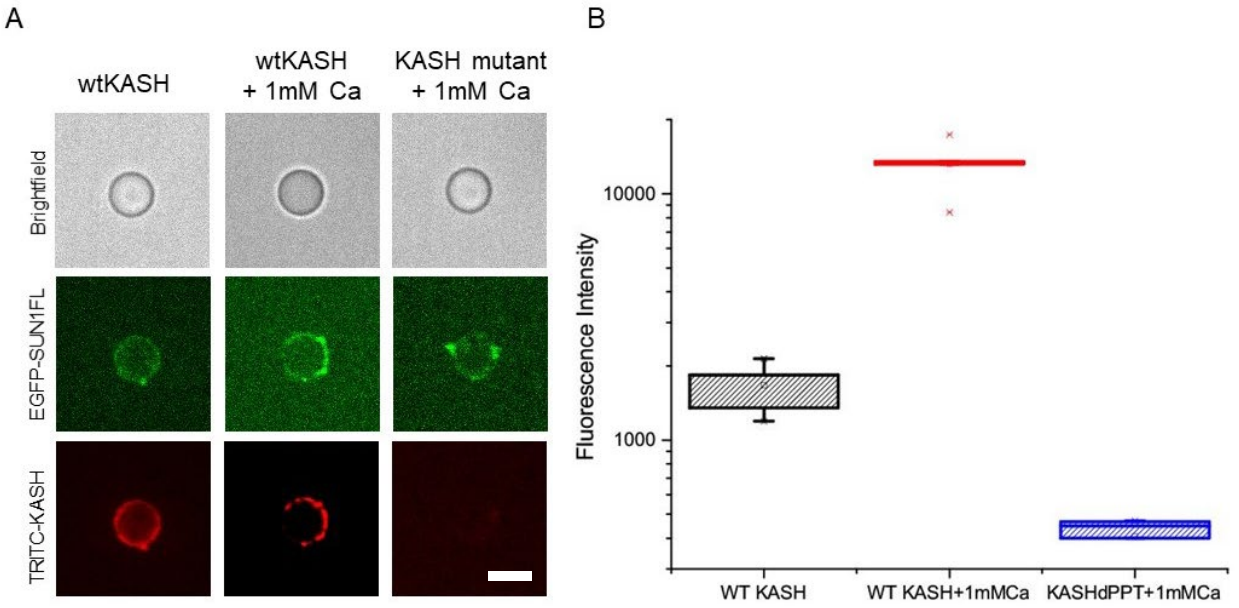

Figure 5.2: Calcium dependent binding affinity between SUN1FL and KASH peptide. (A) Images of beads with reconstituted SUN1FL-KASH interactions in the presence or absence of calcium for both wild type and mutant KASH peptides. (B) Box plots depicting statistical data of the relative fluorescence intensities from 5 beads for each condition. Final concentration of KASH peptides: 500nM. Scale bar: 5 µm

perinuclear space remains a significant technical challenge, the solvent-exposed LDs of FL SUN1 and SUN2 on the surface of ANMs provides a simplified system for testing the effect of manipulating calcium levels on LINC complex assembly. Preliminary studies show calcium-dependent increase in KASH binding of ANMs with SUN1FL (Figure 5.2). The effect is less prominent with SUN2FL. In addition, ANMs may help quantitatively assess the ability of KASH peptides from different nesprins to interact with SUN proteins. This will be especially interesting for the KASH peptides of KASH5 and lymphoid-restricted membrane protein, which unlike the KASH peptides of nesprins 1–3 lack the intermolecular SUN–KASH disulfide bond-forming conserved cysteine present at position -23[141].

Despite being non-essential for the SUN–KASH interaction, it was recently shown that the conserved cysteine residues present in SUN and nesprin proteins are required for actin-dependent nuclear anchorage, yet dispensable for microtubule-dependent

nuclear movement[179]. Therefore, KASH peptides containing this conserved cysteine residue may display differential SUN protein-binding kinetics compared to those that do not. Furthermore, ANMs may finally provide the long sought-after experimental system for defining the mechanism of LINC complex regulation by the luminal ATPase torsinA[236], owing to the lack of a need for protein purification. Besides SUN1 and SUN2, mammals express three additional testis-specific SUN proteins (SUN3, SUN4 and SUN5)[148]. While immunoprecipitation experiments show that SUN3 can associate with nesprin-1 and nesprin-3[237], the ability of SUN4 and SUN5 to interact with KASH proteins remains unknown.

Nevertheless, ANMs provide an ideal experimental platform for future explorations of the ability of these poorly studied SUN proteins to form LINC complexes. The use of ANMs is by no means limited to SUN and KASH proteins. ANMs can provide a simple and powerful experimental platform for structure/function analyses of any membrane protein, nuclear or otherwise. By bridging the gap between *in vitro* studies using purified proteins and *in vivo* imaging-based biochemical studies, ANMs open the door to a previously inaccessible set of experiments designed to provide mechanistic insights into protein behavior, which is invaluable in this post-genomic age. Akin to other attempts to use modular approaches for building synthetic cells or reconstituting cellular processes[3,204], future efforts will be aimed at reconstituting the nuclear lamina and its interaction with the nucleoplasmic domain of SUN proteins within an ANM.

Finally, it might be possible to use ANMs as templates for the reconstitution of an artificial nuclear envelope through a ‘layer-by-layer’ double-membrane assembly approach using poly L-lysine as an electrostatic polymer linker, which has been previously

shown to allow the formation of lipid multilayers via vesicle rupture onto existing supported lipid bilayers[238]. Owing to the ability of the nesprin KASH peptide to directly interact with the SUN protein SUN domain[150,178], ruptured nesprin-containing ER-derived microsomes generated by CFE would presumably coat the ANM containing the reconstituted SUN protein such that the nesprin N-terminus would extend into the solution while its C-terminus would face the ANM.

5.2.2 Understanding TorsinA dynamics and its role in Dystonia

TorsinA is a membrane-embedded AAA+ ATPase that is known to localize to the nuclear envelope and the ER. An autosomal dominant loss-of-function point mutation in TorsinA, ΔE, causes the childhood-onset neurological disease dystonia[239]. Previous studies have shown the shift in localization of TorsinA form the ER to the nuclear envelope depending on its interaction with other activator proteins like LULL1 and LAP1[240,241]. In the nuclear envelope, TorsinA is known to interact with SUN2, nesprin-2G and nesprin-3[241] which are components of the LINC complex. One aspect of impaired nuclear mechanotransduction in dystonia patients could be associated with the reduced efficiency of interaction of TorsinA- ΔE with SUN2 in the inner nuclear membrane[241]. TorsinA function in the nuclear envelope is also believed to be connected to lipid metabolism mediated by hyperactivity of phosphatidic acid phosphatase (lipin) in dystonia patients, as recent discoveries have shown[242]. Using the ANM approach, SUPER template beads can be used to study TorsinA dynamics with different mutants and other interacting proteins which will be difficult to probe in cells. Since the membrane composition can be

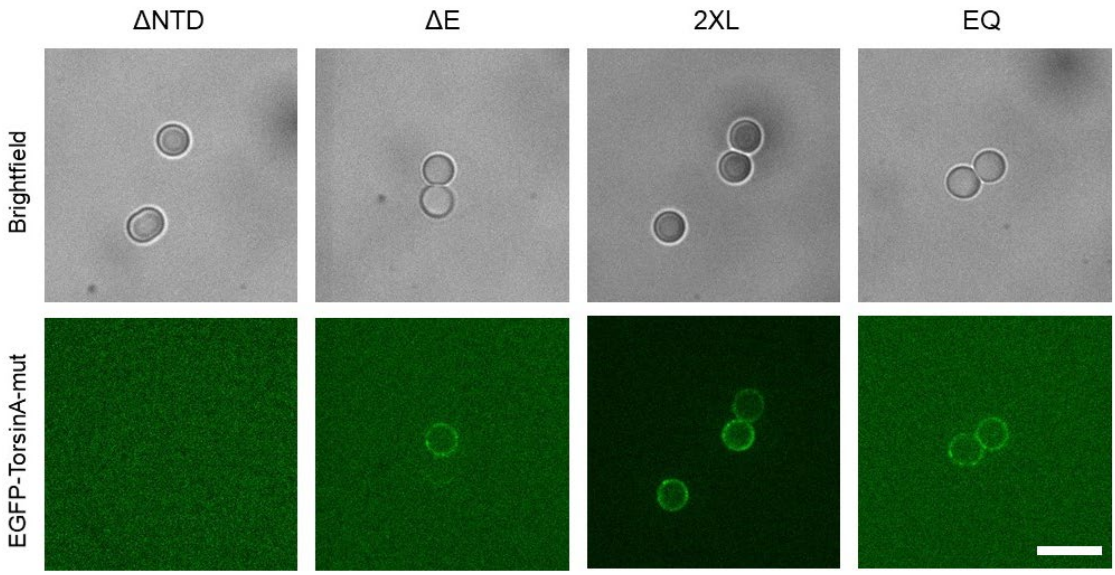

Figure 5.3: Reconstitution of TorsinA mutants on SUPER template beads. Scale bar: 10 µm

experimentally controlled, the effect of lipin-based phosphatidic acid metabolism on TorsinA activity can also be tested in our *in vitro* setup.

By cloning a few TorsinA mutants with N-terminally tagged EGFP, we have tested their reconstitution on SUPER template beads using our HeLa CFE (Figure 5.3). It has been shown before that TorsinA monotopically associates with the ER in its lumen[243]. This was evident from the green fluorescence observed on beads with the wild type protein. The loss-of-function mutant TorsinA-ΔE also seemed to interact with the membrane. The mutant with the deleted monotopic association domain, however, did not show any fluorescence on the beads. This confirms the absence of other hydrophobic regions in TorsinA which could lead to potential membrane interactions. A positive control for membrane insertion which converted the monotopic association domain into a full transmembrane domain (TorsinA-2XL) resulted in high fluorescence intensities on the beads. Finally, TorsinA-EQ also associated with the membrane as expected. EQ mutation inhibits the ability of TorsinA to hydrolyze ATP.

Thus, these preliminary studies demonstrate the potential of such an approach to explore the full range of torsinA functions in presence of SUN proteins (as previously reconstituted) and proteins like LAP1 and LULL1. Also, the formation of clusters on beads can be indicative of homo-oligomerization of torsinA which will be interesting to look at in future studies.

5.2.3 Calcium biosensor as a screen for identifying mechanosensitive channels

The development of a synthetic cell capable of mechanosensing and biosensing opens up the possibility of testing different types of mechanosensitive channels. The use of CFE for reconstitution is well suited for this purpose given the complex structure and gating mechanisms of known mechanosensitive channels. G-GECO is a fast calcium biosensor and its coupled synthesis along with MscL resulted in a high sensitivity to calcium influx. Purified G-GECO can be used as an alternative to detect calcium. However purified G-GECO is chelated to calcium present in bacterial cells. Subsequent sequestration of calcium with EGTA is not sufficient to mediate high ON/OFF ratios of fluorescence upon calcium binding. As has been shown in Chapter 3, the resultant fluorescence intensity is also proportional to the external calcium concentration suggesting some linear dependency in a small concentration range. By swapping the gene for MscL with any other protein, the same protocol can be applied to test for mechanosensitive behavior. Thus, we have developed a standard technique to couple mechanosensation with optical detection. Although a dye leakage assay can be used to mediate the same effect, the heterogeneity in encapsulation using non-microfluidic methods of liposome generation can cause difficulties in detection. Even with microfluidic approaches, the choice of dye will depend on the protein being studied since pore size

may affect diffusion of different dyes across the liposome membrane. Finally, known mechanosensitive mammalian channels like Piezo1 have very small pore diameters with selectivity towards cations[70]. Calcium influx is ideally suited to study their gating mechanisms in response to osmotic shock on these synthetic cells.

Using different populations of such synthetic cells, a screen for various mutants and possible candidates for non-selective or cation-specific mechanosensitive channels can be established. Since membrane tension in liposomes can be correlated to the osmolarity difference between the inner and outer solutions, the effect of different osmotic gradients can also be studied in these systems. While standard orthogonal promotor-based genetic circuits are not yet available for HeLa CFE, previous studies carried out in our lab suggest possible control over extent of protein expression based on plasmid concentrations with the same T7 promotor. The use of HeLa CFE is preferable for the expression of mammalian mechanosensitive channels owing to the presence of microsomes which might ensure better folding kinetics and successful reconstitution into liposomal membranes. Although a comparative study with the standard *E. coli* CFE with larger membrane proteins is yet to be done. Using our HeLa CFE, we have successfully expressed the large Piezo1 channel in bulk reactions (data not shown). We found evidence of Piezo1 localization in the microsomal fraction which is promising for future reconstitution studies.

5.2.4 Shear-based activation of mechanosensitive channels

Another application of the work presented in Chapter 3 is to examine effect of shear stresses on the activation of MscL and other mechanosensitive proteins. Previous theoretical calculations and computational models have shown the possibility of stretch-

activated gating of MscL on liposomes subjected to fluid shear forces[244]. Other channels like Peizo1 are known to be activated in blood vessels[65] and in cells subjected to external fluid shear stresses *in vitro*[71]. But, given the interaction of cell membranes with cytoskeletal proteins, true response to membrane stretch cannot be easily decoupled. Using our synthetic cell model with calcium-based G-GECO fluorescence, one can envision the study of mechanosensitive behavior under fluid flow.

Towards such an attempt, we have developed microfluidic devices capable of capturing CFE encapsulated liposomes within different channel widths. Subsequently, calcium-containing iso-osmotic solutions at different concentrations can be flowed

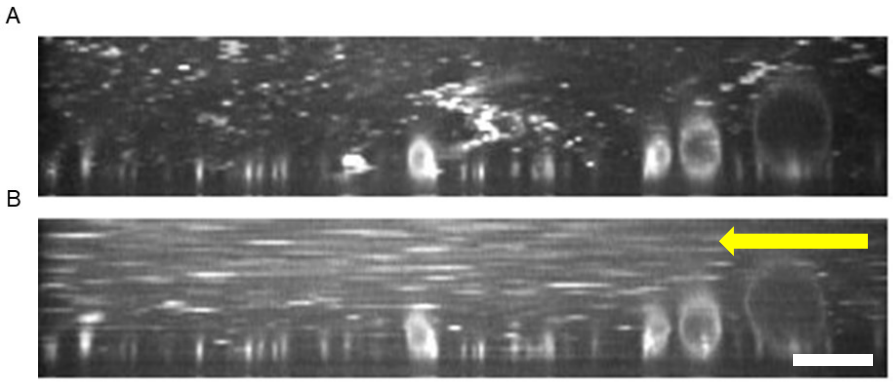

Figure 5.4: Liposomes attached to the bottom surface of a microfluidic channel. (A) No flow, (B) At a flow rate of 50 µL/hr. Yellow arrow indicates the direction of flow. Channel height: 65 µm. Channel width: 300 µm. Scale bar: 25 µm

through the device. The synthetic cells are attached through biotin-streptavidin conjugation on the bottom channel surface. At high enough flow rates, the liposome membranes will experience shear forces which can potentially activate the reconstituted MscL channel. While preliminary studies are underway, the approach is promising in testing shear-induced gating. A 3D reconstructed image using confocal microscopy is shown in Figure 5.4. Attached vesicles are shown before and after application of fluid flow. Tracer particles were used to visualize the flow.

As before, such a setup can be extended to study MscL mutants under varying flow rates and calcium concentrations and to screen for shear-sensitive non-selective or cation-specific channels. Both *E. coli* and HeLa CFE systems can be adapted for use with this setup.

5.2.5 Use of gene circuits for sequential reconstitution of interacting proteins

Using endogenous *E. coli* promotors and transcription factors, the possibility of designing different genetic circuits with control over protein synthesis was previously demonstrated[183]. The use of lac operon along with a σ28 gene amplification circuit enabled induction of protein synthesis with high ON/OFF ratio using IPTG. This gene circuit can be used to study interactions of different proteins in a time-dependent manner. One can start with the expression of a protein like MreB which forms filaments inside the liposomes. Upon induction using osmotic shock, a second protein (like MreC) that interacts with MreB can be synthesized at a different time point. This will allow the observation of real-time protein-protein interactions and change in morphology (in this case) as a consequence of the synthesis of the other protein. Interactions between both soluble and membrane proteins can be studied using this approach. Studies of *in vitro* reconstitution of actin networks inside liposomes can be extended to temporal aspects of polymerization dynamics. The second choice of protein could be any actin binding protein which could alter the morphology of the induced synthetic cells. Another system which has temporal variation coupled to a visual output is the Min oscillator[245,246]. The effect of Min protein interactions as a function of changing concentrations[245] can be studied by the encapsulation of such genetic circuits.

One limitation of this approach could be the depletion of resources for sustaining protein synthesis when using such complicated gene circuits. However, the use of MscL is beneficial to this cause because of its large pore diameter. This can allow the influx of NTPs and amino acids supplemented in the external solution to continue protein synthesis post induction.

Overall, the tools developed in this dissertation are modular and can be applied to a wide range of biological processes. Through the use of different CFE systems, I have demonstrated their utility in tackling pertinent problems in cell and molecular biology.

Bibliography

1. Mazzarello P. A unifying concept: the history of cell theory. *Nat Cell Biol*. 1999;1(1):E13-E15. doi:10.1038/8964

2. Babloyantz A. Molecules, dynamics, and life: An introduction to self-organization of matter. *Wiley-Interscience*. 1986.

3. Liu AP, Fletcher D a. Biology under construction: in vitro reconstitution of cellular function. *Nat Rev Mol Cell Biol*. 2009;10(9):644-650. doi:10.1038/nrm2746

4. Ganzinger KA, Schwille P. More from less – Bottom-up reconstitution of cell biology. *J Cell Sci*. 2019;132(4). doi:10.1242/jcs.227488

5. Vincent Noireaux and Allen P. Liu. The New Age of Cell-Free Biology. *Annu Rev Biomed Eng*. 2020;22:51-77.

6. Singer SJ, Nicolson GL. The Fluid Mosaic Model of the Structure of Cell Membranes. *Science (80-)*. 1972;175(4023):720-731. doi:10.1126/science.175.4023.720

7. Nicolson GL. The Fluid—Mosaic Model of Membrane Structure: Still relevant to understanding the structure, function and dynamics of biological membranes after more than 40years. *Biochim Biophys Acta - Biomembr*. 2014;1838(6):1451-1466. doi:10.1016/j.bbamem.2013.10.019

8. Burla F, Mulla Y, Vos BE, Aufderhorst-Roberts A, Koenderink GH. From mechanical resilience to active material properties in biopolymer networks. *Nat Rev Phys*. 2019;1(4):249-263. doi:10.1038/s42254-019-0036-4

9. Szent-Györgyi AG. The Early History of the Biochemistry of Muscle Contraction. *J Gen Physiol*. 2004;123(6):631-641. doi:10.1085/jgp.200409091

10. Blanchoin L, Amann KJ, Higgs HN, Marchand J-B, Kaiser DA, Pollard TD. Direct observation of

dendritic actin filament networks nucleated by Arp2/3 complex and WASP/Scar proteins. *Nature*. 2000;404(6781):1007-1011. doi:10.1038/35010008

11. Amann KJ, Pollard TD. Direct real-time observation of actin filament branching mediated by Arp2/3 complex using total internal reflection fluorescence microscopy. *Proc Natl Acad Sci*. 2001;98(26):15009-15013. doi:10.1073/pnas.211556398

12. Reymann A-C, Boujemaa-Paterski R, Martiel J-L, et al. Actin Network Architecture Can Determine Myosin Motor Activity. *Science (80-)*. 2012;336(6086):1310-1314. doi:10.1126/science.1221708

13. Bieling P, Li T-D, Weichsel J, et al. Force Feedback Controls Motor Activity and Mechanical Properties of Self-Assembling Branched Actin Networks. *Cell*. 2016;164(1-2):115-127. doi:10.1016/j.cell.2015.11.057

14. Vogel SK, Heinemann F, Chwastek G, Schwille P. The design of MACs (minimal actin cortices). *Cytoskeleton*. 2013;70(11):706-717. doi:10.1002/cm.21136

15. Köster DV, Husain K, Iljazi E, et al. Actomyosin dynamics drive local membrane component organization in an in vitro active composite layer. *Proc Natl Acad Sci*. 2016;113(12):E1645-E1654. doi:10.1073/pnas.1514030113

16. Murrell MP, Gardel ML. F-actin buckling coordinates contractility and severing in a biomimetic actomyosin cortex. *Proc Natl Acad Sci*. 2012;109(51):20820-20825. doi:10.1073/pnas.1214753109

17. Bashirzadeh Y, Liu AP. Encapsulation of the cytoskeleton: towards mimicking the mechanics of a cell. *Soft Matter*. 2019;15(42):8425-8436. doi:10.1039/C9SM01669D

18. Walde P, Cosentino K, Engel H, Stano P. Giant Vesicles: Preparations and Applications. *ChemBioChem*. 2010;11(7):848-865. doi:10.1002/cbic.201000010

19. Liu AP, Fletcher D a. Actin polymerization serves as a membrane domain switch in model lipid bilayers. *Biophys J*. 2006;91(11):4064-4070. doi:10.1529/biophysj.106.090852

20. Liu AP, Richmond DL, Maibaum L, Pronk S, Geissler PL, Fletcher DA. Membrane-induced

bundling of actin filaments. *Nat Phys*. 2008;4(10):789-793. doi:10.1038/nphys1071

21. Simon C, Kusters R, Caorsi V, et al. Actin dynamics drive cell-like membrane deformation. *Nat Phys*. 2019;15(6):602-609. doi:10.1038/s41567-019-0464-1

22. Carvalho K, Tsai F-C, Lees E, Voituriez R, Koenderink GH, Sykes C. Cell-sized liposomes reveal how actomyosin cortical tension drives shape change. *Proc Natl Acad Sci*. 2013;110(41):16456-16461. doi:10.1073/pnas.1221524110

23. Smith BA, Padrick SB, Doolittle LK, et al. Three-color single molecule imaging shows WASP detachment from Arp2/3 complex triggers actin filament branch formation. *Elife*. 2013;2. doi:10.7554/eLife.01008

24. Fygenson DK, Marko JF, Libchaber A. Mechanics of microtubule-based membrane extension. *Phys Rev Lett*. 1997;79(22):4497-4500. doi:10.1103/PhysRevLett.79.4497

25. Hayashi M, Nishiyama M, Kazayama Y, Toyota T, Harada Y, Takiguchi K. Reversible Morphological Control of Tubulin-Encapsulating Giant Liposomes by Hydrostatic Pressure. *Langmuir*. 2016;32(15):3794-3802. doi:10.1021/acs.langmuir.6b00799

26. Perides G, Scherbarth A, Kühn S, Traub P. An electron microscopic study of the interaction in vitro of vimentin intermediate filaments with vesicles prepared from Ehrlich ascites tumor cell lipids. *Eur J Cell Biol*. 1986;41(2):313-325. http://www.ncbi.nlm.nih.gov/pubmed/3758086.

27. Busch DJ, Houser JR, Hayden CC, Sherman MB, Lafer EM, Stachowiak JC. Intrinsically disordered proteins drive membrane curvature. *Nat Commun*. 2015;6(1):7875. doi:10.1038/ncomms8875

28. Donaldson JG. Arfs and membrane lipids: sensing, generating and responding to membrane curvature. *Biochem J*. 2008;414(2):e1-e2. doi:10.1042/BJ20081438

29. Takei K, Haucke V, Slepnev V, et al. Generation of Coated Intermediates of Clathrin-Mediated Endocytosis on Protein-Free Liposomes. *Cell*. 1998;94(1):131-141. doi:10.1016/S0092-8674(00)81228-3

30. Saleem M, Morlot S, Hohendahl A, Manzi J, Lenz M, Roux A. A balance between membrane elasticity and polymerization energy sets the shape of spherical clathrin coats. *Nat Commun*. 2015;6(1):6249. doi:10.1038/ncomms7249

31. Damke H, Baba T, Warnock DE, Schmid SL. Induction of mutant dynamin specifically blocks endocytic coated vesicle formation. *J Cell Biol*. 1994;127(4):915-934. doi:10.1083/jcb.127.4.915

32. Roux A, Uyhazi K, Frost A, De Camilli P. GTP-dependent twisting of dynamin implicates constriction and tension in membrane fission. *Nature*. 2006;441(7092):528-531. doi:10.1038/nature04718

33. Manneville J-B, Casella J-F, Ambroggio E, et al. COPI coat assembly occurs on liquid-disordered domains and the associated membrane deformations are limited by membrane tension. *Proc Natl Acad Sci*. 2008;105(44):16946-16951. doi:10.1073/pnas.0807102105

34. Bacia K, Futai E, Prinz S, et al. Multibudded tubules formed by COPII on artificial liposomes. *Sci Rep*. 2011;1(1):17. doi:10.1038/srep00017

35. Wollert T, Yang D, Ren X, Lee HH, Im YJ, Hurley JH. The ESCRT machinery at a glance. *J Cell Sci*. 2009;122(13):2163-2166. doi:10.1242/jcs.029884

36. Chiaruttini N, Redondo-Morata L, Colom A, et al. Relaxation of Loaded ESCRT-III Spiral Springs Drives Membrane Deformation. *Cell*. 2015;163(4):866-879. doi:10.1016/j.cell.2015.10.017

37. Lee K-H. T Cell Receptor Signaling Precedes Immunological Synapse Formation. *Science (80-)*. 2002;295(5559):1539-1542. doi:10.1126/science.1067710

38. Varma R, Campi G, Yokosuka T, Saito T, Dustin ML. T Cell Receptor-Proximal Signals Are Sustained in Peripheral Microclusters and Terminated in the Central Supramolecular Activation Cluster. *Immunity*. 2006;25(1):117-127. doi:10.1016/j.immuni.2006.04.010

39. Yokosuka T, Sakata-Sogawa K, Kobayashi W, et al. Newly generated T cell receptor microclusters initiate and sustain T cell activation by recruitment of Zap70 and SLP-76. *Nat Immunol*. 2005;6(12):1253-1262. doi:10.1038/ni1272

40. Mossman KD. Altered TCR Signaling from Geometrically Repatterned Immunological Synapses. *Science (80-)*. 2005;310(5751):1191-1193. doi:10.1126/science.1119238

41. Chang VT, Fernandes RA, Ganzinger KA, et al. Initiation of T cell signaling by CD45 segregation at “close contacts.” *Nat Immunol*. 2016;17(5):574-582. doi:10.1038/ni.3392

42. Rohrs JA, Zheng D, Graham NA, Wang P, Finley SD. Computational Model of Chimeric Antigen Receptors Explains Site-Specific Phosphorylation Kinetics. *Biophys J*. 2018;115(6):1116-1129. doi:10.1016/j.bpj.2018.08.018

43. Mukhopadhyay H, de Wet B, Clemens L, et al. Multisite Phosphorylation Modulates the T Cell Receptor ζ -Chain Potency but not the Switchlike Response. *Biophys J*. 2016;110(8):1896-1906. doi:10.1016/j.bpj.2016.03.024

44. Sojo V, Dessimoz C, Pomiankowski A, Lane N. Membrane Proteins Are Dramatically Less Conserved than Water-Soluble Proteins across the Tree of Life. *Mol Biol Evol*. 2016;33(11):2874-2884. doi:10.1093/molbev/msw164

45. Chernomordik L V, Kozlov MM. Mechanics of membrane fusion. *Nat Struct Mol Biol*. 2008;15(7):675-683. doi:10.1038/nsmb.1455

46. Razin M, Ginsburg H. Fusion of liposomes with planar lipid bilayers. *Biochim Biophys Acta - Biomembr*. 1980;598(2):285-292. doi:10.1016/0005-2736(80)90006-1

47. Balch WE, Glick BS, Rothman JE. Sequential intermediates in the pathway of intercompartmental transport in a cell-free system. *Cell*. 1984;39(3):525-536. doi:10.1016/0092-8674(84)90459-8

48. Brunger AT, Cipriano DJ, Diao J. Towards reconstitution of membrane fusion mediated by SNAREs and other synaptic proteins. *Crit Rev Biochem Mol Biol*. 2015;50(3):231-241. doi:10.3109/10409238.2015.1023252

49. Hussain S, Davanger S. The discovery of the soluble N-ethylmaleimide-sensitive factor attachment protein receptor complex and the molecular regulation of synaptic vesicle transmitter release: the 2010 Kavli Prize in neuroscience. *Neuroscience*. 2011;190:12-20. doi:10.1016/j.neuroscience.2011.05.057

50. Struck DK, Hoekstra D, Pagano RE. Use of resonance energy transfer to monitor membrane fusion. *Biochemistry*. 1981;20(14):4093-4099. doi:10.1021/bi00517a023

51. Weber T, Zemelman B V, McNew JA, et al. SNAREpins: Minimal Machinery for Membrane Fusion. *Cell*. 1998;92(6):759-772. doi:10.1016/S0092-8674(00)81404-X

52. Fix M, Melia TJ, Jaiswal JK, et al. Imaging single membrane fusion events mediated by SNARE proteins. *Proc Natl Acad Sci*. 2004;101(19):7311-7316. doi:10.1073/pnas.0401779101

53. Bowen ME, Weninger K, Brunger AT, Chu S. Single Molecule Observation of Liposome-Bilayer Fusion Thermally Induced by Soluble N-Ethyl Maleimide Sensitive-Factor Attachment Protein Receptors (SNAREs). *Biophys J*. 2004;87(5):3569-3584. doi:10.1529/biophysj.104.048637

54. Lai Y, Lou X, Wang C, Xia T, Tong J. Synaptotagmin 1 and Ca2+ drive trans SNARE zippering. *Sci Rep*. 2015;4(1):4575. doi:10.1038/srep04575

55. Yu H, Crisman L, Stowell MHB, Shen J. Functional Reconstitution of Intracellular Vesicle Fusion Using Purified SNAREs and Sec1/Munc18 (SM) Proteins. In: ; 2019:237-249. doi:10.1007/978-1-4939-8760-3_15

56. Kiessling V, Liang B, Kreutzberger AJB, Tamm LK. Planar Supported Membranes with Mobile SNARE Proteins and Quantitative Fluorescence Microscopy Assays to Study Synaptic Vesicle Fusion. *Front Mol Neurosci*. 2017;10(March):1-8. doi:10.3389/fnmol.2017.00072

57. Zhang Y. Energetics, kinetics, and pathway of SNARE folding and assembly revealed by optical tweezers. *Protein Sci*. 2017;26(7):1252-1265. doi:10.1002/pro.3116

58. Quist A, Doudevski I, Lin H, et al. Amyloid ion channels: A common structural link for protein-misfolding disease. *Proc Natl Acad Sci*. 2005;102(30):10427-10432. doi:10.1073/pnas.0502066102

59. Studer A, Demarche S, Langenegger D, Tiefenauer L. Integration and recording of a reconstituted voltage-gated sodium channel in planar lipid bilayers. *Biosens Bioelectron*. 2011;26(5):1924-1928. doi:10.1016/j.bios.2010.06.008

60. Aimon S, Manzi J, Schmidt D, Poveda Larrosa JA, Bassereau P, Toombes GES. Functional Reconstitution of a Voltage-Gated Potassium Channel in Giant Unilamellar Vesicles. Muller DJ, ed. *PLoS One*. 2011;6(10):e25529. doi:10.1371/journal.pone.0025529

61. Santacruz-Toloza, Lucia, Eduardo Perozo and DMP. Purification and reconstitution of functional Shaker K+ channels assayed with a light-driven voltage-control system. *Biochemistry*. 1994;33(6):1295-1299.

62. St-Pierre F, Chavarha M, Lin MZ. Designs and sensing mechanisms of genetically encoded fluorescent voltage indicators. *Curr Opin Chem Biol*. 2015;27:31-38. doi:10.1016/j.cbpa.2015.05.003

63. Hirano-Iwata A, Ishinari Y, Yoshida M, et al. Reconstitution of Human Ion Channels into Solvent-free Lipid Bilayers Enhanced by Centrifugal Forces. *Biophys J*. 2016;110(10):2207-2215. doi:10.1016/j.bpj.2016.04.010

64. Sukharev SI, Blount P, Martinac B, Blattner FR, Kung C. A large-conductance mechanosensitive channel in E. coli encoded by mscL alone. *Nature*. 1994;368(6468):265-268. doi:10.1038/368265a0

65. Cahalan SM, Lukacs V, Ranade SS, Chien S, Bandell M, Patapoutian A. Piezo1 links mechanical forces to red blood cell volume. *Elife*. 2015;4. doi:10.7554/eLife.07370

66. Häse CC, Le Dain AC, Martinac B. Purification and Functional Reconstitution of the Recombinant Large Mechanosensitive Ion Channel (MscL) of Escherichia coli. *J Biol Chem*. 1995;270(31):18329-18334. doi:10.1074/jbc.270.31.18329

67. Sukharev S, Betanzos M, Chiang C-S, Guy HR. The gating mechanism of the large mechanosensitive channel MscL. *Nature*. 2001;409(6821):720-724. doi:10.1038/35055559

68. Maingret F, Patel AJ, Lesage F, Lazdunski M, Honoré E. Lysophospholipids Open the Two-pore Domain Mechano-gated K + Channels TREK-1 and TRAAK. *J Biol Chem*. 2000;275(14):10128-10133. doi:10.1074/jbc.275.14.10128

69. Coste B, Mathur J, Schmidt M, et al. Piezo1 and Piezo2 Are Essential Components of Distinct

Mechanically Activated Cation Channels. *Science (80-)*. 2010;330(6000):55-60. doi:10.1126/science.1193270

70. Syeda R, Florendo MN, Cox CD, et al. Piezo1 Channels Are Inherently Mechanosensitive. *Cell Rep*. 2016;17(7):1739-1746. doi:10.1016/j.celrep.2016.10.033

71. Li J, Hou B, Tumova S, et al. Piezo1 integration of vascular architecture with physiological force. *Nature*. 2014;515(7526):279-282. doi:10.1038/nature13701

72. Cox CD, Bae C, Ziegler L, et al. Removal of the mechanoprotective influence of the cytoskeleton reveals PIEZO1 is gated by bilayer tension. *Nat Commun*. 2016;7(1):10366. doi:10.1038/ncomms10366

73. Stenlund P, Babcock GJ, Sodroski J, Myszka DG. Capture and reconstitution of G protein-coupled receptors on a biosensor surface. *Anal Biochem*. 2003;316(2):243-250. doi:10.1016/S0003-2697(03)00046-0

74. Vélez-Ruiz GA, Sunahara RK. Reconstitution of G Protein-Coupled Receptors into a Model Bilayer System: Reconstituted High-Density Lipoprotein Particles. In: ; 2011:167-182. doi:10.1007/978-1-61779-160-4_8

75. Su X, Ditlev JA, Rosen MK, Vale RD. Reconstitution of TCR Signaling Using Supported Lipid Bilayers. In: ; 2017:65-76. doi:10.1007/978-1-4939-6881-7_5

76. Carbone CB, Kern N, Fernandes RA, et al. In vitro reconstitution of T cell receptor-mediated segregation of the CD45 phosphatase. *Proc Natl Acad Sci*. 2017;114(44):E9338-E9345. doi:10.1073/pnas.1710358114

77. Rigaud JL, Lévy D. Reconstitution of Membrane Proteins into Liposomes. *Methods Enzymol*. 2003;372(2000):65-86. doi:10.1016/S0076-6879(03)72004-7

78. Syeda R, Xu J, Dubin AE, et al. Chemical activation of the mechanotransduction channel Piezo1. *Elife*. 2015;4. doi:10.7554/eLife.07369

79. Bernaudat F, Frelet-Barrand A, Pochon N, et al. Heterologous Expression of Membrane Proteins:

Choosing the Appropriate Host. van Veen HW, ed. *PLoS One*. 2011;6(12):e29191. doi:10.1371/journal.pone.0029191

80. Gecchele E, Merlin M, Brozzetti A, Falorni A, Pezzotti M, Avesani L. A Comparative Analysis of Recombinant Protein Expression in Different Biofactories: Bacteria, Insect Cells and Plant Systems. *J Vis Exp*. 2015;(97). doi:10.3791/52459

81. Chiang P-C, Tanady K, Huang L-T, Chao L. Rupturing Giant Plasma Membrane Vesicles to Form Micron-sized Supported Cell Plasma Membranes with Native Transmembrane Proteins. *Sci Rep*. 2017;7(1):15139. doi:10.1038/s41598-017-15103-3

82. van Meer G, Voelker DR, Feigenson GW. Membrane lipids: where they are and how they behave. *Nat Rev Mol Cell Biol*. 2008;9(2):112-124. doi:10.1038/nrm2330

83. Goers R, Thoma J, Ritzmann N, et al. Optimized reconstitution of membrane proteins into synthetic membranes. *Commun Chem*. 2018;1(1):35. doi:10.1038/s42004-018-0037-8

84. Hardy GJ, Nayak R, Munir Alam S, Shapter JG, Heinrich F, Zauscher S. Biomimetic supported lipid bilayers with high cholesterol content formed by α-helical peptide-induced vesicle fusion. *J Mater Chem*. 2012;22(37):19506. doi:10.1039/c2jm32016a

85. Méléard P, Bagatolli LA, Pott T. Giant Unilamellar Vesicle Electroformation. From Lipid Mixtures to Native Membranes Under Physiological Conditions. *Methods Enzymol*. 2009;465(C):161-176. doi:10.1016/S0076-6879(09)65009-6

86. Khan M, Dosoky N, Williams J. Engineering Lipid Bilayer Membranes for Protein Studies. *Int J Mol Sci*. 2013;14(11):21561-21597. doi:10.3390/ijms141121561

87. van Weerd J, Karperien M, Jonkheijm P. Supported Lipid Bilayers for the Generation of Dynamic Cell-Material Interfaces. *Adv Healthc Mater*. 2015;4(18):2743-2779. doi:10.1002/adhm.201500398

88. Montal M, Darszon A, Schindler H. Functional reassembly of membrane proteins in planar lipid bilayers. *Q Rev Biophys*. 1981;14(1):1-79. doi:10.1017/S0033583500002079

89. Winterhalter M. Black lipid membranes. *Curr Opin Colloid Interface Sci*. 2000;5(3-4):250-255.

doi:10.1016/S1359-0294(00)00063-7

90. Funakoshi K, Suzuki H, Takeuchi S. Lipid bilayer formation by contacting monolayers in a microfluidic device for membrane protein analysis. *Anal Chem*. 2006;78(24):8169-8174. doi:10.1021/ac0613479

91. Renauld S, Cortes S, Bersch B, Henry X, De Waard M, Schaack B. Functional reconstitution of cell-free synthesized purified Kv channels. *Biochim Biophys Acta - Biomembr*. 2017;1859(12):2373-2380. doi:10.1016/j.bbamem.2017.09.002

92. Najem JS, Dunlap MD, Rowe ID, et al. Activation of bacterial channel MscL in mechanically stimulated droplet interface bilayers. *Sci Rep*. 2015;5(1):13726. doi:10.1038/srep13726

93. Ritchie TK, Grinkova YV, Bayburt TH, et al. Reconstitution of Membrane Proteins in Phospholipid Bilayer Nanodiscs. In: ; 2009:211-231. doi:10.1016/S0076-6879(09)64011-8

94. Dong Y, Chen S, Zhang S, et al. Folding DNA into a Lipid-Conjugated Nanobarrel for Controlled Reconstitution of Membrane Proteins. *Angew Chemie*. 2018;130(8):2094-2098. doi:10.1002/ange.201710147

95. Rigaud J-L, Levy D, Mosser G, Lambert O. Detergent removal by non-polar polystyrene beads. *Eur Biophys J*. 1998;27(4):305-319. doi:10.1007/s002490050138

96. Pistorius AMA, Stekhoven FMAHS, Boveegeurts PHM, Degrip WJ. Quantitative Analysis of Residual Detergent in Proteoliposomes by Fourier Transform Infrared Spectroscopy. *Anal Biochem*. 1994;221(1):48-52. doi:10.1006/abio.1994.1376

97. Nicholls P, Hildebrandt V, Wrigglesworth JM. Orientation and reactivity of cytochrome aa3 heme groups in proteoliposomes. *Arch Biochem Biophys*. 1980;204(2):533-543. doi:10.1016/0003-9861(80)90065-X

98. Tunuguntla R, Bangar M, Kim K, Stroeve P, Ajo-Franklin CM, Noy A. Lipid Bilayer Composition Can Influence the Orientation of Proteorhodopsin in Artificial Membranes. *Biophys J*. 2013;105(6):1388-1396. doi:10.1016/j.bpj.2013.07.043

99. Gale, Ernest F. and JPF. Effect of nucleic acids on protein synthesis and amino-acid incorporation in disrupted staphylococcal cells. *Nature*. 1954;173(4417):1223-1227.

100. Bank, A. and PAM. Protein synthesis in a cell free human reticulocyte system: ribosome function in thalassemia. *J Clin Invest*. 1966;45(3):330-336.

101. Paul C. Zamecnik, Ivan D. Frantz, Jr., Robert B. Loftfield MLS. Incorporation in vitro of radioactive carbon from carboxyl-labeled DL-Alanine and glycine into proteins of normal and malignant rat livers. *J Biol Chem*. 1948;175:299-314.

102. Littlefield, John W. and EBK. Incorporation of C14-amino acids into ribonucleoprotein particles from the Ehrlich mouse ascites tumor. *J Biol Chem*. 1957;224(1):13-30.

103. Marcus A, Feeley J, Volcani T. Protein Synthesis in Imbibed Seeds III. Kinetics of Amino Acid Incorporation Ribosome Activation, and Polysome Formation. *Plant Physiol*. 1966;41(7):1167-1172. doi:10.1104/pp.41.7.1167

104. Nirenberg M. Historical review: Deciphering the genetic code – a personal account. *Trends Biochem Sci*. 2004;29(1):46-54. doi:10.1016/j.tibs.2003.11.009

105. PELHAM HRB, JACKSON RJ. An Efficient mRNA-Dependent Translation System from Reticulocyte Lysates. *Eur J Biochem*. 1976;67(1):247-256. doi:10.1111/j.1432-1033.1976.tb10656.x

106. Craig D, Howell MT, Gibbs CL, Hunt T, Jackson RJ. Plasmid cDNA-directed protein synthesis in a coupled eukaryotic in vitro transcription-translation system. *Nucleic Acids Res*. 1992;20(19):4987-4995. doi:10.1093/nar/20.19.4987

107. Chong S. Overview of Cell-Free Protein Synthesis: Historic Landmarks, Commercial Systems, and Expanding Applications. *Curr Protoc Mol Biol*. 2014;108(1). doi:10.1002/0471142727.mb1630s108

108. Kuruma Y, Ueda T. The PURE system for the cell-free synthesis of membrane proteins. *Nat Protoc*. 2015;10(9):1328-1344. doi:10.1038/nprot.2015.082

109. Quast RB, Kortt O, Henkel J, et al. Automated production of functional membrane proteins using

eukaryotic cell-free translation systems. *J Biotechnol*. 2015;203:45-53. doi:10.1016/j.jbiotec.2015.03.015

110. Sachse R, Dondapati SK, Fenz SF, Schmidt T, Kubick S. Membrane protein synthesis in cell-free systems: From bio-mimetic systems to bio-membranes. *FEBS Lett*. 2014;588(17):2774-2781. doi:10.1016/j.febslet.2014.06.007

111. Brödel AK, Sonnabend A, Kubick S. Cell-free protein expression based on extracts from CHO cells. *Biotechnol Bioeng*. 2014;111(1):25-36. doi:10.1002/bit.25013

112. Ferencz CM, Guigas G, Veres A, Neumann B, Stemmann O, Weiss M. In vitro reconstitution of the endoplasmic reticulum. *Curr Protoc Cell Biol*. 2017;2017(September):11.22.1-11.22.16. doi:10.1002/cpcb.30

113. Zemella A, Thoring L, Hoffmeister C, Kubick S. Cell-Free Protein Synthesis: Pros and Cons of Prokaryotic and Eukaryotic Systems. *ChemBioChem*. 2015;16(17):2420-2431. doi:10.1002/cbic.201500340

114. van Dalen A, Hegger S, Killian JA, de Kruijff B. Influence of lipids on membrane assembly and stability of the potassium channel KcsA. *FEBS Lett*. 2002;525(1-3):33-38. doi:10.1016/S0014-5793(02)03061-2

115. Awayda MS, Ismailov II, Berdiev BK, Benos DJ. A cloned renal epithelial Na+ channel protein displays stretch activation in planar lipid bilayers. *Am J Physiol Physiol*. 1995;268(6):C1450-C1459. doi:10.1152/ajpcell.1995.268.6.C1450

116. Berrier C, Guilvout I, Bayan N, et al. Coupled cell-free synthesis and lipid vesicle insertion of a functional oligomeric channel MscL. *Biochim Biophys Acta - Biomembr*. 2011;1808(1):41-46. doi:10.1016/j.bbamem.2010.09.018

117. Price CE, Kocer A, Kol S, van der Berg JP, Driessen AJM. In vitro synthesis and oligomerization of the mechanosensitive channel of large conductance, MscL, into a functional ion channel. *FEBS Lett*. 2011;585(1):249-254. doi:10.1016/j.febslet.2010.11.057

118. Kobilka BK. The role of cytosolic and membrane factors in processing of the human β-2

adrenergic receptor following translocation and glycosylation in a cell-free system. *J Biol Chem*. 1990;265(13):7610-7618.

119. Goren MA, Fox BG. Wheat germ cell-free translation, purification, and assembly of a functional human stearoyl-CoA desaturase complex. *Protein Expr Purif*. 2008;62(2):171-178. doi:10.1016/j.pep.2008.08.002

120. Kuruma Y, Stano P, Ueda T, Luisi PL. A synthetic biology approach to the construction of membrane proteins in semi-synthetic minimal cells. *Biochim Biophys Acta - Biomembr*. 2009;1788(2):567-574. doi:10.1016/j.bbamem.2008.10.017

121. Hamada S, Tabuchi M, Toyota T, et al. Giant vesicles functionally expressing membrane receptors for an insect pheromone. *Chem Commun*. 2014;50(22):2958. doi:10.1039/c3cc48216b

122. Falk MM. Cell-free synthesis and assembly of connexins into functional gap junction membrane channels. *EMBO J*. 1997;16(10):2703-2716. doi:10.1093/emboj/16.10.2703

123. Kalmbach R, Chizhov I, Schumacher MC, Friedrich T, Bamberg E, Engelhard M. Functional Cell-free Synthesis of a Seven Helix Membrane Protein: In situ Insertion of Bacteriorhodopsin into Liposomes. *J Mol Biol*. 2007;371(3):639-648. doi:10.1016/j.jmb.2007.05.087

124. Long AR, O'Brien CC, Alder NN. The Cell-Free Integration of a Polytopic Mitochondrial Membrane Protein into Liposomes Occurs Cotranslationally and in a Lipid-Dependent Manner. Cobine P, ed. *PLoS One*. 2012;7(9):e46332. doi:10.1371/journal.pone.0046332

125. Wuu JJ, Swartz JR. High yield cell-free production of integral membrane proteins without refolding or detergents. *Biochim Biophys Acta - Biomembr*. 2008;1778(5):1237-1250. doi:10.1016/j.bbamem.2008.01.023

126. Caschera F, Noireaux V. Integration of biological parts toward the synthesis of a minimal cell. *Curr Opin Chem Biol*. 2014;22. doi:10.1016/j.cbpa.2014.09.028

127. Scott A, Noga MJ, de Graaf P, Westerlaken I, Yildirim E, Danelon C. Cell-Free Phospholipid Biosynthesis by Gene-Encoded Enzymes Reconstituted in Liposomes. van Veen HW, ed. *PLoS One*. 2016;11(10):e0163058. doi:10.1371/journal.pone.0163058

128. Adamala KP, Martin-Alarcon DA, Guthrie-Honea KR, Boyden ES. Engineering genetic circuit interactions within and between synthetic minimal cells. *Nat Chem*. 2017;9(5):431-439. doi:10.1038/nchem.2644

129. Caschera F, Lee JW, Ho KKY, Liu AP, Jewett MC. Cell-free compartmentalized protein synthesis inside double emulsion templated liposomes with: In vitro synthesized and assembled ribosomes. *Chem Commun*. 2016;52(31):5467-5469. doi:10.1039/c6cc00223d

130. Van Nies P, Westerlaken I, Blanken D, Salas M, Mencía M, Danelon C. Self-replication of DNA by its encoded proteins in liposome-based synthetic cells. *Nat Commun*. 2018;9(1). doi:10.1038/s41467-018-03926-1

131. Majumder S, Willey PT, DeNies MS, Liu AP, Luxton GWG. A synthetic biology platform for the reconstitution and mechanistic dissection of LINC complex assembly. *J Cell Sci*. 2019;132(4):jcs219451. doi:10.1242/jcs.219451

132. Hetzer MW. The Nuclear Envelope. *Cold Spring Harb Perspect Biol*. 2010;2(3):a000539-a000539. doi:10.1101/cshperspect.a000539

133. Watson ML. Further Observations on the Nuclear Envelope of the Animal Cell. *J Biophys Biochem Cytol*. 1959;6(2):147-156. doi:10.1083/jcb.6.2.147

134. Burke B, Stewart CL. The nuclear lamins: flexibility in function. *Nat Rev Mol Cell Biol*. 2013;14(1):13-24. doi:10.1038/nrm3488

135. Otsuka S, Ellenberg J. Mechanisms of nuclear pore complex assembly – two different ways of building one molecular machine. *FEBS Lett*. 2018;592(4):475-488. doi:10.1002/1873-3468.12905

136. Knockenhauer KE, Schwartz TU. The Nuclear Pore Complex as a Flexible and Dynamic Gate. *Cell*. 2016;164(6):1162-1171. doi:10.1016/j.cell.2016.01.034

137. Alam SG, Zhang Q, Prasad N, et al. The mammalian LINC complex regulates genome transcriptional responses to substrate rigidity. *Sci Rep*. 2016;6(1):38063. doi:10.1038/srep38063

138. Lombardi ML, Lammerding J. Keeping the LINC: the importance of nucleocytoskeletal coupling in

intracellular force transmission and cellular function. *Biochem Soc Trans*. 2011;39(6):1729-1734. doi:10.1042/BST20110686

139. Meinke P, Schirmer EC. LINC'ing form and function at the nuclear envelope. *FEBS Lett*. 2015;589(19PartA):2514-2521. doi:10.1016/j.febslet.2015.06.011

140. Tapley EC, Starr DA. Connecting the nucleus to the cytoskeleton by SUN–KASH bridges across the nuclear envelope. *Curr Opin Cell Biol*. 2013;25(1):57-62. doi:10.1016/j.ceb.2012.10.014

141. Horn HF. LINC Complex Proteins in Development and Disease. In: ; 2014:287-321. doi:10.1016/B978-0-12-397920-9.00004-4

142. Janin A, Bauer D, Ratti F, Millat G, Méjat A. Nuclear envelopathies: a complex LINC between nuclear envelope and pathology. *Orphanet J Rare Dis*. 2017;12(1):147. doi:10.1186/s13023-017-0698-x

143. Roux KJ, Crisp ML, Liu Q, et al. Nesprin 4 is an outer nuclear membrane protein that can induce kinesin-mediated cell polarization. *Proc Natl Acad Sci*. 2009;106(7):2194-2199. doi:10.1073/pnas.0808602106

144. Luxton GG, Starr DA. KASHing up with the nucleus: novel functional roles of KASH proteins at the cytoplasmic surface of the nucleus. *Curr Opin Cell Biol*. 2014;28:69-75. doi:10.1016/j.ceb.2014.03.002

145. Starr DA. Role of ANC-1 in Tethering Nuclei to the Actin Cytoskeleton. *Science (80-)*. 2002;298(5592):406-409. doi:10.1126/science.1075119

146. Malone CJ, Fixsen WD, Horvitz HR, Han M. UNC-84 localizes to the nuclear envelope and is required for nuclear migration and anchoring during C. elegans development. *Development*. 1999;126(14):3171-3181. http://www.ncbi.nlm.nih.gov/pubmed/10375507.

147. Chang W, Worman HJ, Gundersen GG. Accessorizing and anchoring the LINC complex for multifunctionality. *J Cell Biol*. 2015;208(1):11-22. doi:10.1083/jcb.201409047

148. Sosa BA, Kutay U, Schwartz TU. Structural insights into LINC complexes. *Curr Opin Struct Biol*.

2013;23(2):285-291. doi:10.1016/j.sbi.2013.03.005

149. Stewart-Hutchinson PJ, Hale CM, Wirtz D, Hodzic D. Structural requirements for the assembly of LINC complexes and their function in cellular mechanical stiffness. *Exp Cell Res*. 2008;314(8):1892-1905. doi:10.1016/j.yexcr.2008.02.022

150. Ostlund C, Folker ES, Choi JC, Gomes ER, Gundersen GG, Worman HJ. Dynamics and molecular interactions of linker of nucleoskeleton and cytoskeleton (LINC) complex proteins. *J Cell Sci*. 2009;122(22):4099-4108. doi:10.1242/jcs.057075

151. Zhou Z, Du X, Cai Z, et al. Structure of Sad1-UNC84 Homology (SUN) Domain Defines Features of Molecular Bridge in Nuclear Envelope. *J Biol Chem*. 2012;287(8):5317-5326. doi:10.1074/jbc.M111.304543

152. Nie S, Ke H, Gao F, et al. Coiled-Coil Domains of SUN Proteins as Intrinsic Dynamic Regulators. *Structure*. 2016;24(1):80-91. doi:10.1016/j.str.2015.10.024

153. Slaughter BD, Li R. Toward Quantitative “In Vivo Biochemistry” with Fluorescence Fluctuation Spectroscopy. Kellogg D, ed. *Mol Biol Cell*. 2010;21(24):4306-4311. doi:10.1091/mbc.e10-05-0451

154. Hennen J, Saunders CA, Mueller JD, Luxton GWG. Fluorescence fluctuation spectroscopy reveals differential SUN protein oligomerization in living cells. Misteli T, ed. *Mol Biol Cell*. 2018;29(9):1003-1011. doi:10.1091/mbc.E17-04-0233

155. Lei K, Zhu X, Xu R, et al. Inner Nuclear Envelope Proteins SUN1 and SUN2 Play a Prominent Role in the DNA Damage Response. *Curr Biol*. 2012;22(17):1609-1615. doi:10.1016/j.cub.2012.06.043

156. Lei K, Zhang X, Ding X, et al. SUN1 and SUN2 play critical but partially redundant roles in anchoring nuclei in skeletal muscle cells in mice. *Proc Natl Acad Sci*. 2009;106(25):10207-10212. doi:10.1073/pnas.0812037106

157. Ding X, Xu R, Yu J, Xu T, Zhuang Y, Han M. SUN1 Is Required for Telomere Attachment to Nuclear Envelope and Gametogenesis in Mice. *Dev Cell*. 2007;12(6):863-872.

doi:10.1016/j.devcel.2007.03.018

158. Liu Q, Pante N, Misteli T, et al. Functional association of Sun1 with nuclear pore complexes. *J Cell Biol*. 2007;178(5):785-798. doi:10.1083/jcb.200704108

159. Lu W, Gotzmann J, Sironi L, et al. Sun1 forms immobile macromolecular assemblies at the nuclear envelope. *Biochim Biophys Acta - Mol Cell Res*. 2008;1783(12):2415-2426. doi:10.1016/j.bbamcr.2008.09.001

160. Talamas JA, Hetzer MW. POM121 and Sun1 play a role in early steps of interphase NPC assembly. *J Cell Biol*. 2011;194(1):27-37. doi:10.1083/jcb.201012154

161. Pucadyil TJ, Schmid SL. Supported Bilayers with Excess Membrane Reservoir: A Template for Reconstituting Membrane Budding and Fission. *Biophys J*. 2010;99(2):517-525. doi:10.1016/j.bpj.2010.04.036

162. Ho KKY, Murray VL, Liu AP. *Engineering Artificial Cells by Combining HeLa-Based Cell-Free Expression and Ultrathin Double Emulsion Template*. Vol 128. Elsevier Ltd; 2015. doi:10.1016/bs.mcb.2015.01.014

163. Luxton GWG, Gomes ER, Folker ES, Vintinner E, Gundersen GG. Linear arrays of nuclear envelope proteins harness retrograde actin flow for nuclear movement. *Science*. 2010;329(5994):956-959. doi:10.1126/science.1189072

164. Mikami S, Kobayashi T, Machida K, Masutani M, Yokoyama S, Imataka H. N-terminally truncated GADD34 proteins are convenient translation enhancers in a human cell-derived in vitro protein synthesis system. *Biotechnol Lett*. 2010;32(7):897-902. doi:10.1007/s10529-010-0251-7

165. Murray CJ, Baliga R. Cell-free translation of peptides and proteins:from high throughput screening to clinical production. *Curr Opin Chem Biol*. 2013;17(3):420-426. doi:10.1016/j.cbpa.2013.02.014

166. Rosenblum G, Cooperman BS. Engine out of the chassis: Cell-free protein synthesis and its uses. *FEBS Lett*. 2014;588(2):261-268. doi:10.1016/j.febslet.2013.10.016

167. Zemella A, Grossmann S, Sachse R, Sonnabend A, Schaefer M, Kubick S. Qualifying a eukaryotic

cell-free system for fluorescence based GPCR analyses. *Sci Rep*. 2017;7(1):3740. doi:10.1038/s41598-017-03955-8

168. Kai L, Orbán E, Henrich E, Proverbio D, Dötsch V, Bernhard F. Co-translational Stabilization of Insoluble Proteins in Cell-Free Expression Systems. In: ; 2015:125-143. doi:10.1007/978-1-4939-2205-5_7

169. Schwarz D, Dötsch V, Bernhard F. Production of membrane proteins using cell-free expression systems. *Proteomics*. 2008;8(19):3933-3946. doi:10.1002/pmic.200800171

170. van Meer G, Voelker DR, Feigenson GW. Membrane lipids: where they are and how they behave. *Nat Rev Mol Cell Biol*. 2008;9(2):112-124. doi:10.1038/nrm2330

171. Schultz J. SMART: a web-based tool for the study of genetically mobile domains. *Nucleic Acids Res*. 2000;28(1):231-234. doi:10.1093/nar/28.1.231

172. Xu S, Cramer WA, Peterson AA, Hermodson M, Montecucco C. Dynamic properties of membrane proteins: reversible insertion into membrane vesicles of a colicin E1 channel-forming peptide. *Proc Natl Acad Sci*. 1988;85(20):7531-7535. doi:10.1073/pnas.85.20.7531

173. Starr DA, Fridolfsson HN. Interactions Between Nuclei and the Cytoskeleton Are Mediated by SUN-KASH Nuclear-Envelope Bridges. *Annu Rev Cell Dev Biol*. 2010;26(1):421-444. doi:10.1146/annurev-cellbio-100109-104037

174. Hodzic DM, Yeater DB, Bengtsson L, Otto H, Stahl PD. Sun2 Is a Novel Mammalian Inner Nuclear Membrane Protein. *J Biol Chem*. 2004;279(24):25805-25812. doi:10.1074/jbc.M313157200

175. Turgay Y, Ungricht R, Rothballer A, et al. A classical NLS and the SUN domain contribute to the targeting of SUN2 to the inner nuclear membrane. *EMBO J*. 2010;29(14):2262-2275. doi:10.1038/emboj.2010.119

176. Adamczak R, Porollo A, Meller J. Accurate prediction of solvent accessibility using neural networks-based regression. *Proteins Struct Funct Bioinforma*. 2004;56(4):753-767. doi:10.1002/prot.20176

177. Padmakumar VC. The inner nuclear membrane protein Sun1 mediates the anchorage of Nesprin-2 to the nuclear envelope. *J Cell Sci*. 2005;118(15):3419-3430. doi:10.1242/jcs.02471

178. Sosa BA, Rothballer A, Kutay U, Schwartz TU. LINC Complexes Form by Binding of Three KASH Peptides to Domain Interfaces of Trimeric SUN Proteins. *Cell*. 2012;149(5):1035-1047. doi:10.1016/j.cell.2012.03.046

179. Cain NE, Jahed Z, Schoenhofen A, et al. Conserved SUN-KASH Interfaces Mediate LINC Complex-Dependent Nuclear Movement and Positioning. *Curr Biol*. 2018;28(19):3086-3097.e4. doi:10.1016/j.cub.2018.08.001

180. Majumder S, Garamella J, Wang Y-L, DeNies M, Noireaux V, Liu AP. Cell-sized mechanosensitive and biosensing compartment programmed with DNA. *Chem Commun*. 2017;53(53):7349-7352. doi:10.1039/C7CC03455E

181. Carlson ED, Gan R, Hodgman CE, Jewett MC. Cell-free protein synthesis: Applications come of age. *Biotechnol Adv*. 2012;30(5):1185-1194. doi:10.1016/j.biotechadv.2011.09.016

182. Tayar AM, Karzbrun E, Noireaux V, Bar-Ziv RH. Propagating gene expression fronts in a one-dimensional coupled system of artificial cells. *Nat Phys*. 2015;11(12):1037-1041. doi:10.1038/nphys3469

183. Garamella J, Marshall R, Rustad M, Noireaux V. The All E. coli TX-TL Toolbox 2.0: A Platform for Cell-Free Synthetic Biology. *ACS Synth Biol*. 2016;5(4):344-355. doi:10.1021/acssynbio.5b00296

184. Pardee K, Slomovic S, Nguyen PQ, et al. Portable, On-Demand Biomolecular Manufacturing. *Cell*. 2016;167(1):248-259.e12. doi:10.1016/j.cell.2016.09.013

185. Ng PP, Jia M, Patel KG, et al. A vaccine directed to B cells and produced by cell-free protein synthesis generates potent antilymphoma immunity. *Proc Natl Acad Sci*. 2012;109(36):14526-14531. doi:10.1073/pnas.1211018109

186. Iwane Y, Hitomi A, Murakami H, Katoh T, Goto Y, Suga H. Expanding the amino acid repertoire of ribosomal polypeptide synthesis via the artificial division of codon boxes. *Nat Chem*. 2016;8(4):317-325. doi:10.1038/nchem.2446

187. Chemla Y, Ozer E, Schlesinger O, Noireaux V, Alfonta L. Genetically expanded cell-free protein synthesis using endogenous pyrrolysyl orthogonal translation system. *Biotechnol Bioeng*. 2015;112(8):1663-1672. doi:10.1002/bit.25587

188. Hong SH, Kwon Y-C, Jewett MC. Non-standard amino acid incorporation into proteins using Escherichia coli cell-free protein synthesis. *Front Chem*. 2014;2. doi:10.3389/fchem.2014.00034

189. Takahashi MK, Chappell J, Hayes CA, et al. Rapidly Characterizing the Fast Dynamics of RNA Genetic Circuitry with Cell-Free Transcription–Translation (TX-TL) Systems. *ACS Synth Biol*. 2015;4(5):503-515. doi:10.1021/sb400206c

190. Ho KKY, Lee JW, Durand G, Majumder S, Liu AP. Protein aggregation with poly(vinyl) alcohol surfactant reduces double emulsion-encapsulated mammalian cell-free expression. Yuan F, ed. *PLoS One*. 2017;12(3):e0174689. doi:10.1371/journal.pone.0174689

191. Pohorille A, Deamer D. Artificial cells: prospects for biotechnology. *Trends Biotechnol*. 2002;20(3):123-128. doi:10.1016/S0167-7799(02)01909-1

192. Fujii S, Matsuura T, Sunami T, Nishikawa T, Kazuta Y, Yomo T. Liposome display for in vitro selection and evolution of membrane proteins. *Nat Protoc*. 2014;9(7):1578-1591. doi:10.1038/nprot.2014.107

193. Arriaga LR, Datta SS, Kim SH, et al. Ultrathin shell double emulsion templated giant unilamellar lipid vesicles with controlled microdomain formation. *Small*. 2014;10(5):950-956. doi:10.1002/smll.201301904

194. Zhao Y, Araki S, Wu J, et al. An Expanded Palette of Genetically Encoded Ca2+ Indicators. *Science (80-)*. 2011;333(6051):1888-1891. doi:10.1126/science.1208592

195. Noireaux V, Libchaber A. A vesicle bioreactor as a step toward an artificial cell assembly. *Proc Natl Acad Sci*. 2004;101(51):17669-17674. doi:10.1073/pnas.0408236101

196. Lee LM, Liu AP. A microfluidic pipette array for mechanophenotyping of cancer cells and mechanical gating of mechanosensitive channels. *Lab Chip*. 2015;15(1):264-273. doi:10.1039/C4LC01218F

197. Heureaux J, Chen D, Murray VL, Deng CX, Liu AP. Activation of a Bacterial Mechanosensitive Channel in Mammalian Cells by Cytoskeletal Stress. *Cell Mol Bioeng*. 2014;7(3):307-319. doi:10.1007/s12195-014-0337-8

198. Su S, Phua SC, DeRose R, et al. Genetically encoded calcium indicator illuminates calcium dynamics in primary cilia. *Nat Methods*. 2013;10(11):1105-1107. doi:10.1038/nmeth.2647

199. Utada AS, Lorenceau E, Link DR, Kaplan PD, Stone HA, Weitz DA. Monodisperse Double Emulsions Generated from a Microcapillary Device. *Science (80-)*. 2005;308(5721):537-541. doi:10.1126/science.1109164

200. Ho KKY, Lee LM, Liu AP. Mechanically activated artificial cell by using microfluidics. *Sci Rep*. 2016;6(August):32912. doi:10.1038/srep32912

201. Shin J, Noireaux V. An E. coli Cell-Free Expression Toolbox: Application to Synthetic Gene Circuits and Artificial Cells. *ACS Synth Biol*. 2012;1(1):29-41. doi:10.1021/sb200016s

202. Siuti P, Yazbek J, Lu TK. Synthetic circuits integrating logic and memory in living cells. *Nat Biotechnol*. 2013;31(5):448-452. doi:10.1038/nbt.2510

203. Garamella J, Majumder S, Liu AP, Noireaux V. An Adaptive Synthetic Cell Based on Mechanosensing, Biosensing, and Inducible Gene Circuits. *ACS Synth Biol*. 2019;8(8):1913-1920. doi:10.1021/acssynbio.9b00204

204. Majumder S, Liu AP. Bottom-up synthetic biology: modular design for making artificial platelets. *Phys Biol*. 2017;15(1):013001. doi:10.1088/1478-3975/aa9768

205. Chiarabelli C, Stano P, Luisi PL. Chemical approaches to synthetic biology. *Curr Opin Biotechnol*. 2009;20(4):492-497. doi:10.1016/j.copbio.2009.08.004

206. Hutchison CA, Chuang R-Y, Noskov VN, et al. Design and synthesis of a minimal bacterial genome. *Science (80-)*. 2016. doi:10.1126/science.aad6253

207. Schwille P. Jump-starting life? Fundamental aspects of synthetic biology. *J Cell Biol*. 2015;210(5):687-690. doi:10.1083/jcb.201506125

208. Ishikawa K, Sato K, Shima Y, Urabe I, Yomo T. Expression of a cascading genetic network within liposomes. *FEBS Lett*. 2004;576(3):387-390. doi:10.1016/j.febslet.2004.09.046

209. Caschera F, Noireaux V. Compartmentalization of an all- E. coli Cell-Free Expression System for the Construction of a Minimal Cell. *Artif Life*. 2016;22(2):185-195. doi:10.1162/ARTL_a_00198

210. Lu Y. Cell-free synthetic biology: Engineering in an open world. *Synth Syst Biotechnol*. 2017;2(1):23-27. doi:10.1016/j.synbio.2017.02.003

211. Vogele K, Frank T, Gasser L, et al. Towards synthetic cells using peptide-based reaction compartments. *Nat Commun*. 2018;9(1):1-7. doi:10.1038/s41467-018-06379-8

212. Lentini R, Martín NY, Forlin M, et al. Two-Way Chemical Communication between Artificial and Natural Cells. *ACS Cent Sci*. 2017;3(2):117-123. doi:10.1021/acscentsci.6b00330

213. Deng N-N, Yelleswarapu M, Zheng L, Huck WTS. Microfluidic Assembly of Monodisperse Vesosomes as Artificial Cell Models. *J Am Chem Soc*. 2017;139(2):587-590. doi:10.1021/jacs.6b10977

214. Garenne D, Noireaux V. Cell-free transcription–translation: engineering biology from the nanometer to the millimeter scale. *Curr Opin Biotechnol*. 2019;58:19-27. doi:10.1016/j.copbio.2018.10.007

215. Green AA, Silver PA, Collins JJ, Yin P. Toehold switches: De-novo-designed regulators of gene expression. *Cell*. 2014;159(4):925-939. doi:10.1016/j.cell.2014.10.002

216. Lutz R. Independent and tight regulation of transcriptional units in Escherichia coli via the LacR/O, the TetR/O and AraC/I1-I2 regulatory elements. *Nucleic Acids Res*. 1997;25(6):1203-1210. doi:10.1093/nar/25.6.1203

217. Sun ZZ, Hayes CA, Shin J, Caschera F, Murray RM, Noireaux V. Protocols for Implementing an Escherichia coli Based TX-TL Cell-Free Expression System for Synthetic Biology. *J Vis Exp*. 2013;(79). doi:10.3791/50762

218. Marshall R, Maxwell CS, Collins SP, Beisel CL, Noireaux V. Short DNA containing χ sites

enhances DNA stability and gene expression in E. coli cell-free transcription-translation systems. *Biotechnol Bioeng*. 2017;114(9):2137-2141. doi:10.1002/bit.26333

219. Shin J, Noireaux V. Efficient cell-free expression with the endogenous E. Coli RNA polymerase and sigma factor 70. *J Biol Eng*. 2010;4(1):8. doi:10.1186/1754-1611-4-8

220. Martinac B. Mechanosensitive ion channels: molecules of mechanotransduction. *J Cell Sci*. 2004;117(12):2449-2460. doi:10.1242/jcs.01232

221. Chen H, Meisburger SP, Pabit SA, Sutton JL, Webb WW, Pollack L. Ionic strength-dependent persistence lengths of single-stranded RNA and DNA. *Proc Natl Acad Sci*. 2012;109(3):799-804. doi:10.1073/pnas.1119057109

222. Rechendorff K, Witz G, Adamcik J, Dietler G. Persistence length and scaling properties of single-stranded DNA adsorbed on modified graphite. *J Chem Phys*. 2009;131(9):095103. doi:10.1063/1.3216111

223. Nurse P, Marians KJ. Purification and Characterization of Escherichia coli MreB Protein. *J Biol Chem*. 2013;288(5):3469-3475. doi:10.1074/jbc.M112.413708

224. Salje J, van den Ent F, de Boer P, Löwe J. Direct Membrane Binding by Bacterial Actin MreB. *Mol Cell*. 2011;43(3):478-487. doi:10.1016/j.molcel.2011.07.008

225. Maeda YT, Nakadai T, Shin J, Uryu K, Noireaux V, Libchaber A. Assembly of MreB filaments on liposome membranes: A synthetic biology approach. *ACS Synth Biol*. 2012;1(2):53-59. doi:10.1021/sb200003v

226. Tinevez J-Y, Schulze U, Salbreux G, Roensch J, Joanny J-F, Paluch E. Role of cortical tension in bleb growth. *Proc Natl Acad Sci*. 2009;106(44):18581-18586. doi:10.1073/pnas.0903353106

227. Thoring L, Wüstenhagen DA, Borowiak M, Stech M, Sonnabend A, Kubick S. Cell-Free Systems Based on CHO Cell Lysates: Optimization Strategies, Synthesis of “Difficult-to-Express” Proteins and Future Perspectives. Budisa N, ed. *PLoS One*. 2016;11(9):e0163670. doi:10.1371/journal.pone.0163670

228. Morimoto A, Shibuya H, Zhu X, et al. A conserved KASH domain protein associates with telomeres, SUN1, and dynactin during mammalian meiosis. *J Cell Biol*. 2012;198(2):165-172. doi:10.1083/jcb.201204085

229. Jahed Z, Mofrad MRK. Mechanical LINCs of the nuclear envelope: Where SUN meets KASH. *Extrem Mech Lett*. 2018;20:99-103. doi:10.1016/j.eml.2018.01.010

230. Wegener KL, Campbell ID. Transmembrane and cytoplasmic domains in integrin activation and protein-protein interactions (Review). *Mol Membr Biol*. 2008;25(5):376-387. doi:10.1080/09687680802269886

231. Chavan TS, Muratcioglu S, Marszalek R, et al. Plasma membrane regulates Ras signaling networks. *Cell Logist*. 2015;5(4):e1136374. doi:10.1080/21592799.2015.1136374

232. Jahed Z, Soheilypour M, Peyro M, Mofrad MRK. The LINC and NPC relationship – it's complicated! *J Cell Sci*. 2016;129(17):3219-3229. doi:10.1242/jcs.184184

233. Lin DH, Stuwe T, Schilbach S, et al. Architecture of the symmetric core of the nuclear pore. *Science (80-)*. 2016;352(6283):aaf1015-aaf1015. doi:10.1126/science.aaf1015

234. Ungricht R, Kutay U. Establishment of NE asymmetry—targeting of membrane proteins to the inner nuclear membrane. *Curr Opin Cell Biol*. 2015;34:135-141. doi:10.1016/j.ceb.2015.04.005

235. Krapf D. Compartmentalization of the plasma membrane. *Curr Opin Cell Biol*. 2018;53:15-21. doi:10.1016/j.ceb.2018.04.002

236. Saunders CA, Luxton GWG. LINCing Defective Nuclear-Cytoskeletal Coupling and DYT1 Dystonia. *Cell Mol Bioeng*. 2016;9(2):207-216. doi:10.1007/s12195-016-0432-0

237. Göb E, Schmitt J, Benavente R, Alsheimer M. Mammalian Sperm Head Formation Involves Different Polarization of Two Novel LINC Complexes. Bryk M, ed. *PLoS One*. 2010;5(8):e12072. doi:10.1371/journal.pone.0012072

238. Heath GR, Li M, Polignano IL, et al. Layer-by-Layer Assembly of Supported Lipid Bilayer Poly-<scp>l</scp> -Lysine Multilayers. *Biomacromolecules*. 2016;17(1):324-335.

doi:10.1021/acs.biomac.5b01434

239. Charlesworth G, Bhatia KP, Wood NW. The genetics of dystonia: new twists in an old tale. *Brain*. 2013;136(7):2017-2037. doi:10.1093/brain/awt138

240. Goodchild RE, Buchwalter AL, Naismith T V., et al. Access of torsinA to the inner nuclear membrane is activity dependent and regulated in the endoplasmic reticulum. *J Cell Sci*. 2015;128(15):2854-2865. doi:10.1242/jcs.167452

241. Vander Heyden AB, Naismith T V., Snapp EL, Hodzic D, Hanson PI. LULL1 Retargets TorsinA to the Nuclear Envelope Revealing an Activity That Is Impaired by the DYT1 Dystonia Mutation. Hegde RS, ed. *Mol Biol Cell*. 2009;20(11):2661-2672. doi:10.1091/mbc.e09-01-0094

242. Grillet M, Gonzalez BD, Sicart A, et al. Torsins Are Essential Regulators of Cellular Lipid Article Torsins Are Essential Regulators of Cellular Lipid Metabolism. 2016:235-247. doi:10.1016/j.devcel.2016.06.017

243. Nery FC, Armata IA, Farley JE, et al. TorsinA participates in endoplasmic reticulum-associated degradation. *Nat Commun*. 2011;2(1):393. doi:10.1038/ncomms1383

244. Pak OS, Young Y-N, Marple GR, Veerapaneni S, Stone HA. Gating of a mechanosensitive channel due to cellular flows. *Proc Natl Acad Sci*. 2015;112(32):9822-9827. doi:10.1073/pnas.1512152112

245. Vecchiarelli AG, Li M, Mizuuchi M, et al. Membrane-bound MinDE complex acts as a toggle switch that drives Min oscillation coupled to cytoplasmic depletion of MinD. *Proc Natl Acad Sci*. 2016;113(11):E1479-E1488. doi:10.1073/pnas.1600644113

246. Litschel T, Ramm B, Maas R, Heymann M, Schwille P. Beating vesicles: Encapsulated protein oscillations cause dynamic membrane deformations. *Angew Chemie Int Ed*. 2018. doi:10.1002/anie.201808750